MESOSCALE CONVECTIVE SYSTEMS

Robert A. Houze Jr.
Department of Atmospheric Sciences
University of Washington
Seattle, Washington, USA

Received 19 January 2004; revised 5 August 2004; accepted 8 November 2004; published 31 December 2004.

[1] Mesoscale convective systems (MCSs) have regions of both convective and stratiform precipitation, and they develop mesoscale circulations as they mature. The upward motion takes the form of a deep-layer ascent drawn into the MCS in response to the latent heating and cooling in the convective region. The ascending layer overturns as it rises but overall retains a coherent layer structure. A middle level layer of inflow enters the stratiform region of the MCS from a direction determined by the large-scale flow and descends in response to diabatic cooling at middle-to-low levels. A middle level mesoscale convective vortex (MCV) develops in the stratiform region, prolongs the MCS, and may contribute to tropical cyclone development. The propagation of an MCS may have a discrete component but may further be influenced by waves and disturbances generated both in response to the MCS and external to the MCS. Waves of a larger scale may affect the propagation velocity by phase locking with the MCS in a cooperative mode. The horizontal scale of an MCS may be limited either by a balance between the formation rate of convective precipitation and dissipation of stratiform precipitation or by the Rossby radius of the MCV. The vertical redistribution of momentum by an MCS depends on the size of the stratiform region, while the net vertical profile of heating of the large-scale environment depends on the amount of stratiform rain. Regional variability of the stratiform rain from MCSs affects the large-scale circulation's response to MCS heating. *INDEX TERMS:* 3329 Meteorology and Atmospheric Dynamics: Mesoscale meteorology; 3354 Meteorology and Atmospheric Dynamics: Precipitation (1854); 3384 Meteorology and Atmospheric Dynamics: Waves and tides; 3314 Meteorology and Atmospheric Dynamics: Convective processes; 3324 Meteorology and Atmospheric Dynamics: Lightning; *KEYWORDS:* convective processes, mesoscale meteorology, precipitation.

Citation: Houze, R. A., Jr. (2004), Mesoscale convective systems, *Rev. Geophys.*, *42*, RG4003, doi:10.1029/2004RG000150.

1. INTRODUCTION

[2] Large ice clouds spread by winds aloft dominate the view of Earth from space. These cirriform cloud tops emanate from cyclones, both tropical and extratropical, and from large convective storms. Mesoscale convective systems (MCSs) are the largest of the convective storms. They form when clouds occurring in response to convective instability amalgamate and organize upscale into a single cloud system with a very large upper cirriform cloud structure and rainfall covering large contiguous rain areas. They account for a large proportion of precipitation in both the tropics and warmer midlatitudes. Long-lasting, slow moving MCSs are a major cause of flooding, and these systems often contain hail, strong winds, and even tornadoes. MCSs over the ocean sometimes evolve into tropical cyclones. In producing all these effects, MCSs take on a variety of forms. A broad descriptive definition of an MCS that includes most, if not all, of its forms is a cumulonimbus cloud system that produces a contiguous precipitation area $\sim$100 km or more in at least one direction. *Houze* [1993] suggested a similar definition and further noted that the dynamics of an MCS are often more complex than those of individual cumulonimbus clouds or lines of cumulonimbus. When the individual cumulonimbus clouds and/or lines of cumulonimbus group together in these cloud systems, additional phenomena appear. In particular, the MCS often contains a large region of stratiform precipitation and [*Houze*, 1993, p. 334] ''mesoscale circulations. . .induced by the large conglomerate of convective and stratiform clouds and precipitation.'' MCSs exhibit a variety of cloud and precipitation structures [*Houze et al.*, 1990]. A special case of MCS is the mesoscale convective complex (MCC), defined by *Maddox* [1980] as a long-lasting, quasi-circular, extremely cold topped MCS.

[3] MCSs are an important link between atmospheric convection and the larger-scale atmospheric circulation. For example, they are associated in various ways with larger-scale wave motions [e.g., *Payne and McGarry*, 1977; *Hodges and Thorncroft*, 1997; *Houze et al.*, 2000; *Carbone et al.*, 2002], and some of the largest MCSs occur over the Pacific Ocean warm pool as a fundamental ingredient of intraseasonal and interannual climate variations [*Nakazawa*, 1988; *Chen et al.*, 1996]. This review explores both the internal structure and dynamics of MCSs and the interactions between MCSs and larger scales of motion.

[4] Much of what we know about MCSs and MCCs has come from field projects and modeling studies carried out in the 1970s and 1980s. Those defining studies were synthesized by *Cotton and Anthes* [1989, chapter 10] and *Houze* [1993, chapter 9]. *Fritsch and Forbes* [2001] subsequently

8755-1209/04/2004RG000150*$15.00*
Paper number 2004RG000150

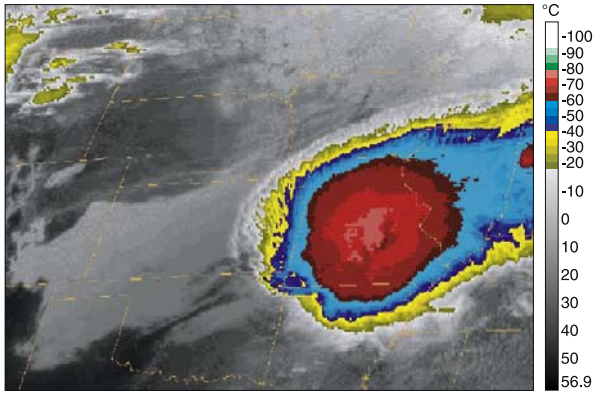

Figure 1. Infrared satellite image of a mesoscale convective system over Missouri. Courtesy of J. Moore, St. Louis University, St. Louis, Missouri.

have summarized work on MCSs carried out up to about 1995. The present review continues this process of synthesis. It is organized around the following major aspects of MCS structure and interaction of MCSs with the larger-scale atmospheric circulation: (1) the nature of the ascent of the buoyant air in MCSs, (2) the middle level inflow and descent of potentially negatively buoyant air, (3) the development of a middle level vortex within the MCS, (4) modes of MCS propagation, (5) factors limiting the lifetime and size of an MCS, (6) feedback of MCSs to larger scales of motion via momentum transport and heating, and (7) the global distribution and impact of MCSs.

2. FUNDAMENTAL ELEMENTS OF MCS STRUCTURE

[5] Figure 1 shows an example of the infrared temperature of the cloud shield of a mature MCS. The area of cloud top temperature $<-70°C$ is approximately the size of the state of Missouri ($\sim 10^5$ km^2 in area). This area of cold cloud exceeds the size of an individual cumulonimbus by 2–3 orders of magnitude. Precipitation and circulations develop on a scale somewhat similar to the cold cloud top in MCSs like this one, thus establishing the MCS as a mesoscale, as opposed to convective-scale or synoptic-scale, phenomenon. The precipitation in an MCS (by definition) is contiguous across a region at least 100 km in dimension. Radar echoes show that the precipitation divides distinctly into a convective and a stratiform region [*Houze*, 1977; *McAnelly and Cotton*, 1989; *Houze et al.*, 1990]. The convective region consists of intense, vertically extending cores, while the stratiform region is of a more uniform (but not perfectly uniform) texture of lighter precipitation (Figure 2). The stratiform precipitation is partly produced by the dissipation of older convective cells and partly produced by broader-sloping mesoscale layer ascent [*Houze et al.*, 1989; *Houze*, 1993; *Yuter and Houze*, 1995a, 1995b; *Houze*, 1997]. The horizontal pattern formed by the areas of convective cells in relation to the stratiform rain varies and is an important indicator of the internal dynamics of the MCS [*Houze et al.*, 1990; *Loehrer and Johnson*, 1995; *Parker and Johnson*, 2000]. The stratiform region has a cloud base in the middle troposphere under the region of ascent owing to a combined effect of layer lifting and the accumulation of older, weakening, and expanding buoyant elements aloft (Figure 3). Below cloud base is a region of net descent, owing to the cooling of mid tropospheric environmental air by melting and evaporation of precipitation particles falling out of the stratiform cloud aloft. Juxtaposed with the stratiform cloud and precipitation are convective cells, with cumulus-scale updrafts extending upward from the boundary layer and precipitation-driven downdrafts in their lower portions. The net effect of this arrangement of convective and stratiform processes is a characteristically different vertical distribution of heating in the convective and stratiform regions. The convective region exhibits net heating at all levels (Figure 4a). The convective-scale downdrafts are insufficient to counteract completely the condensational heating in the convective updrafts. The stratiform region has net heating aloft, where upward air motion and condensation prevail, but cooling in the lower troposphere, where melting and evaporation of precipitation particles prevail. These heating profiles constitute two distinct wavelengths of forcing; the convective heating wavelength is $2H$, while the stratiform wavelength is H, where H represents the depth of the troposphere. These two wavelengths of forcing produce distinct effects on the large-scale environment of the MCS [*Nicholls et al.*, 1991; *Mapes*, 1993; *Mapes and Houze*, 1995]. These modes will be further discussed in sections 7 and 10. Because of the long lifetime of an MCS, solar and infrared radiative heating modify the latent heating profiles. As shown by *Houze* [1982], the radiative heating is concentrated aloft and exaggerates the heating maximum aloft in the stratiform region. The radiative processes thus do not change the basic shapes of the curves in Figure 4. The greater the proportion of stratiform rain produced by an MCS, the more the vertical profile of net heating becomes elevated and intensified. The global implications of the stratiform precipitation fraction will be explored in section 10.

3. UPDRAFTS IN MCSs

3.1. Parcel Lifting

[6] The defining property of a convective cloud is that condensation occurs in nonhydrostatic buoyant upward air

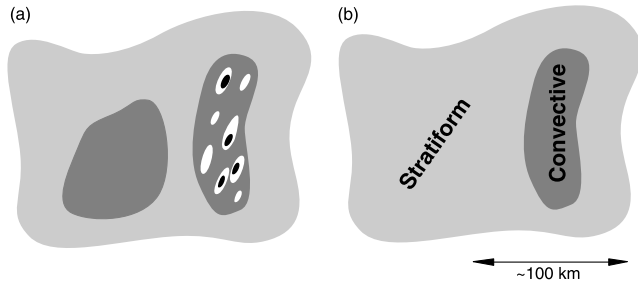

Figure 2. (a) Idealization of a horizontal map of radar reflectivity (b) divided into convective and stratiform regions. From *Houze* [1997].

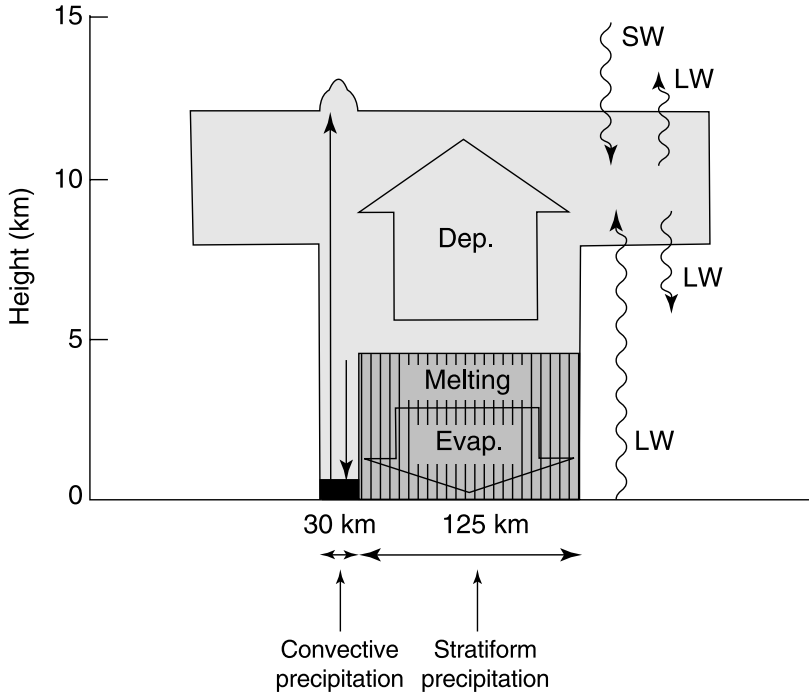

Figure 3. Schematic of a tropical mesoscale convective system in its mature stage. LW and SW indicate long- and short-wave radiation, respectively. Light shading indicates cloud. Vertical lines with medium shading indicate stratiform precipitation. Black indicates convective precipitation. Straight, solid arrows indicate convective updrafts and downdrafts. Wide, open arrows indicate mesoscale ascent and subsidence in the stratiform region, where vapor deposition (Dep.) and evaporation (Evap.) occur. Adapted from *Houze* [1982], courtesy of the Meteorological Society of Japan.

currents. One tradition regards this upward air motion as occurring in the form of bubbles or "parcels" of warm, moist (high equivalent potential temperature θ_e) air originating in the boundary layer, accelerating upward after being forced above the local level of free convection, entraining varying amounts of environmental air via in-cloud turbulence as they rise, then decelerating and eventually stopping and spreading out laterally at or near a level of neutral buoyancy. The parcel view of lifting in convective clouds has inspired conceptual models of convective clouds such as that of *Raymond and Blyth* [1986] (Figure 5). *Riehl and Malkus* [1958] had the parcel view in mind when they postulated that the high-θ_e air characterizing the tropical upper troposphere must arrive there in the form of undiluted air parcels originating in the planetary boundary layer (i.e., the "lucky" parcels in Figure 5). The entraining

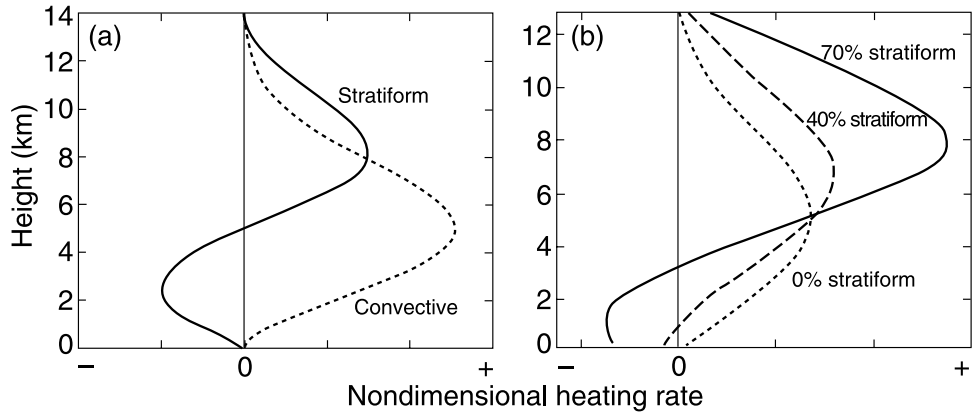

Figure 4. (a) Idealized profiles of net heating associated with convective and stratiform precipitation in a mesoscale convective system. The *x* axis is nondimensional until precipitation amounts are specified for the convective and stratiform regions. (b) Profiles of net heating by a mesoscale convective system with different fractions of stratiform precipitation. Adapted from *Schumacher et al.* [2004].

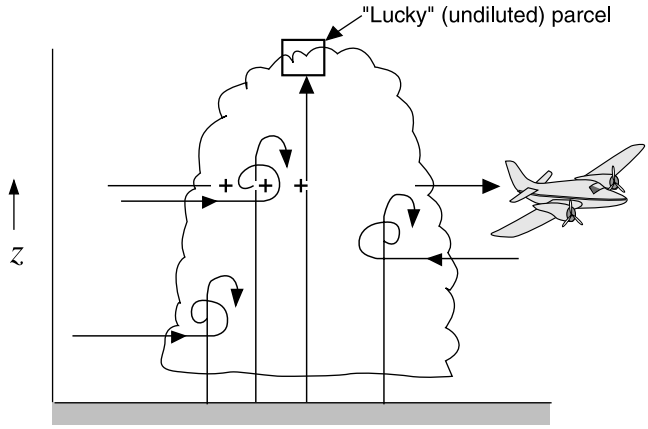

Figure 5. Sketch of a cumulus cloud composed of entraining air parcels. As parcels rise from below cloud base, they may entrain environmental air from some level, lose buoyancy, and decelerate accordingly. "Lucky" parcels experience no entrainment and rise undiluted to the environment's level of zero buoyancy. Reprinted from *Houze* [1993] with permission from Elsevier.

parcel model also serves as the basis of several well-known convective parameterization schemes [e.g., *Ooyama*, 1971; *Yanai et al.*, 1973; *Arakawa and Schubert*, 1974].

3.2. Layer Lifting

[7] Another traditional view considers the upward air motion maintaining a mature MCS to occur in the form of a deep slantwise ascending layer of air. *Ludlam* [1980] reviewed this layer view qualitatively. A series of papers by Moncrieff and colleagues [*Moncrieff and Miller*, 1976; *Moncrieff*, 1978, 1981, 1992; *Thorpe et al.*, 1982; *Crook and Moncrieff*, 1988] (for a synopsis of this work, see *Cotton and Anthes* [1989, pp. 497–505]) have quantified this view for the case of an idealized steady state two-dimensional convective storm. A key assumption of the theory is that the storm may be characterized by a prescribed decrease in hydrostatic pressure across the updraft at middle levels. If the large-scale environment is unstably stratified and sheared, air must flow through the storm along a unique set of streamlines. The geometry of the streamlines is deduced from conservation of entropy, mass, momentum, and vorticity along streamlines. Similar reasoning is employed to determine the streamlines of the downdraft fed by middle level inflow on the rear side of the storm. For a typical environment of strong low level shear the updraft consists of a layer ascending on a slantwise path through the storm (Figure 6).

3.3. Gravity Wave Interpretation of Layer Lifting

[8] Since the Moncrieff theory is for steady state conditions and prescribed environmental stability and shear, it provides no explanation for why the layer inflow and ascent initially develop in an MCS. A physical explanation of the layer inflow to convective updraft regions of MCSs is suggested by the work of *Schmidt and Cotton* [1990] and *Pandya and Durran* [1996]. These studies ran nonlinear high-resolution models and simulated the detailed behavior of a mesoscale system consisting of a squall line and trailing-stratiform region. Then they interpreted the simulation in terms of gravity wave responses to the heating by the MCS. *Pandya and Durran* [1996] averaged the diabatic heating field in the region of the convective line over a 2-hour period (Figure 7a). Then they input the averaged heating field into the model and let the model respond, yielding the horizontal wind field shown in Figure 7b. *Fovell* [2002] performed a similar analysis on a squall line simulation and obtained the result in Figure 8. The fields of horizontal velocity component in Figures 7 and 8 are consistent with a gravity wave response to the mean heating in the convective line. The gravity wave response leads to a 3- to 6-km layer of inflow air entering the convective region, rising and exiting as the middle to upper level front-to-rear flow. This result suggests that the deep-layer inflow occurs once the convective cells have "organized,"

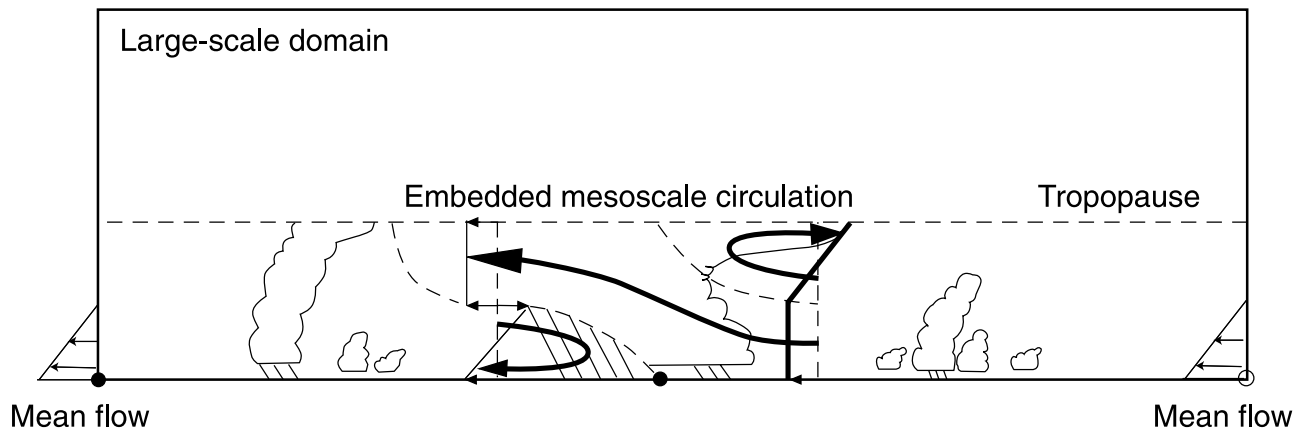

Figure 6. Schematic diagram showing the airflow relative to a two-dimensional, steady state mesoscale convective system in a large-scale environment of given wind shear. The environmental air entering the updraft is potentially unstable, and there is a pressure decrease across the system from right to left at middle levels. The streamlines are those required by conservation of mass, momentum, entropy, and vorticity. Adapted from *Moncrieff* [1992].

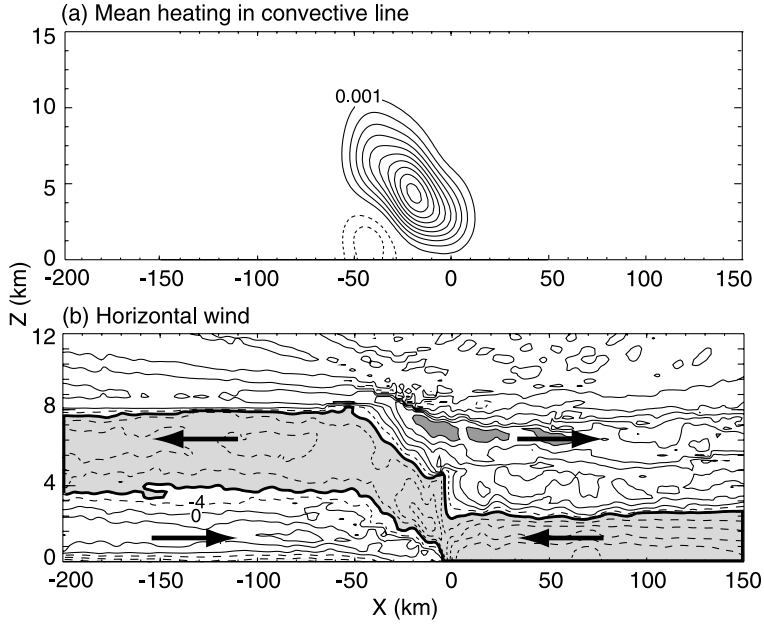

Figure 7. Two-dimensional model simulation results for a leading-line/trailing-stratiform squall line mesoscale convective system (MCS). (a) Time mean thermal forcing meant to represent the forcing from the leading convective line alone. Contour interval is 0.001 K s^{-1}. (b) Horizontal velocity at time t = 6 hours generated by the thermal forcing in Figure 7a. Horizontal velocity contours are at intervals of 4 m s^{-1}. Arrows indicate direction of the horizontal flow. Cold pool forward boundary is at x = 0. Bold contour and shading emphasize layer inflow constituting the layer ascent of air originating ahead of the storm and rising through it. Adapted from *Pandya and Durran* [1996].

that is, clustered into one mesoscale group that constitutes a quasi-steady heat source. A layer of inflow is then drawn up through the system as a gravity wave response to the heating. The middle level inflow from the rear of the system is also part of the pattern. This middle level inflow descends to lower levels and converges with the layer of air entering in the lowest 3 km ahead of the storm. The upper level outflow ahead of the system is also part of the gravity wave response to the mean heating pattern. The deep layer of inflow air entering from ahead and rising over the cold pool in this gravity wave response contrasts sharply with any notion that the updraft air reaching high levels in an MCS must always rise out of the planetary boundary layer where θ_e is highest. Most likely, the deep convection of an incipient and developing system is rooted in the boundary layer in its early stages; then once the storm has reached

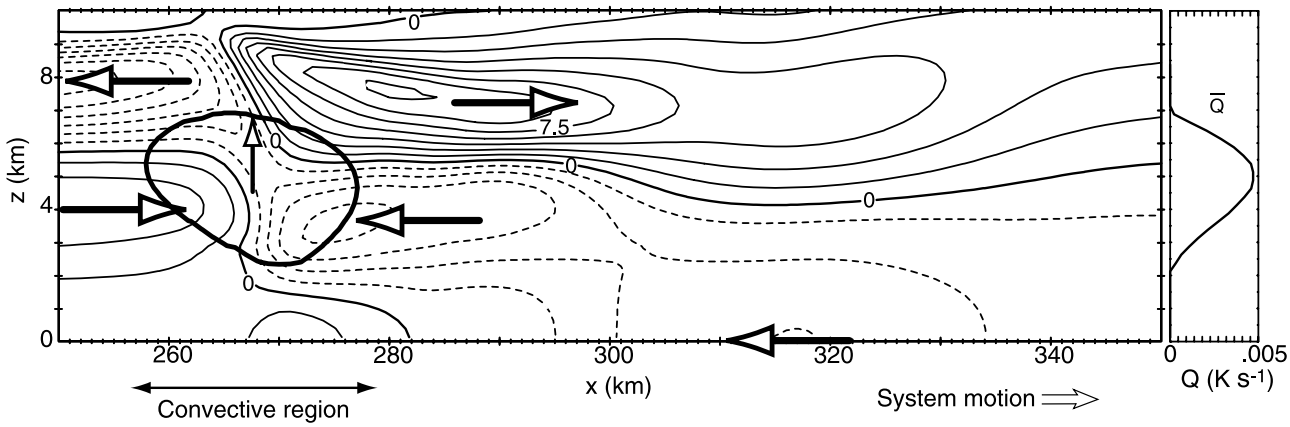

Figure 8. Response to convective region heating in a simulated MCS. The circle outlined by the bold line shows the area in which heating was applied. Contours show the horizontal velocity response to the mean convective region heating profile indicated in the right-hand panel. Contours of perturbation horizontal wind in the plane of the cross section are at intervals of 1.5 m s^{-1}, with dashed contours indicating right-to-left flow in the cross section. Large arrows emphasize direction of motion. Adapted from *Fovell* [2002].

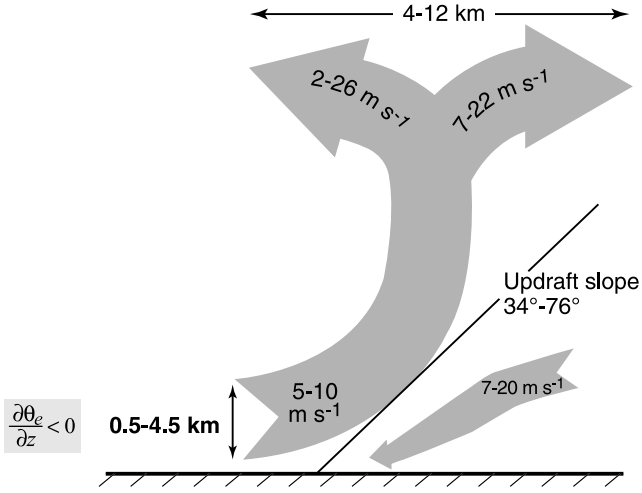

Figure 9. Schematic of airflow in the convective regions of an MCS over the western tropical Pacific as observed by airborne Doppler radar in Tropical Ocean–Global Atmosphere Coupled Ocean-Atmosphere Response Experiment (TOGA COARE). The numbers (from bottom to top) indicate the observed ranges of values of the depth of the inflow layer, horizontal relative velocity of inflow and outflow air currents, the slope of the updraft (angle measured relative to the ocean surface), and the width of the divergent region aloft. The horizontal directional differences of the low level updraft inflow and middle level downdraft inflow were often significantly different from 180°. Based on figures and tables from *Kingsmill and Houze* [1999a].

maturity, an organized convective region forms and constitutes a relatively steady heat source to which the environment must adjust via gravity wave dynamics.

3.4. Stratification Within the Ascending Layer

[9] In the Moncrieff theory (Figure 6) the equivalent potential temperature (θ_e) is conserved along streamlines. The thermodynamic stratification within the updraft layer is therefore the same in the exiting air as in the entering air. Since the air in the rising layer is potentially unstable, small-scale convective cells would be expected to form as soon as the rising layer becomes saturated. Without such a release of instability the highest-θ_e air in the lowermost levels of the rising layer of air has no chance to reach the tropopause. In this sense, the layer ascent model seems at odds with the parcel view, which allows the undiluted parcels to reach the highest levels as the potentially unstable layer overturns [*Riehl and Malkus*, 1958].

[10] Nonetheless, recent studies suggest that the layer lifting mode indeed operates when the layer is potentially unstable. Oceanic tropical convection observed over the west Pacific warm pool in the Tropical Ocean–Global Atmosphere Coupled Ocean-Atmosphere Response Experiment (TOGA COARE) provided an excellent opportunity to document the layer lifting aspects of MCSs. *Kingsmill and Houze* [1999a] examined an enormous set of airborne Doppler data obtained by National Oceanic and Atmospheric Administration (NOAA) aircraft in TOGA COARE. These data included 33 dual-Doppler analyses from 25 different MCS cases as well as countless single Doppler sweeps from the vertically scanning Doppler radars. The schematic in Figure 9 summarizes the results gleaned from airborne Doppler radar flights in and around the convective regions of TOGA COARE MCSs. The updrafts were nearly always slantwise and consisted of finite layers of air rising over an apparent downdraft cold pool. The layer of air composing the sloping updraft ranged from 0.5 to 4.5 km in depth, notably deeper than the planetary boundary layer. This layer of air was potentially unstable ($\partial\theta_e/\partial z < 0$) but, nonetheless, maintained a well-defined layered structure in radar radial velocity data that was consistent with the postulated structure of the Moncrieff model in Figure 6.

[11] *Moncrieff and Klinker* [1997] inferred deep layer inflow into large mesoscale convective systems in TOGA COARE by a rather different approach. They simulated a TOGA COARE case within a global model, which had a resolution of ~80 km (T213). The model parameterized convection and cloud microphysics on the grid scale and resolved very large cloud clusters. Despite the coarse resolution, mesoscale convective systems formed in the model and exhibited realistic features such as the curved region of convective ascent and the mesoscale rear inflow under a broad anvil (Figure 10). One of the simulated features was a deep layer of inflow from ahead of the cloud system. Moncrieff and Klinker were concerned that the system might have been the result of aliasing smaller systems onto a large model-resolvable scale. However, systems of the size of that in Figure 10 were indeed observed during TOGA COARE [e.g., see *Chen et al.*, 1996, Figure 12]. Although MCSs of this extreme size can occur and may sometimes be resolved by general circulation models (GCMs), there are likely many other situations in which smaller MCSs are aliased upscale in GCMs. Climate models likely miss MCSs altogether and fall back on parcel-based parameterizations of convection.

[12] *Bryan and Fritsch* [2000] examined the behavior of layer ascent of unstable air in several midlatitude MCSs. They analyzed radar and sounding data and ran a numerical model to simulate the observed cases. Their results are summarized in Figure 11. Both soundings and the model showed a deep (several kilometers thick) layer of inflow into the convective region of the MCS. As in the TOGA COARE MCSs the layer of air composing the sloping layered updraft was potentially unstable but, nonetheless, retained a coherent layer structure as it ascended. *Bryan and Fritsch* [2000] referred to this phenomenon as a "moist absolutely unstable layer (or MAUL)." The question raised by this result as well as by the Moncrieff theory (Figure 6) is the following: How does a layer of potentially unstable air retain the structure of a coherent rising layer of air after the layer becomes saturated?

3.5. Overturning Within the Layer of Ascent

[13] One possibility is that the absolute instability created when the layer saturates allows for overturning within the layer but the overturning does not completely break the flow

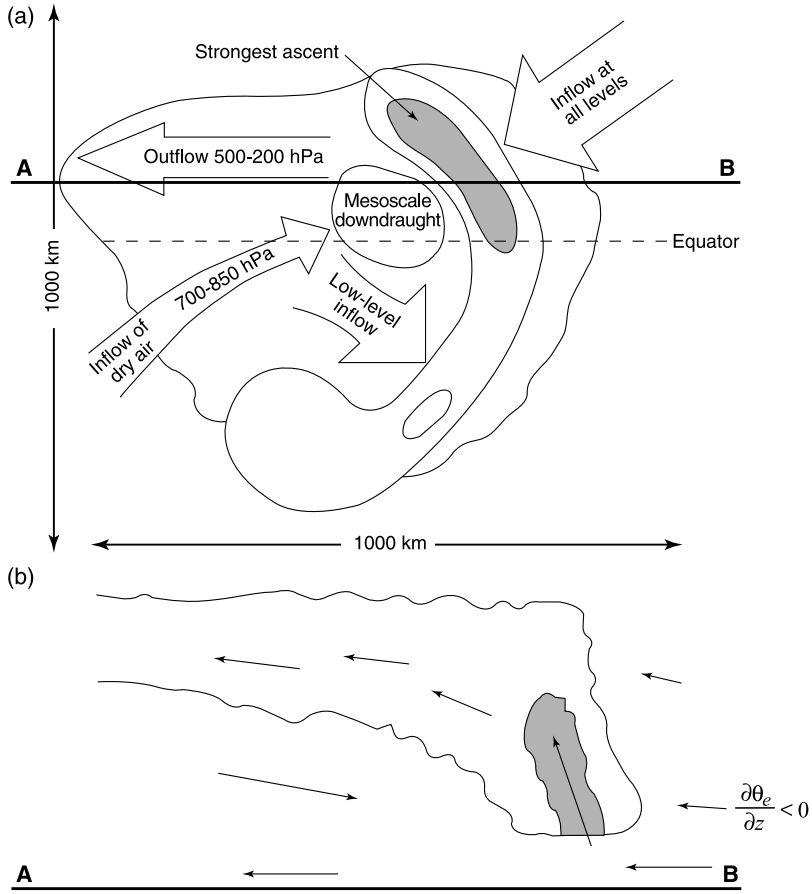

Figure 10. Conceptual model of a supercluster, which is a large mesoscale convective system of the type that occurs over the western tropical Pacific. (a) Plan view and (b) zonal vertical cross section along line AB. Note the depth of the inflow layer at B. From *Moncrieff and Klinker* [1997].

down such that the layer loses its coherence in the air motion field. Some evidence to this effect was found by *Mechem et al.* [2002]. They further examined TOGA COARE MCSs by numerical modeling and confirmed the layer inflow and ascent of potentially unstable air into these tropical oceanic convective systems. Figure 12 shows trajectories into the leading convective region of a simulated TOGA COARE MCS. The trajectories show layer lifting, in that all the trajectories originating in a 6-km-deep layer ahead of the system ascend (Figure 12b). However, the vertical projections of trajectories in Figure 12b show further that the air overturned within the layer. Inflow air originally at the bottom of the ascending layer ends up at the top of the layer (note how the yellow and purple trajectories cross during the ascent). In this regard the realistic trajectories in the inflow layer do not remain vertically in the same relative positions as they do in the Moncrieff idealization but rather exchange vertical positions within the confines of the rising layer. The Mechem et al. trajectories suggest that some sort of mixing process occurs to reverse the vertical profile of θ_e within the ascending layer even while the layer maintains a coherent structure. Three-dimensionality apparently is required for this overturning of the θ_e profile, and horizontal projections of the trajectories do show that the model trajectories spread out laterally (Figure 12c). It is possible that mixing also occurs on the subgrid scale. The model used to calculate the trajectories parameterized the subgrid-scale mixing, so whatever this process is cannot easily be determined from the model trajectories.

[14] *Zipser* [1977] suggested a way of thinking about the smaller-scale mixing in the updraft by blending parcel thinking with the layer model. He postulated a conceptual model (Figure 13), in which environmental air approaches the convective region of the MCS with Moncrieff-type ascending-layer trajectories (the ambient subcloud and cloud layer air in Figure 13), but when the air in the ascending layer saturates, parcel processes become active within a ''crossover zone.'' Parcels arriving in the crossover zone from the subcloud levels may entrain air arriving in the zone with lower θ_e (i.e., from the upper part of the ambient cloud layer). A buoyant parcel in the crossover zone will rise to a height corresponding to the θ_e, determined by the amount of entrainment experienced by the parcel. A set of such parcels occurring with random degrees of entrainment would allow air to rise to various levels of zero buoyancy where it would continue down shear on a more horizontal trajectory. The parcel processes envisaged to occur in the crossover zone thus constitute a mechanism allowing for the layer

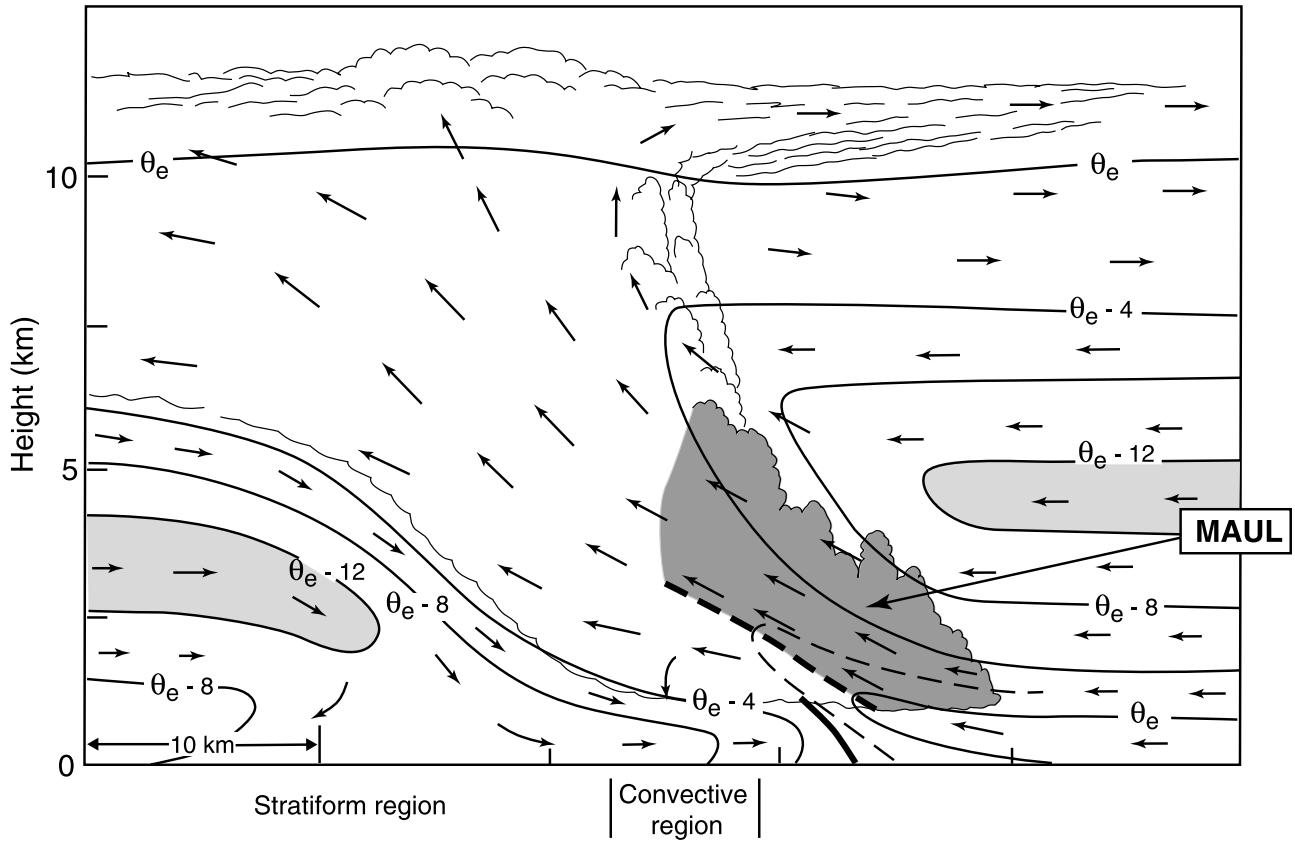

Figure 11. Idealized cross section through slab convective overturning. Flow vectors are system-relative, scalloped lines indicate cloud boundaries, solid lines are θ_e contours every 4 K (thin dashed line is an intermediate contour, and bold dashed line marks axis of highest values), bold solid line indicates outflow boundary or frontal zone, light shading highlights middle level layer of low-θ_e air, and dark shading depicts the moist absolutely unstable layer (MAUL). Adapted from *Bryan and Fritsch* [2000].

of ascent to neutralize its θ_e profile by the time it reaches the upper levels of the organized MCS.

[15] A further detail of Zipser's conceptual model is that air entering the convective region of the MCS from middle levels has such low θ_e that it must sink. The cellular aspect of the ascent layer implied by the crossover zone idea allows passageways for this extremely low-θ_e air to filter through the line and sink. *Rotunno et al.* [1988] show further that the temporal pulsing of a line of convection produces windows of time in which the low-θ_e air can pass across it.

3.6. Nature of Cells Embedded in the Deep Layer of Ascent

[16] Since *Zipser*'s [1977] crossover zone paper several conceptual models have been proposed to describe the small-scale cellular structure embodied within the deep layer of ascent of an MCS, especially those exhibiting the leading-line/trailing-stratiform squall structure. In broad outline the conceptual model of *Houze et al.* [1989] (Figure 14) has the mean flow attributes of the Moncrieff layer-overturning model (compare Figures 6 and 14). However, the convective region shows an embedded cellular structure, designed to be consistent with the typical radar echo structure of a leading-line/trailing-stratiform MCS. The postulated cellular structure suggests that the layer of front-to-rear ascent contains flow perturbations to account for a sequence of precipitation cells (new, mature, and old) similar to that postulated by *Browning et al.* [1976] for multicellular hailstorms. These cells are imagined to trigger as the lower tropospheric layer of potentially unstable air feeding the convective region becomes saturated and hence absolutely unstable. The postulated cells mix the entering environmental inflow layer vertically before it reemerges as the ascending front-to-rear flow.

[17] *Yuter and Houze* [1995b] suggested that the individual convective cells developing in response to the instability of the layer of upward ascent act as "particle fountains" to distribute precipitation particles throughout the MCS (Figure 15). Each particle fountain is a manifestation of gravity sorting of the precipitation particles growing in a small-scale intense updraft core. The heavier rain and graupel particles fall out directly downward from the updraft to form the reflectivity cores identified as "cells" on radar. Meanwhile, the more moderately sized ice particles are spread by the expanding buoyant parcels over a wider area, and they form the raw material of the stratiform cloud deck that becomes thick and persistent in the MCS. Buoyant

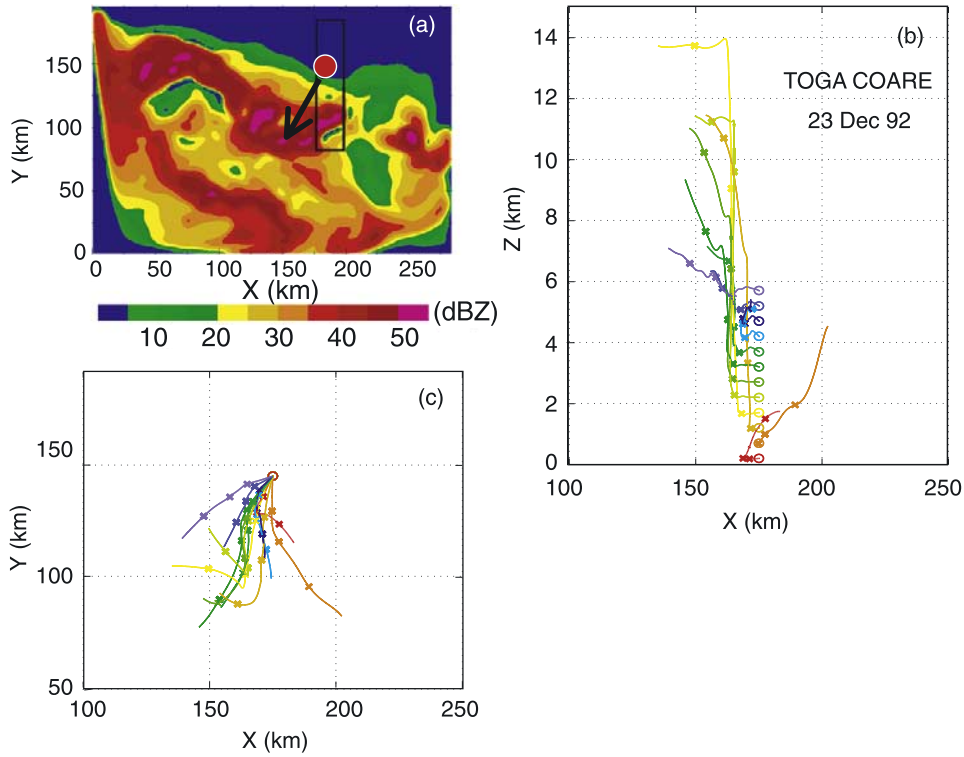

Figure 12. (a) Model-simulated reflectivity (dBZ) for an MCS over the western tropical Pacific. The box in Figure 12a indicates the horizontal span of the initial tracer distribution used in trajectory calculations. Twelve trajectories were calculated over 3.5 hours of model time. Initial tracer locations are located 500 m apart in a vertical column. Initial location is marked by the small circle. Arrow indicates general direction of low level flow. (b) Projection of the trajectory paths onto the *x*-*z* (west-east) vertical plane and (c) projection onto the *x*-*y* (horizontal) plane. Origins are indicated by circles; hourly positions are shown by crosses. Adapted from *Mechem et al.* [2002].

parcels spread the ice particles over a broader area as they expand laterally by simple pressure decrease with height. In addition, the ascending front-to-rear layer spreads the influence of the particle fountains by advecting them into the stratiform region. *Fritsch and Forbes* [2001] emphasized that the slantwise layer lifting was a key component promoting the broad saturated upper cloud region of MCSs and MCCs. The net result is that ice particles formed in the small-scale rising parcels embedded within the broader ascending layer seed the ascending layer flow so that a widespread deep stratiform cloud deck can develop. The lateral spreading of updraft trajectories seen in Figure 12c also contributes to the expansion of the zone influenced by the particle fountains in the upper levels of the stratiform region of the MCS.

[18] The dynamical mechanism of the embedded cellular structure has been examined by numerical modeling. *Yang and Houze* [1995a] suggested that the embedded cells within the ascent layer are triggered at the nose of the cold pool and then propagate rearward as trapped gravity waves (Figure 16). This process requires the deep inflow layer to become stabilized soon after it ascends over the gust front in order for the layer to support gravity wave motion. The results of *Pandya and Durran* [1996, Figure 3] suggest that the ascent layer is, indeed, essentially stable for most of its course through the MCS. *Fovell and Tan* [1998], however, argue that the cells moving back from the nose of the cold pool are buoyant elements (Figure 17a). The buoyant parcel (shaded ellipse in Figure 17b) has a circulation produced by the buoyancy pressure gradient force [*Houze*, 1993, p. 225]. The wind in the mean layer of ascent advects the buoyancy element and its pressure gradient–driven circulation rearward over the cold pool, where it becomes cut off from the cold pool nose as its circulation entrains prestorm environment air into the wake of the buoyant cell (Figure 17c). *Fovell and Tan* [1998] find that eventually the buoyant element takes on the properties of a trapped gravity wave, though not as quickly as suggested by *Yang and Houze* [1995a]. As it moves rearward, the overturning circulation of the cell, whether it is a gravity wave or buoyant element, disperses hydrometeors as a particle fountain (Figure 15).

[19] *Bryan and Fritsch* [2003] have recently used a numerical model with extremely high resolution to show that the cells may have a lateral component of circulation in which the buoyancy elements overturn in rolls aligned along the shear within the overturning layer. Figure 18 indicates the geometry of the rolls. These elongated cells would appear to explain the common observation of cigar-shaped cells oriented at an oblique angle to the line of cells in squall line

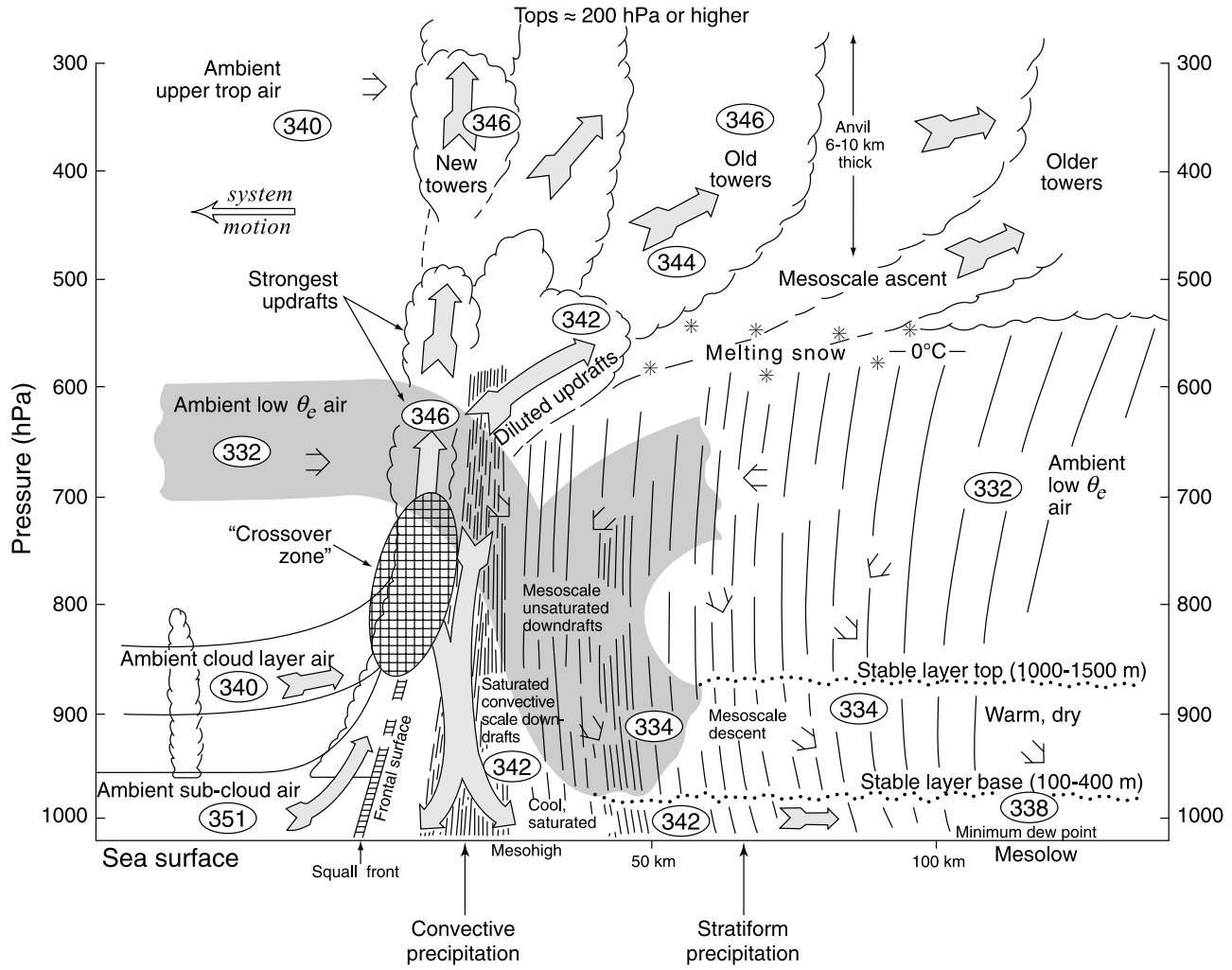

Figure 13. Idealization of a tropical oceanic mesoscale convective system with leading-line/trailing-stratiform structure. Parcels of subcloud boundary layer air rise and form the basic convective updrafts. Ambient cloud layer air is entrained into the updrafts. The updraft parcels rise till they lose their buoyancy by entrainment or by encountering a stable layer in the environment. Entrainment of ambient low-θ_e air weakens updrafts and forms convective-scale downdrafts, which sink to the surface in the convective precipitation zone. Note that the system has three-dimensionality such that the updraft and downdraft trajectories are not collocated, and the convective region contains a "crossover zone" where convective-scale updrafts and downdrafts coexist. Adapted from *Zipser* [1977].

MCSs [*Ligda*, 1956; *Houze et al.*, 1990]. (Look ahead to Figure 23 to see a schematic of this typical cell geometry.)

4. MIDDLE LEVEL INFLOW INTO MCS DOWNDRAFTS

[20] The leading-line/trailing-stratiform type of MCS typically exhibits "rear inflow," which is a layer of low-θ_e air that enters the MCS from the rear below the trailing anvil cloud of the stratiform region and descends toward the leading convective line (Figure 14). The descent is gradual across the stratiform region but often takes a sudden plunge downward as it approaches the immediate rear of a region of active convective cells.

[21] A common assumption is that the descending rear inflow is "driven" by thermodynamic processes, namely, cooling by sublimation, melting, and evaporation of precipitation particles falling from the trailing-stratiform cloud layer of the squall line MCS. However, the proximate cause of the rear inflow is likely dynamic. *Schmidt and Cotton* [1990] performed numerical simulations of a squall line MCS and identified gravity waves responding to the heating in the convective line. They argued that when these waves occurred in a sheared environment, rearward gravity wave propagation at upper levels altered the wind structure at upper levels so as to produce a channel of rear inflow. This view seems consistent with the more general results of *Pandya and Durran* [1996], who showed that the middle level inflow is an integral part of the overall gravity wave response to the mean heating in the convective region (Figure 7).

[22] While likely not the proximate case of the rear inflow, microphysical feedbacks can strengthen the middle

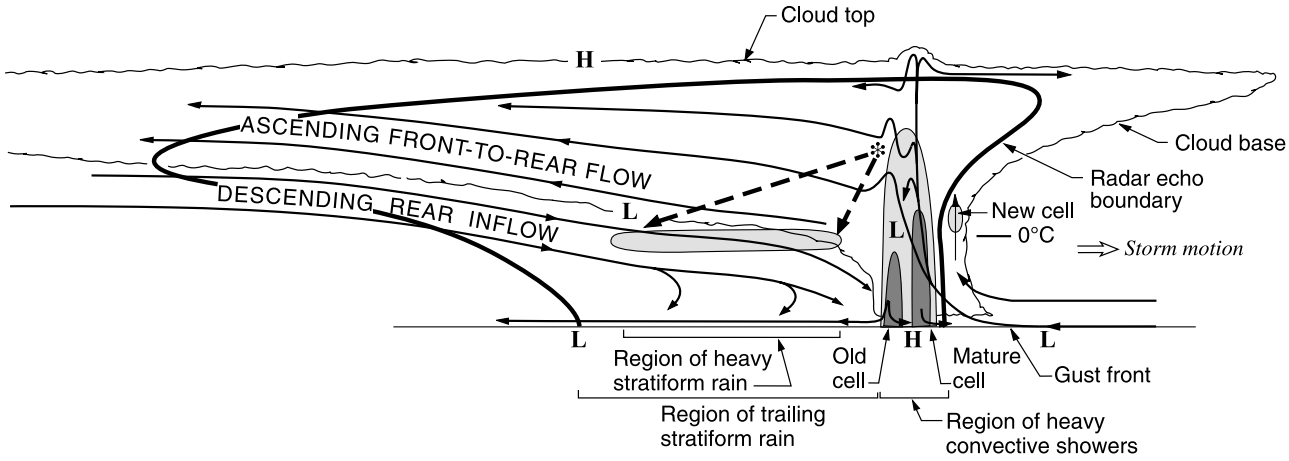

Figure 14. Conceptual model of the kinematic, microphysical, and radar echo structure of a convective line with trailing-stratiform precipitation viewed in a vertical cross section oriented perpendicular to the convective line (and generally parallel to its motion). Intermediate and strong radar reflectivity is indicated by medium and dark shading, respectively. H and L indicate centers of positive and negative pressure perturbations, respectively. Dashed-line arrows indicate fallout trajectories of ice particles passing through the melting layer. From *Houze et al.* [1989].

level inflow and force it to descend. *Zipser* [1969] and *Leary* [1980] estimated the rate of rain evaporation below the melting level. *Leary and Houze* [1979] analyzed and computed the rate of the cooling by melting within the bright band layer. The cooling rates were found to be substantial and widespread enough to affect the mesoscale rate of descent in the stratiform region. A frequent assumption is that the melting initiates the descent. However, *Braun and Houze* [1997] used modeling to document the effects of sublimation just below the trailing-stratiform cloud of a midlatitude squall line MCS and found that the sinking started with sublimation when the environmental middle level inflow first went under the trailing-stratiform cloud deck before the inflow descended to the melting layer. This conclusion is consistent with the earlier finding of *Gamache and Houze* [1982] that the mesoscale downdraft in a tropical Atlantic MCS appeared to start above the melting level. In another model simulation, *Yang and Houze* [1995b] isolated the two-dimensional rear inflow induced by the system itself. They found that evaporation, melting, and sublimation in the stratiform region all contributed substantially to the evolution and strength of the rear inflow (as suggested by *Smull and Houze* [1987] and *Lafore and Moncrieff* [1989]) but that these effects alone could not produce the strength of middle level rear inflow observed in the strongest rear inflow cases.

[23] *Smull and Houze* [1987] documented several cases of rear inflow and presented evidence that while middle level rear inflow was ubiquitous in leading-line/trailing-stratiform systems, often it was weak. *Chong et al.* [1987] and *Klimowski* [1994] have analyzed Doppler radar data in strong squall line systems that had weak rear inflow. Both studies found that this weaker rear inflow developed over time as the system matured. While an MCS (particularly an idealized two-dimensional squall line MCS) can develop its own rear inflow, it has difficulty developing strong rear inflow. *Skamarock et al.* [1994] showed that the rear inflow could be strengthened when vortices induced at the ends of the line reinforced the rear inflow toward the center of the line. *Zhang and Gao* [1989] showed that the rear inflow could be much stronger if aided by the large-scale environmental flow (for further discussion of this point, see *Houze* [1993, section 9.2.3.6]).

[24] In summary, the middle level rear-to-front flow of a leading-line/trailing-stratiform type of MCS appears, at the most fundamental level, to be a gravity wave response to heating in the convective line. Sublimation, melting, and evaporation of precipitation particles encourage the middle level inflow to descend when it comes under the trailing-stratiform cloud deck. However, processes deriving directly from the storm itself do not appear to account for the strength of some observed rear inflows. For the stronger rear inflows the squall line must have line end vortices, or it must occur in an environment that strongly feeds middle level air into the rear of the leading-line/trailing-stratiform system.

[25] As noted in section 2, the structure of the precipitation within an MCS does not always take the form of a leading line with a trailing-stratiform region. *McAnelly and Cotton* [1989] commented on the diversity of patterns formed by the convective and stratiform regions. *Houze et al.* [1990] identified a spectrum of MCS internal structure, with about one third of Oklahoma MCSs bearing no structural similarity to the leading-line/trailing-stratiform archetype. *Rickenbach and Rutledge* [1998] found a variety of linear and nonlinear structures in MCSs over the tropical Pacific. Sometimes a dominant line of convection is hard to identify, or lines of various orientations appear and disappear intermittently. It is important to examine the concept of

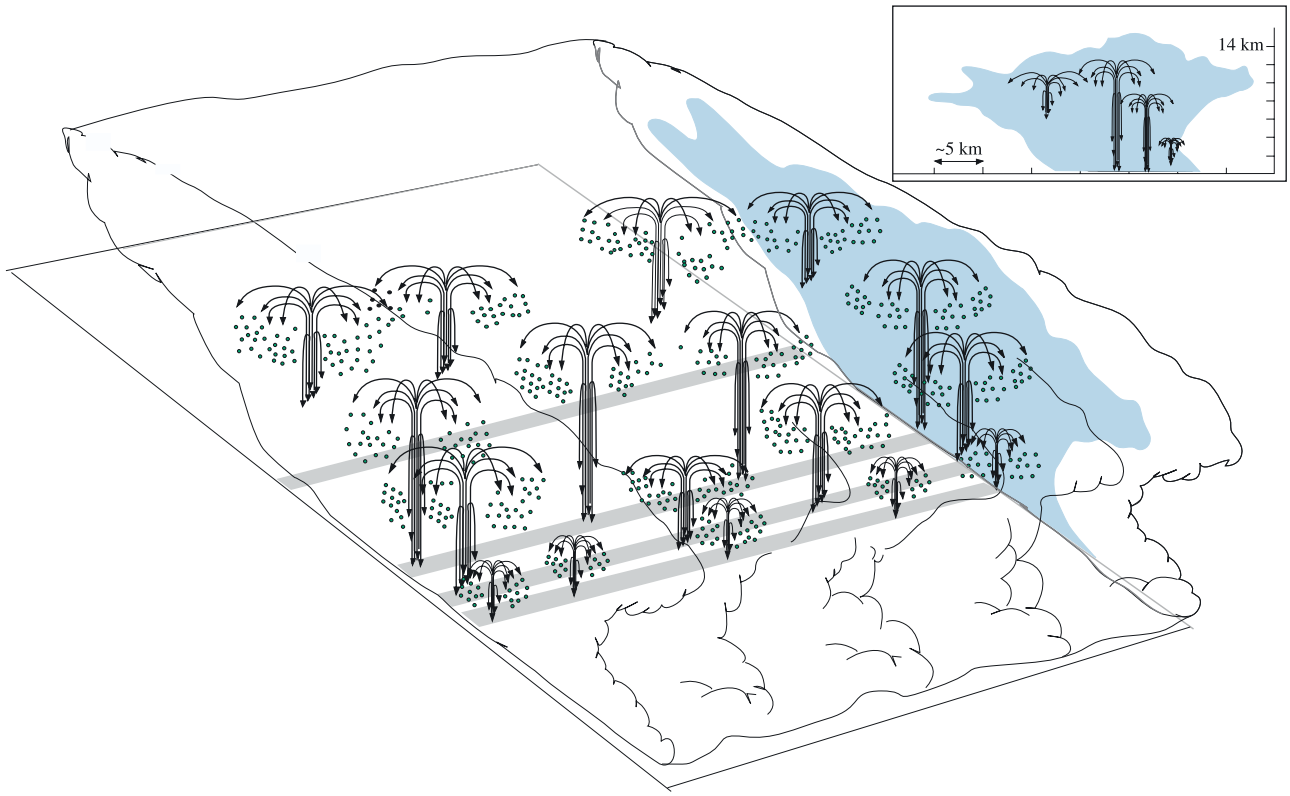

Figure 15. Conceptual model of an ensemble of particle fountains in a multicellular MCS. Shaded area represents radar reflectivity along a cross section perpendicular to the convective region. Cloud boundary is indicated by the scalloped outline. Inset shows approximate scales and arrangement of the largest particle fountains relative to the radar echo. From *Yuter and Houze* [1995b].

middle level inflow to an MCS in the more general context of the full variety of observed three-dimensional MCS structures, of which leading-line/trailing-stratiform systems are only one characteristic structure.

[26] Without a dominant, moving, leading convective line the concept of rear inflow becomes vague, since the system as a whole does not have particularly well-defined front and rear sides. However, even when clear leading-line/trailing-stratiform structure is absent, strong middle level inflow occurs. *Kingsmill and Houze* [1999a] analyzed airborne Doppler radar data obtained in 25 aircraft missions in and around the stratiform regions of mesoscale convective systems over the west Pacific warm pool during TOGA COARE. They found that the middle level inflow was well defined in both single- and dual-Doppler radar data. The flow into the stratiform regions was generally strong, and the direction of the inflow was evidently determined by the direction of the middle level large-scale environmental flow relative to the storm (Figure 19).

[27] In significant ways the middle level inflows examined by *Kingsmill and Houze* [1999a] resembled the rear inflow of two-dimensional squall line MCSs in that they were sandwiched between distinct flows at lower and upper levels and sloped downward as they extended into the stratiform region. The flow typically entered the stratiform precipitation region at the 4- to 7-km level, in the "anvil" region, where the stratiform echo was located aloft but not reaching the surface. As the flow penetrated farther into the stratiform region, where echo extended down to the sea surface, it crossed the radar bright band (associated with the melting level) and continued down into the rain layer. This sequence suggests that the middle level inflow feeds the mesoscale downdraft as a result of cooling by sublimation of snow below the anvil on the outer perimeter of the system, melting ice particles in the bright band layer, and evaporation of rain below (just as in the squall line–type of MCS described above). Since these microphysical-thermodynamic processes determine only the vertical component of motion (i.e., the subsidence), the horizontal direction of the middle level airflow supplying the mesoscale downdraft must be determined by other factors.

[28] Although the middle level inflows in MCSs of the type examined by *Kingsmill and Houze* [1999a] resembled the "rear inflow" seen in squall lines, and were likely driven downward by the same microphysical-thermodynamic processes, they do not necessarily enter from the trailing side of the system. Indeed, a nonsquall MCS may have no well-defined front or rear side. Rather the direction from which the middle level inflow enters appears to be determined to a large extent by the flow in the large-scale environment. Figure 20 shows the observed relationship of the middle level inflow to the environmental wind in the cases analyzed by *Kingsmill and Houze* [1999a]. Earth-relative wind was used in these plots because mesoscale system motion was

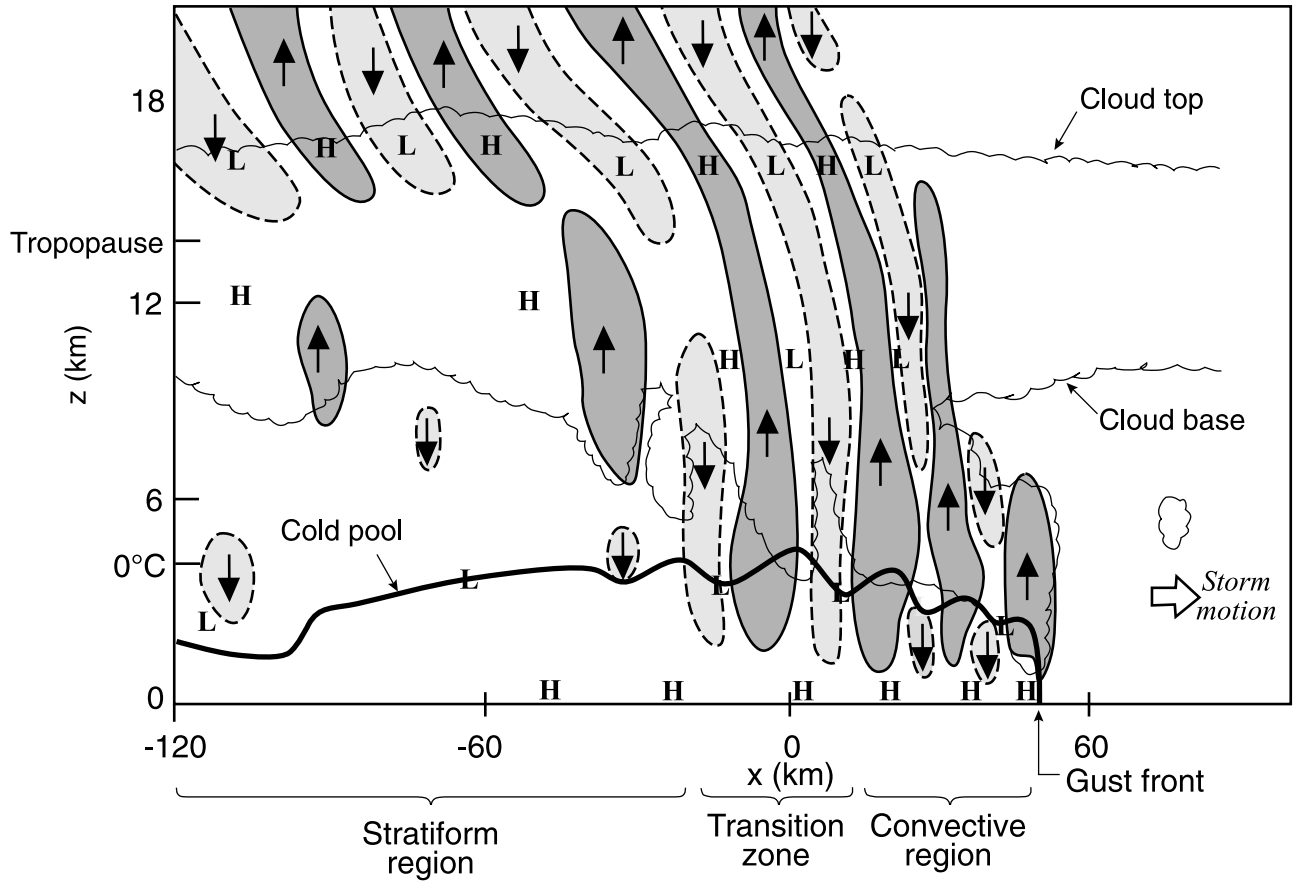

Figure 16. Schematic model of the gravity wave structure of a simulated multicellular MCS at a mature stage of development. Updrafts >1 m s^{-1} are heavily shaded. Downdrafts <−1 m s^{-1} are lightly shaded. Bold line is the cold pool outline defined by the −1 K potential temperature perturbation. Cloud outline is for the 0.5 g kg^{-1} contour of nonprecipitating hydrometeor mixing ratio. L and H indicate centers of low and high perturbation pressure, respectively. From *Yang and Houze* [1995a].

difficult to determine from the aircraft radar data owing to the limited sampling time, complex structures, and discrete modes of propagation. Generally, the cells and larger mesoscale systems moved slowly. Motions relative to embedded convective cells were determined but not shown here because they lead to conclusions consistent with those determined in the Earth-relative frame. The plots in Figures 20a–20d show statistics of the directional difference between the environmental wind and inflow velocity at four different levels. The middle level inflows come from all directions. However, there was a tendency for directional differences between the radar-observed inflow velocity and the environmental winds to be minimized at the 400- to 500-hPa level (Figures 20b and 20c), which coincides with the height of the stratiform region inflow. The distribution of the directional differences at 400–500 hPa is negatively skewed, suggesting that the large-scale winds at these levels turned clockwise (in most cases cyclonically) as they entered the stratiform inflows. In addition, the maximum values of middle level inflow wind within the storm were generally greater than the large-scale environmental wind speed, as is evident from the high frequency of magnitude ratios <1 in Figures 20e–20h. These results suggest that horizontal pressure gradients within the stratiform precipitation were accelerating the large-scale winds as they penetrated the system (as proposed by *Smull and Houze* [1987] for cases of "rear inflow").

[29] From these studies it appears that "rear inflow" behind squall lines may be a particularly clear example of the more general phenomenon of middle level inflow into a stratiform region of an MCS. Any well-defined MCS is likely to have a stratiform rain area made up of material produced earlier in active convective cells and either left behind or advected from those cells [*Houze*, 1993, 1997]. The snow, melting snow, and rain falling in the stratiform region cool the inflow and cause it to sink gradually over the breadth of the stratiform region. The air on which these processes act enters the MCS from whatever direction the large-scale ambient flow dictates.

5. MIDDLE LEVEL MESOSCALE VORTICES

[30] One implication of the vertical structure of heating in an MCS (Figure 4) is that a vortex tends to form in middle levels at the base of the stratiform cloud (Figure 21). The formation of a mesoscale vortex in the stratiform region of an MCS was first noticed in the tropics [e.g., *Houze*, 1977; *Gamache and Houze*, 1982]. However, it is even more

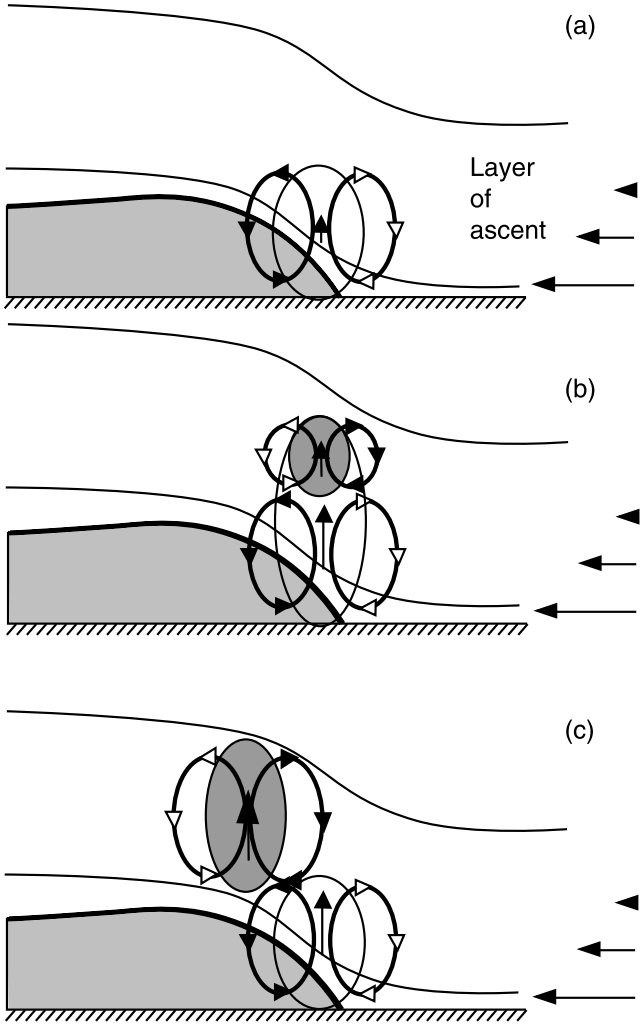

Figure 17. Interpretation of an updraft cell (open oval) in the convective region of an MCS as a buoyancy element. (a) Circulation tendency at the nose of the cold pool (shaded). (b) Positively buoyant region (shaded oval) with associated circulation tendency forced by the perturbation pressure field. (c) Same as Figure 17b but at a later time. Adapted from *Fovell and Tan* [1998].

prominent in midlatitude MCSs. In a case study of synoptic and satellite data, *Menard and Fritsch* [1989] and *Zhang and Fritsch* [1988] in a modeling study pointed out that an MCC can develop a middle level mesoscale vortex in its mature and later stages. *Cotton et al.* [1989] found middle level positive relative vorticity in a composite analysis of MCCs. This feature is now called a "mesoscale convective vortex" or MCV. *Bartels and Maddox* [1991] compiled a satellite-based climatology of MCVs over the United States by identifying spiral-banded structures in the visible satellite images of the middle level cloud remains of old MCSs. Associating the observed MCVs with sounding data, they found that the MCVs were favored by weak flow, weak vertical shear, weak background relative vorticity, and strong gradients of humidity. They further concluded that the MCVs could be explained by the stretching term of the vorticity equation.

[31] *Menard and Fritsch* [1989] and *Cotton et al.* [1989] suggested that this middle level vortex could become inertially stable. Thus energy would be retained by the system that otherwise would propagate away in the large-scale environment's gravity wave response to the convective disturbance. The stable mesoscale vortex, according to this reasoning, would be supported by a secondary (vertical-radial) circulation and therefore have a built-in mechanism for supporting continued release of potential instability in air drawn into and upward through the system.

[32] The middle level vortex forms in the stratiform region of an MCS at the level of maximum convergence (Figure 4). In midlatitudes the Coriolis force accentuates the development of MCVs. *Fortune et al.* [1992] suggested the MCV in midlatitude storms might have a baroclinic character analogous to a larger-scale frontal cyclone. However, model simulations carried out later have indicated a fluid dynamical explanation for MCV formation in a leading-line/trailing-stratiform MCS and a more specific role of the Coriolis force. *Skamarock et al.* [1994] showed that trailing "bookend" vortices form on each end of the squall line and that a midlatitude cyclonic MCV can develop from the bookend vortex favored by the Coriolis force (Figure 22). This type of development leads to a distortion of the trailing-stratiform precipitation region, where the stratiform region is biased toward the poleward end of the line (Figure 23b). The stratiform region behind the poleward end of the line is advected rearward by the cyclonic flow, while dry air is advected toward the central and equatorward ends of the line. It takes several hours for the Coriolis force to act and form the asymmetric structure. The echo structure in the earlier

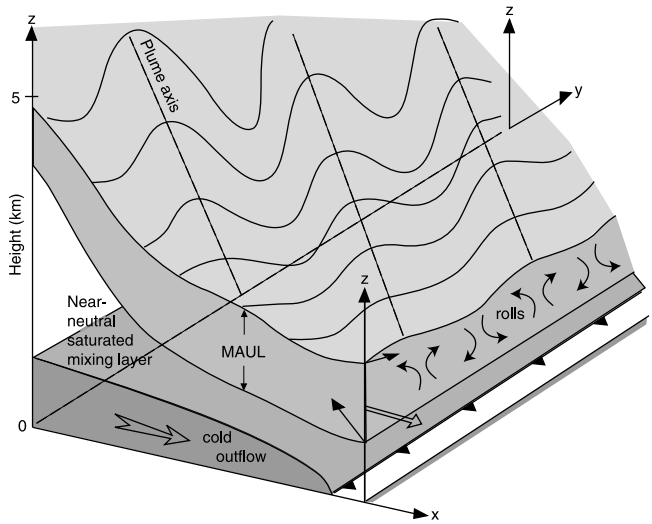

Figure 18. Schematic of rolls in the convective region of an MCS. Bold solid arrows at the top and bottom of the MAUL indicate the ground-relative wind flow. The double-line arrow indicates the shear vector. In this schematic the plumes axes are not perpendicular to the surface gust front (as they are in the numerical simulation). Note the shear vector may not be perpendicular to the gust front. From *Bryan and Fritsch* [2003].

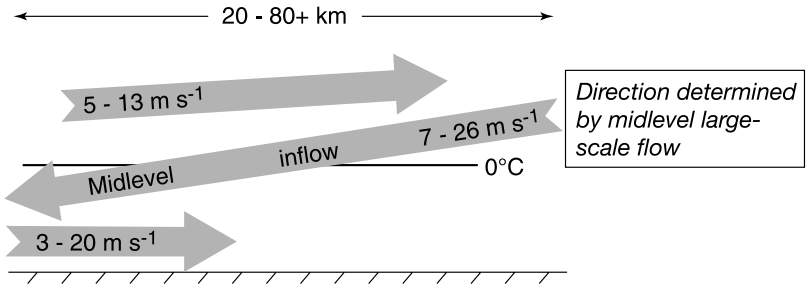

Figure 19. Schematic of airflow in the stratiform regions of a mesoscale convective system over the western tropical Pacific as observed by airborne Doppler radar in TOGA COARE. The numbers indicate the observed ranges of values of the horizontal relative wind velocity and the horizontal scale of the middle level inflow. Based on figures and tables of *Kingsmill and Houze* [1999a].

stages of the MCS tends to be symmetric, with the stratiform region more or less centered behind the convective line (Figure 23a).

[33] *Parker and Johnson* [2000] further examined the symmetric and asymmetric paradigms of MCS structure identified by *Houze et al.* [1990]. They used radar data over the central United States to track 88 MCSs and analyzed how the echo structure evolved in each case. They determined that the spatial arrangement of the stratiform precipitation relative to the convective line on radar was a function of the life cycle stage of the MCS and that several variations on the structural paradigms could occur (Figure 24). The most common life cycle scenario (trajectory 1 in Figure 24) sees an initial line of convective cells develop a stratiform region first in a symmetric juxtaposition with the line and then evolving into an asymmetric form. Evidently, the system became more asymmetric as the Coriolis force had longer to act. The second most common evolution (trajectory 2 in Figure 24) had the only stratiform precipitation forming on the northeast end of the convective line, as old cells weakened and new ones formed on the southwest end of the line. After time went by, it too took on an asymmetric form, with the stratiform precipitation on the northern end of the line being swirled around to the rear of the system. The third most common pattern of echo development (trajectory 3 in Figure 24) showed stratiform precipitation developing ahead of the convective line, a system behavior also seen by *Houze and Rappaport* [1984] also in a tropical case.

[34] While the Coriolis force accentuates MCV development in midlatitudes, especially in asymmetric squall lines, the development of a mesoscale middle level vortex in the stratiform region also occurs in squall systems at tropical latitudes [e.g., *Gamache and Houze* 1982]. The effect is not, however, strong enough to generate asymmetric squall line structures as seen in midlatitudes.

[35] *Bosart and Sanders* [1981] found that the long-lived, self-regenerating MCS that produced the famous Johnstown, Pennsylvania, flood was characterized by a middle level cyclonic vortex detectable by the synoptic sounding network. *Knievel and Johnson* [2002, 2003] have used profiler data from a mesonetwork to describe an MCV. Their vorticity budget indicates that the middle level vortex is made up both of vorticity advected in from the environment and generated by the MCS perturbation itself. *Bosart and Sanders* [1981] postulated that within and near the MCS the vertical circulation of the evidently balanced or quasi-balanced circulation was responsible for the regeneration of the convection.

[36] *Raymond and Jiang* [1990] provided a theoretical framework for such a circulation associated with a heating anomaly of the type associated with an MCS. They suggested that an environment of weak middle level shear but stronger low level shear (as observed in MCV environments [*Bartels and Maddox*, 1991]) could support a mesoscale rotational circulation in an MCS. The postulated circulation consisted of a warm core vortex characterized by a positive potential vorticity anomaly (i.e., MCV) in middle levels beneath a negative potential vorticity anomaly at upper levels. The idealized MCV overlays a cold pool, presumably formed by precipitation evaporation and melting associated with the MCS. Using a numerical model, *Chen and Frank* [1993] found MCV formation consistent with the theory of *Raymond and Jiang* [1990]. Their result is depicted in Figure 21. The middle level vortex forms in the stratiform region of the MCS. As the stratiform cloud develops, air in middle-to-upper levels saturates over the mesoscale breadth of the storm. The saturation causes the Rossby radius of deformation to become smaller since the buoyancy frequency is determined by the moist static stability rather than the dry static stability, and the stratiform cloud deck is made up of buoyant air from the upper portions of previously more active convective cells (as discussed by *Houze* [1997]). The buoyancy of the middle-to-upper level cloud leads to a low-pressure perturbation at the base of the stratiform cloud, and the lowered Rossby radius allows a quasi-balanced cyclonic vortex to form there (Figure 21b).

[37] *Fritsch et al.* [1994] combined concepts from *Rotunno et al.* [1988], *Raymond and Jiang* [1990], and their own detailed mesoanalysis of a major MCS over the United States in a conceptual model (Figure 25). They found that the MCV that develops in the stratiform region of the MCS can grow upscale and become somewhat larger and much longer lived than the parent MCS. Such

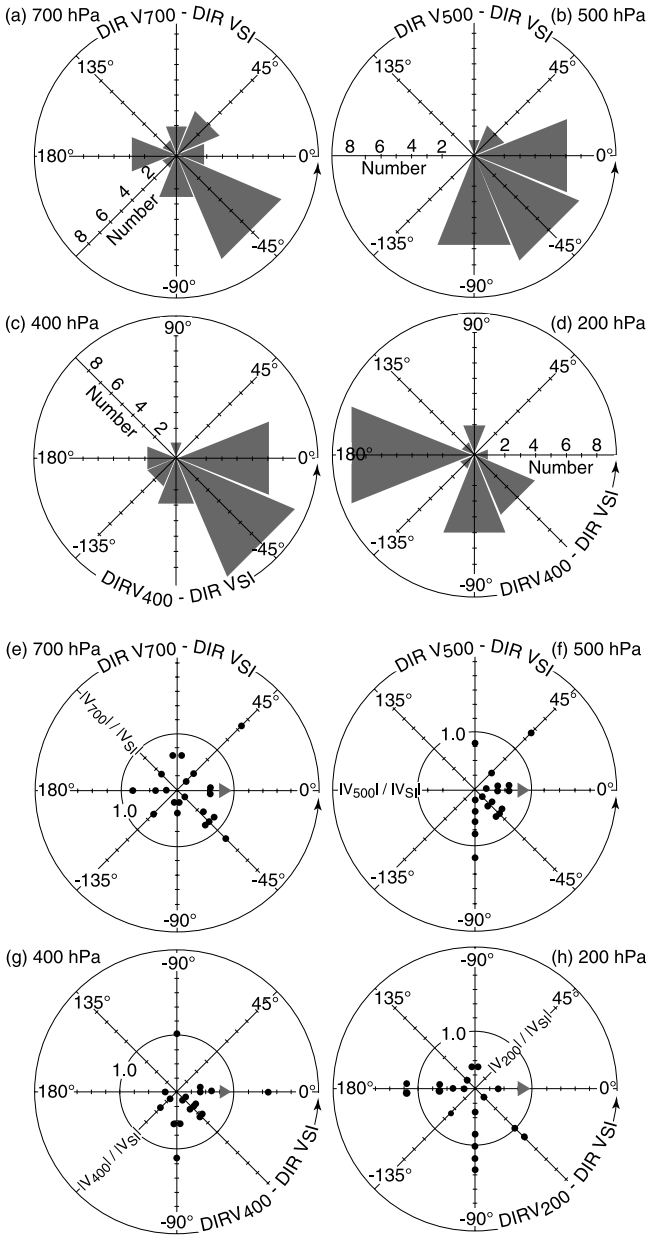

Figure 20. Winds in relation to MCSs observed in TOGA COARE. Plots compare large-scale environmental wind and stratiform wind flow (V_{SI}) in an Earth-relative frame. (a–d) Polar histograms of the directional difference between Earth-relative large-scale wind direction and Earth-relative cell propagation direction. (e–h) Polar scatterplots of the ratio between Earth-relative large-scale wind speed and Earth-relative cell propagation speed as a function of directional difference. The shaded arrow represents a reference vector of unit length. Adapted from *Kingsmill and Houze* [1999a].

was evidently the type of mesovortex described by *Bosart and Sanders* [1981]. These results suggest that the MCV may achieve a state of near balanced flow. *Davis and Weisman* [1994] examined numerically the potential vorticity development associated with the formation of an MCV in an asymmetric squall line. They found a pattern of balanced ascent on the warmer side of the MCS and sinking on the colder side, consistent with *Raymond and Jiang*'s [1990] theory. However, they found that while a warm core vortex of the type discussed by *Raymond and Jiang* [1990] and *Fritsch et al.* [1994] may achieve a state of quasi-balance, it must go through an unbalanced convective phase while part of the convection is evolving into a stratiform region. Consistent with this notion, *Fritsch et al.* [1994] found that a sequence of MCSs occurred in the long-lived mesovortex. Thus, in some extreme cases, an MCS can foster the development of a longer-lived vortex that can, in turn, support development of new MCSs within the long-lived vortex. *Fritsch et al.* [1994] further investigated the mechanism by which the MCV may promote the formation of new convection extending the overall life of the MCS. They found, in the case they studied, that the subsequent MCSs tended to break out in the center of the vortex (i.e., not at the edge of the low level cold pool). They hypothesized that some sort of temporal or spatial nonhomogeneity of the low level cold pool (such as might be promoted by mesoscale banding of the precipitation) allows the warm boundary layer to penetrate horizontally toward the center of the region occupied by the middle level vortex.

[38] Another aspect of the MCV was brought out in a modeling study by *Zhang* [1992]. He described the low as

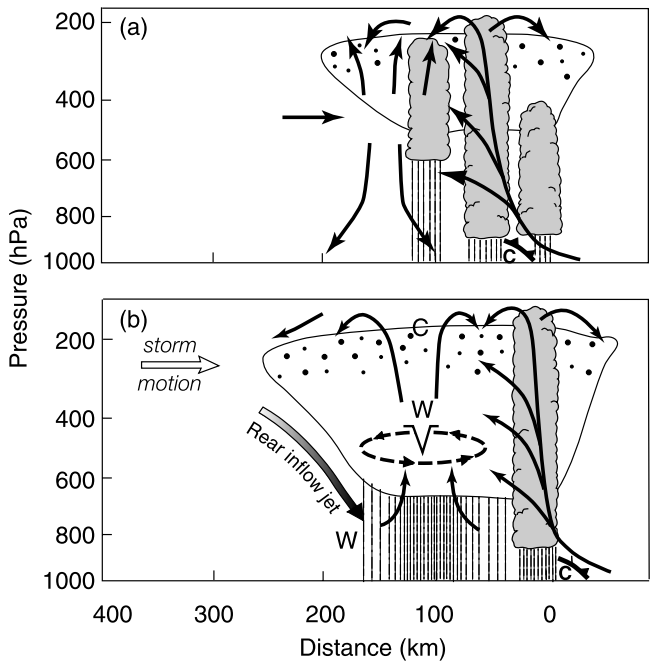

Figure 21. Schematic diagrams of the structure of an MCS with the leading convective line (shading) and the trailing-stratiform rain region (outlined) and the associated mesovortex at (a) initial stage and (b) mesovortex genesis stage. The solid arrows represent the mesoscale circulation. The shaded arrow indicates the location of a rear inflow. W and C mark the regions of positive and negative temperature anomalies, respectively; V and dashed-line arrows denote a middle level mesoscale vortex. From *Chen and Frank* [1993].

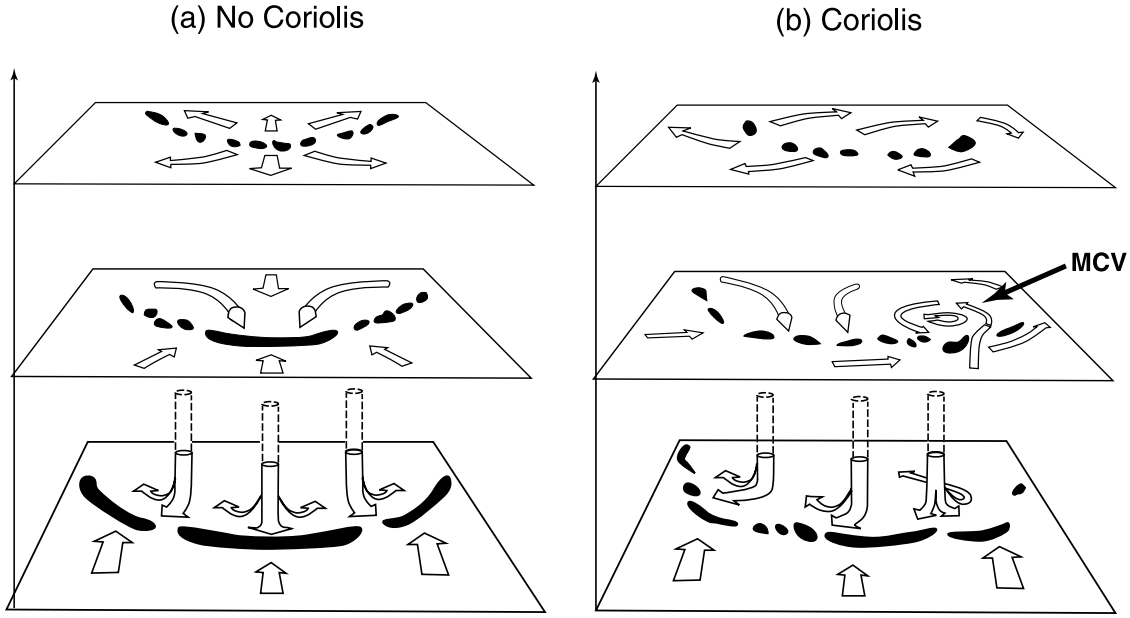

Figure 22. Conceptual model of a Northern Hemisphere squall line that has evolved with and without Coriolis forcing. The view is looking down from the east. The planes represent surface and middle and upper level cross sections. Two-dimensional arrows denote flow in the plane, and three-dimensional tubes denote flow out of the plane. The dotted tubes depict descending flow. MCV indicates an incipient mesoscale convective vortex. Solid areas denote regions of active convection. Adapted from *Skamarock et al.* [1994].

being a cold core low rather than a warm core. The cold core evidently developed from evaporative cooling and/or cooling by melting below the base of the stratiform cloud. *Jorgensen and Smull* [1993], analyzing airborne Doppler radar data, showed that the cyclonic ''bookend'' vortex (of the type in Figure 22) in a midlatitude MCS consisted of two intertwined flows: a rising warm flow on the north side and a cold sinking flow on the south side. Evidently, the middle level vortex is not always easily classifiable as being purely warm or cold core. Some studies have focused on the cold branch of the circulation [e.g., *Zhang*, 1992]. The modeling study of *Chen and Frank* [1993] emphasized the saturated warm branch of the vortex. We note, however, that Figure 21, taken from the *Chen and Frank* [1993] article, is a two-dimensional cross section through a highly three-dimensional storm, and the rear inflow in Figure 21b appears in the schematic sketch to be detached from the vortex. Three-dimensional analysis of the model results, however, shows that the subsiding unsaturated rear inflow depicted in Figure 21b is actually circulating cyclonically

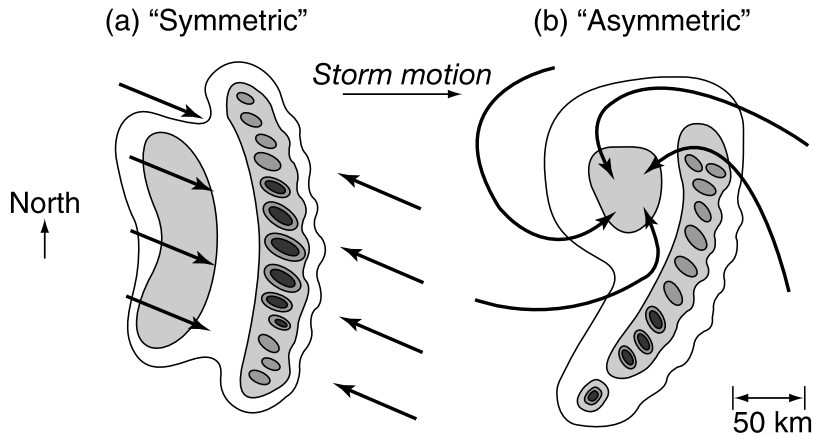

Figure 23. (a) Symmetric and (b) asymmetric paradigms of leading-line/trailing-stratiform squall line MCS structure in the Northern Hemisphere. Contour thresholds indicate radar reflectivity of increasing intensity. Convective regions have cores of maximum reflectivity (dark shading). Stratiform regions are centered on the areas of medium intensity echo (light shading) with no maximum reflectivity cores. Streamlines indicate low level wind direction. Adapted from *Houze et al.* [1989, 1990].

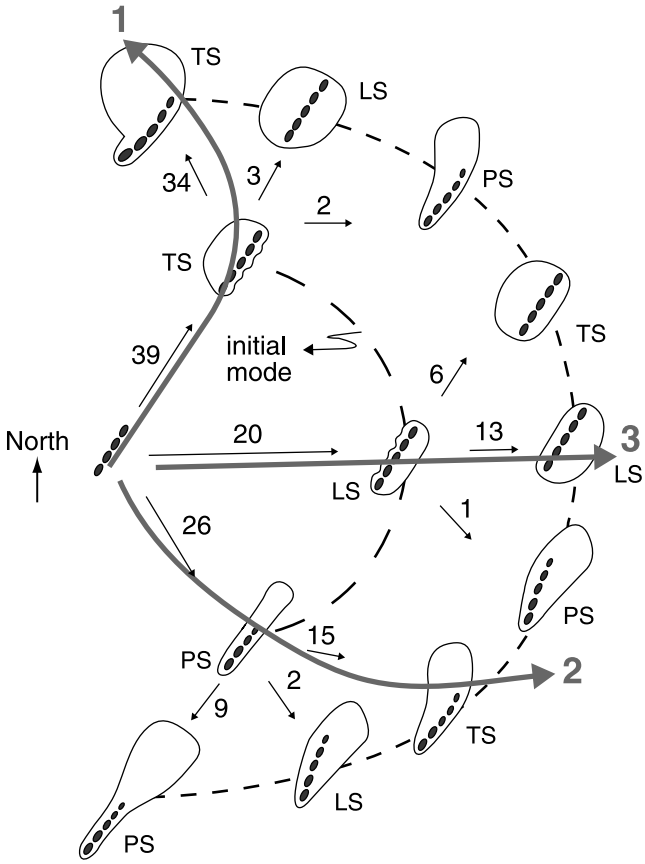

Figure 24. Patterns of evolution of stratiform precipitation in squall lines over the United States. Labels along each evolutionary pathway denote the initial and final modes of stratiform precipitation production. Smaller numbers are the total number of cases following each step. Shaded arrows (labeled 1, 2, and 3) are the most common pathways. Idealized composite positions of convective elements and stratiform precipitation are depicted schematically along each pathway. Abbreviations are for trailing stratiform (TS), leading stratiform (LS), and parallel stratiform (PS).

around the vortex center and is intertwined with the warm saturated air circulating around the vortex center (S. S. Chen, personal communication, 2004).

6. ROLE OF MCSs IN TROPICAL CYCLONE DEVELOPMENT

[39] Satellite data show that tropical cyclones spin up from MCSs. It appears that the MCVs in the stratiform regions of the MCSs are the origin of tropical cyclone circulations. It has been suggested that the middle level vortex in the stratiform region evolves into a deep tropical cyclone circulation [*Velasco and Fritsch*, 1987; *Miller and Fritsch*, 1991; *Fritsch et al.*, 1994; *Fritsch and Forbes*, 2001]. *Bister and Emanuel* [1997] suggested that cooling below the base of the stratiform cloud (of the type discussed by *Zhang* [1992]) is involved in the extension of the middle level vortex downward in tropical MCSs. They proposed that when the cooling-induced MCV extended low enough, it could connect with the boundary layer and develop into a tropical cyclone. The mechanism by which the developing cyclone builds downward and connects with the surface layer, however, remains unclear. *Ritchie and Holland* [1997], *Simpson et al.* [1997], and *Ritchie et al.* [2003] hypothesize that the primary hurricane vortex forms and builds downward when two or more MCSs interact. According to this idea each MCS spins up its own MCV in the stratiform region of the MCS as a result of the profile of heating aloft and cooling at lower levels (Figure 25). When two or more MCVs are in close proximity, they begin to rotate around a common axis and amalgamate into a common vortex. This hypothesis was inspired by several observed cases such as Tropical Cyclone Oliver (1993), illustrated in Figure 26, which identifies the MCSs and locations of associated individual mesoscale vortex centers (identified by aircraft) rotating around a centroid that eventually became the cyclone center (note the Southern Hemisphere rotation). *Ritchie et al.* [2003] argue from modeling evidence that the interaction between unequal middle level vortices will result in the stronger vortex executing a small inner loop while absorbing most of the circulation associated with the weaker vortex. The "victorious" vortex becomes stronger, thickens vertically, and joins with a preexisting surface low. Overall, there seems to be little doubt that the stratiform region MCVs of MCSs are building blocks of the developing cyclone, but much remains to be learned about how the MCSs interact, build a larger cyclone vortex at middle levels, and build downward. This remains a topic of active research.

7. MODES OF MCS PROPAGATION

7.1. Cold Pools

[40] A traditional notion regarding MCSs is that they propagate by "cold pool dynamics." The idea is that negatively buoyant air arriving at the surface as part of the storm's downdrafts spreads out as a gravity current with a leading edge that shoves conditionally unstable environmental air upward past its level of free convection, thus generating new cloud at a leading edge of the storm. This process may fully account for movement of many smaller individual cumulonimbus clouds. MCSs are larger entities composed of multiple intense convective cells accompanied often by a stratiform region. Cold pools generated by these individual convective cells in an MCS typically spread out at the surface and combine to form a large mesoscale cold pool covering a contiguous area on the scale of the entire MCS. This combined cold pool acting as a gravity current can influence MCS propagation velocity by simply forcing unstable air upward on the periphery of the MCS. *Rotunno et al.* [1988] determined that a two-dimensional propagating line of convective storms could be maintained if the horizontal vorticity generated by the advancing cold pool was just offset by the horizontal vorticity generated by buoyant updraft cells forming at the cold pool boundary. However, MCSs are often rather complex combinations of

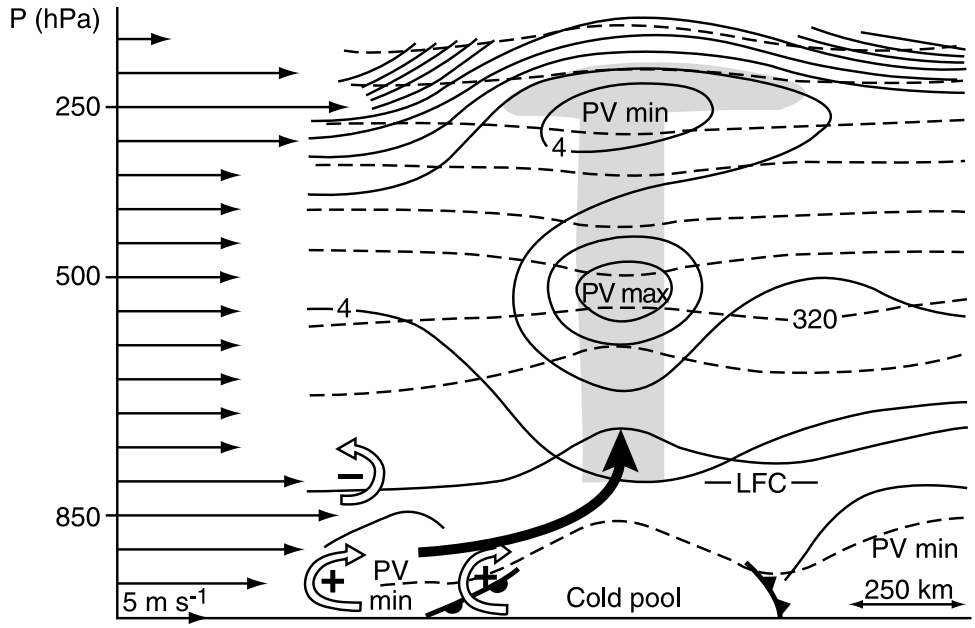

Figure 25. Conceptual diagram of the structure and redevelopment mechanism of a mesoscale warm core vortex associated with an MCS. Thin arrows along the ordinate indicate the vertical profile of the environmental wind. Open arrows with plus or minus signs indicate the sense of the vorticity component perpendicular to the plane of the cross section produced by the cold pool and by the environmental vertical wind shear. The bold solid arrow indicates the updraft axis created by the vorticity distribution. Frontal symbols indicate outflow boundaries. Dashed lines are potential temperature (5 K intervals), and solid lines are potential vorticity (2×10^{-7} m^2 s^{-1} K kg^{-1} intervals). The system is propagating left to right at about 5–8 m s^{-1} and is being overtaken by air of high equivalent potential temperature in the low level jet. Air overtaking the vortex ascends isentropic surfaces, reaches its level of free convection (LFC), and thereby initiates deep convection. Shading indicates cloud. From *Fritsch et al.* [1994].

multiple cumulonimbus cells, arranged in various lines and/or groups, combined with stratiform regions, which can also take on a variety of structures, and cold pool dynamics alone do not seem to account for all aspects of the propagation of these complex mesoscale phenomena.

7.2. Layer Overturning

[41] The cold pool propagation concept does not consider the mesoscale dynamics of the free atmosphere above the boundary layer; it simply offers a mechanism for helping near-surface parcels of air located on the periphery of an MCS to rise above their level of free convection. In section 3 we discussed the organized deep layer of lifting that characterizes an MCS, along with a deep layer of subsiding negatively buoyant air. A theory of propagation of an MCS must account for horizontal displacement of this organized deep tropospheric system of overturning. The Moncrieff theory offers some limited insight into the propagation of such a system. This theory shows that the pressure gradient that must exist at middle levels across a two-dimensional, steady state MCS in a sheared and potentially unstable environment requires a propagation speed that is a function of the stability and shear of the environment. Thus once an MCS has become organized and has achieved steady state with deep layer overturning, it must propagate at a certain rate to maintain dynamical consistency. This rate turns out to be reasonable under shear and stability conditions similar to those of observed MCSs. However, since steady state is assumed, the theory offers no dynamical cause and effect relationship to explain the propagation. In sections 7.3–7.6 we discuss several dynamical theories that have been offered to explain the deep tropospheric structure and propagation of MCSs in dynamical terms.

7.3. Discrete Propagation

[42] Both cold pool dynamics and layer-overturning theory suggest a continuous progression of a mesoscale group or line of convective cells. However, sometimes a group or line of convective cells makes a discrete jump, with new cells forming well ahead of the likely gust front location. An example (brought to the author's attention by R. Fovell (personal communication, 2004)) is shown in Figure 27. The light blue line of low reflectivity identified as the "fine line" is caused by the sharp change of index of refraction at the leading edge of the cold pool. Numerous new cells were forming 10–30 km ahead of the fine line. Clearly, these new cells were not triggered by the cold pool underrunning the air ahead of the storm.

[43] *Corfidi et al.* [1996] and *Fritsch and Forbes* [2001] expressed this behavior in terms of a kinematic formula, in which the propagation velocity is the sum of two velocity vectors: the mean large-scale environmental wind velocity (a proxy for the cold pool propagation velocity of an individual cumulonimbus) plus a "low level jet" wind

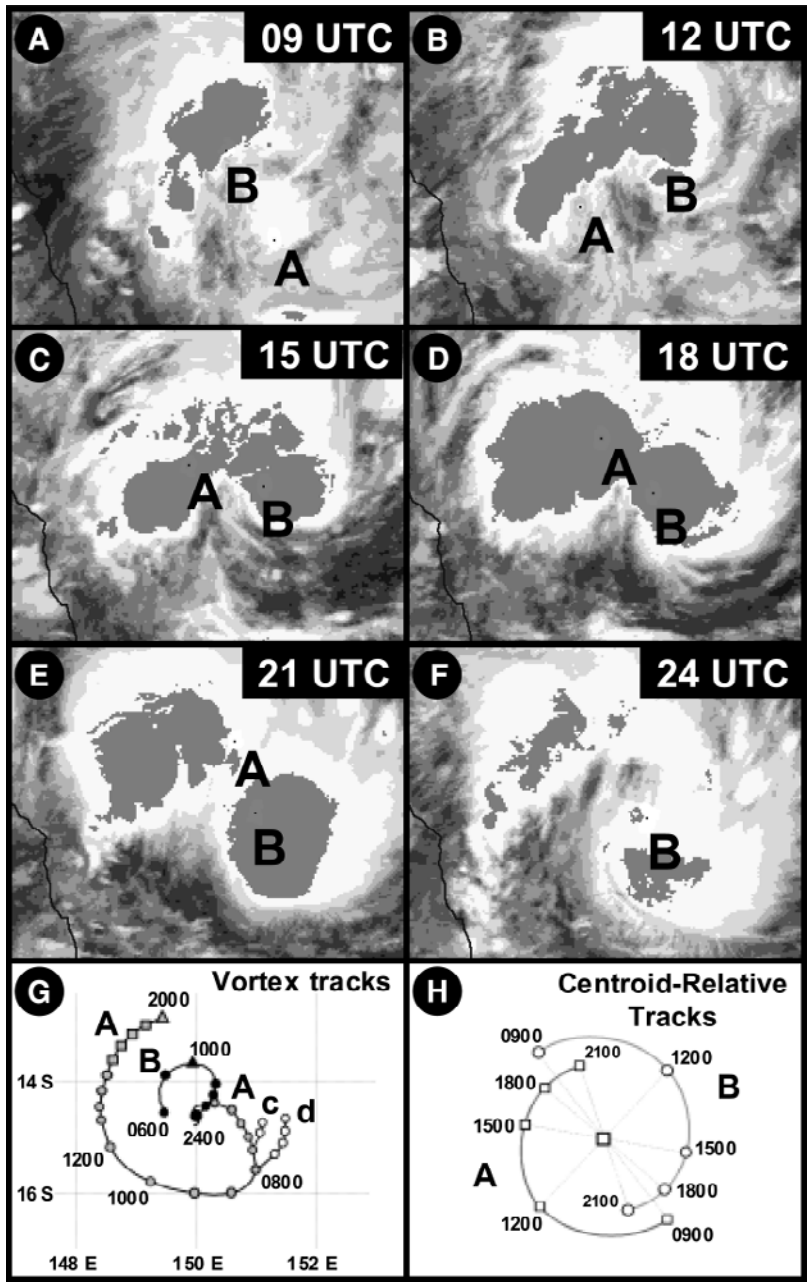

Figure 26. (a–f) The locations of two mesoscale vortices (A and B) during the development of Tropical Cyclone Oliver (located off the coast of northeastern Australia) superimposed on satellite imagery from 0900 UTC 4 February to 0000 UTC 5 February 1993. (g) Tracks of four mesoscale vortices (A, B, c, and d) obtained from radar data. The positions are not evenly spaced, and so times (in UTC) of some of the vortex positions are marked. (h) Centroid-relative tracks of mesovortices A and B from 0900 UTC to 2100 UTC 4 February. From *Ritchie et al.* [2003], adapted from *Simpson et al.* [1997].

vector (which is a proxy for the discrete jumping). This kinematic model assumes the discrete jumping is the way the MCS moves progressively closer to the region of highest boundary layer θ_e. This particular empirical model applies primarily to MCCs over continents where low level jets occur in the lee of major mountain ranges (especially the Rockies and Andes). Such a jet is probably only one possible environmental control that can make the boundary layer on one side or another of an MCS more favorable for regeneration of convection. The root cause of the discrete propagation begs a dynamical explanation.

[44] *Crook and Moncrieff* [1988] found that cells were likely to form ahead of an MCS, without the aid of cold pool triggering, when lifting on a scale larger than the MCS was affecting the air entering the convective system. Their model results showed that when the MCS was occurring in the context of larger-scale lifting, the air just ahead of the MCS, but yet at a distance from the cold pool, was brought to near saturation by the larger-scale lifting, and any random perturbation could trigger convection ahead of the cold pool zone. During the Global Atmospheric Research Program Atlantic Tropical Experiment (GATE), discrete propagation

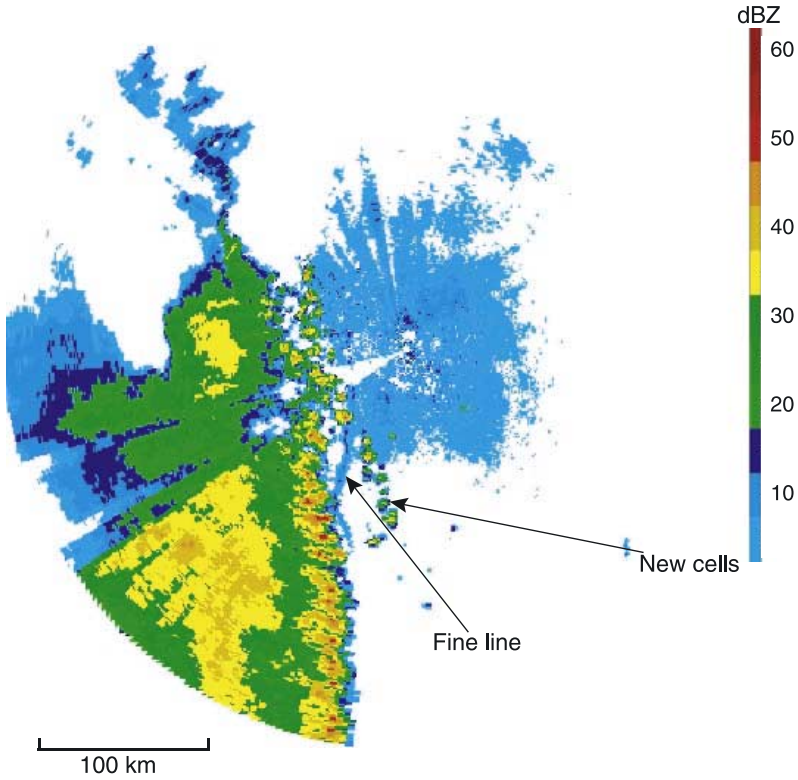

Figure 27. Radar reflectivity pattern, with WSR-88D radar, Vance Air Force Base, Oklahoma, at 0700 UTC 21 June 2003. Maximum range is 230 km. Courtesy of R. Fovell, University of California, Los Angeles.

was found to be a prominent feature of squall line MCSs over west Africa and the tropical eastern Atlantic, and this led to the suggestion that gravity wave dynamics were somehow responsible for the discrete jumping of the line of convection [*Houze*, 1977; *Fortune*, 1980; *Houze and Betts*, 1981]. Consistent with the *Crook and Moncrieff* [1988] results, the cells forming ahead of the gust front (e.g., those forming ahead of the fine line in Figure 27) could have been favored by gravity wave action producing ascent of the environmental air on a scale larger than the MCS itself.

[45] This suggestion raises the broad question of the relationship of wave dynamics to the propagation of MCSs. The following question then arises: What would be the origin of waves or wave-like disturbances in connection with MCSs? There are two possibilities: either wave-like disturbances are triggered by the MCS itself or waves originate from some other cause and become linked to the convection.

7.4. Disturbances Triggered by the MCS Itself

[46] Waves triggered by the MCS itself arise because in a region of precipitating convection, there is net positive buoyancy produced by the latent heat gained by air when precipitation falls out. The vertical displacement of air caused by the buoyancy disturbs the atmosphere, and the dry environment of the MCS adjusts to this buoyant displacement by a spectrum of disturbances (similar to bores), which move at gravity wave speed and have the net effect of displacing environmental mass downward [*Bretherton and Smolarkiewicz*, 1989; *Nicholls et al.*, 1991; *Mapes*, 1993; *Mapes and Houze*, 1995]. Disturbances move at speeds inversely proportional to their vertical wavelength. The shorter-wavelength disturbances remain longer in the vicinity of the MCS and thus may trigger new convective cells in the near field of the MCS.

[47] *Schmidt and Cotton* [1990] identified two main modes traveling at gravity wave speeds away from a model-simulated MCS. The updrafts of these modes are illustrated in Figure 28. The deep updraft is associated with the rapidly propagating mode. The case illustrated is for zero shear in the environment, and mirror image modes propagate away from the disturbance to the left (ULW) and right (URW). The shallower updrafts in the lower half of the troposphere (LLW and LRW) move at about half the speed of the deeper disturbances. They are thought to force new convective cells on or near the flanks of the storm. This mechanism for new cell development does not require a cold pool and may operate at a distance from the current storm. *Abdullah* [1949] and *Tepper* [1950] hypothesized that bores at lower levels may result from the cold pool acting as a piston on the boundary layer air (topped by a stable layer) ahead of the cold pool. *Nicholls et al.* [1991] and *Mapes* [1993],

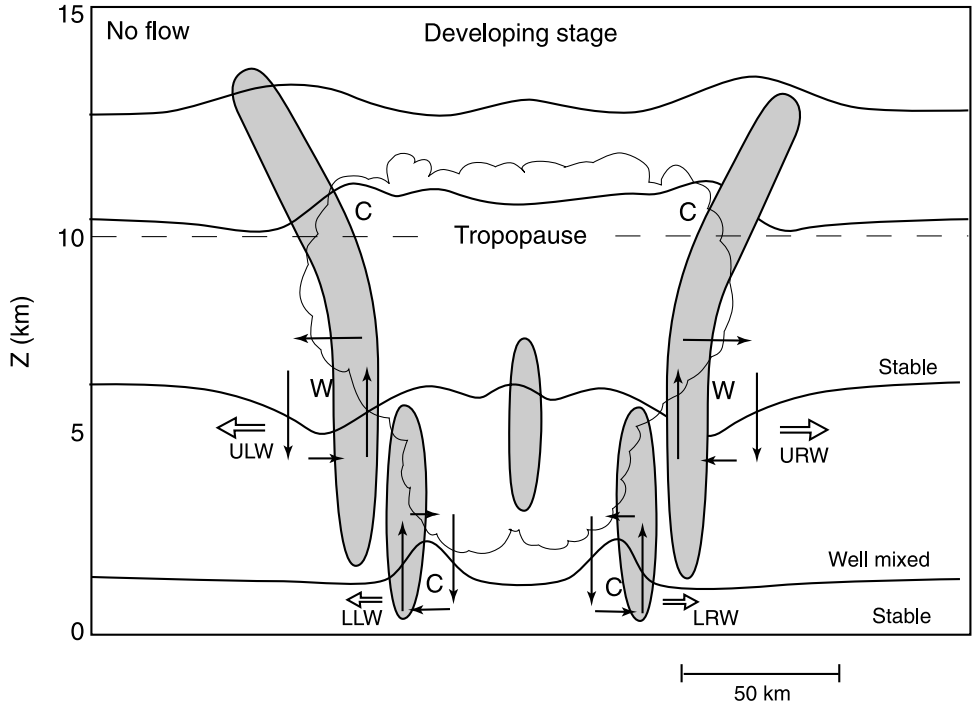

Figure 28. Conceptual model of disturbances generated by an MCS in the case of no shear. The solid lines represent potential temperature contours associated with primary disturbances. The labels C and W represent regions of cold and warm air, respectively. ULW (URW) refers to upper left (right) waves; LLW (LRW) refers to lower left (right) waves. Double arrows represent disturbance movement. Thin arrows denote perturbations in vertical and horizontal wind components. The primary updraft zones are shaded. From *Schmidt and Cotton* [1990].

however, determined that a spectrum of bores emanates from an MCS as a result of the entire vertical profile of mass divergence (or vertical gradient of latent heat release) associated with an MCS. The cold pool divergence at low levels is only one part of this overall divergence profile. Consistent with *Schmidt and Cotton*'s [1990] result (Figure 28), *Nicholls et al.* [1991] and *Mapes* [1993] found the dominant modes associated with observed MCS mass divergence profiles to be a rapidly moving deep bore and a shallower bore moving at half the speed of the deep mode in the environment of MCSs. *Nicholls et al.* [1991] and *Mapes and Houze* [1995] associated the deep, rapidly moving mode associated with the convective region's deep layer of heating and the shallower, more slowly moving bore with the stratiform region's heating aloft and cooling in the lower troposphere (Figure 4). *Mapes* [1993] noted that these bores, unlike gravity waves, produce a net upward displacement of air in the lower troposphere in the vicinity of an MCS. He referred to the destabilizing effect of this upward motion on the environment and likely concomitant triggering of new convection in the near field of the MCS as "gregarious convection." This process would be consistent with results of *Crook and Moncrieff* [1988], who found that lifting of the air over a broad area ahead of the MCS favored the formation of cells ahead of the system, without the necessity of cold pool lifting. As noted in section 7.3, the cells forming ahead of the gust front fine line in Figure 27 could have been triggered in this way.

7.5. Waves Generated External to the MCS

[48] From years of weather observation and forecasting for aviators in Nigeria, with information limited to scattered surface observations, occasional soundings, and pilot reports, *Hamilton and Archbold* [1945] synthesized a remarkably accurate conceptual model of what we now recognize as a squall line MCS with a trailing-stratiform region. In addition to their accurate factual description of the MCS they offered a dynamical interpretation, in which they speculated that the typical MCS "disturbance line" behaved according to the idea "that a single traveling disturbance shifts the various air particles while they are under its influence, somewhat after the manner of a wave at sea." Regarding factors controlling the movement of the system, they noted that

> It is tempting to argue that the disturbance line must be carried along in the prevailing upper wind current, where the bulk of its cloud is. However, this ignores the variations of wind in the neighborhood of the disturbance line.... We therefore offer very tentatively the following remarks based on the assumption that we are dealing essentially with a wave disturbance.

They then compared the motion of the disturbance line to that of a simple gravity wave in a stratified liquid in a channel and concluded that the motion of such a wave was not unlike that of the observed disturbance lines.

[49] *Hamilton and Archbold*'s [1945] intuition that the traveling disturbance had wave-like properties did not

garner much support in their time, probably because convection as a form of instability release seems in many respects inherently non-wave-like. However, the idea gained popularity when it was shown theoretically that a wave could interact constructively with convection. This concept was developed formally in papers by *Hayashi* [1970], *Lindzen* [1974], *Raymond* [1976, 1983, 1984], *Davies* [1979], *Emanuel* [1982], *Silva Dias et al.* [1984], *Xu and Clark* [1984], *Nehrkorn* [1986], *Cram et al.* [1992], and others. In analyzing this interaction, *Lindzen* [1974] drew an analogy to tropical cyclone dynamics. *Charney and Eliassen* [1964] had introduced the term ''conditional instability of the second kind'' (CISK) to describe a hypothesized cooperative interaction in which friction layer convergence in a cyclone drives deep convection and associated heating to strengthen and/or perpetuate a warm core cyclone. So Lindzen dubbed the interaction of wave dynamics and convective clouds ''wave-CISK'' on the basis that the convergence and upward motion in the circulation of an inviscid mesoscale or larger-scale wave (rather than frictional convergence) can maintain a deep convective heat source, which, in turn, strengthens or maintains the wave. This hypothesis is consistent with *Crook and Moncrieff*'s [1988] later finding that convergence and upward motion (e.g., due to a wave) on a scale larger than the MCS favors convective development and more intense, larger convective systems. In the formation of wave-CISK theory the convective heating is parameterized by assuming that its strength is proportional to the wave-scale vertical air motion and is distributed vertically according to a prescribed profile. *Emanuel* [1982], *Raymond* [1983, 1984], *Silva Dias et al.* [1984], *Nehrkorn* [1986], and *Cram et al.* [1992] have proposed that the wave-CISK relationship between a gravity wave and an individual MCS makes the structure and propagation of the MCS one and the same as that of the wave in the spirit of *Hamilton and Archbold*'s [1945] suggestion. Wave-CISK has never been completely satisfactory as a quantitative way of determining preferred mesoscale modes because of its sensitivity to the assumed heating profile. However, the notion that an MCS and a wave can interact constructively remains a useful concept in understanding the observed behavior of MCSs. Interestingly, the most realistic results emerge from wave-CISK calculations when the assumed heating profile of the convection has a maximum in the upper troposphere [e.g., see *Nehrkorn*, 1986; *Cram et al.*, 1992], which is consistent with MCSs having substantial stratiform regions (Figure 4b).

[50] In wave-MCS interactive theory either the wave or the convection may initially occur independently of the other before they become locked together in a mutually beneficial manner. Several recent studies indicate that MCSs sometimes adopt the propagation velocity of a wave arising from some mechanism separate from or larger in scale than the MCS. For example, *Chen et al.* [1996] analyzed infrared satellite imagery in the western tropical Pacific by plotting the centroids of all closed contours of 208 K infrared temperature located near the equator (3°N–10°S) in a time-longitude format (Figure 29). Each centroid was plotted as the center point of an ellipse whose size is proportional to the area covered by the closed contour element in the satellite data. The larger ellipses correspond to MCSs. Generally, the pattern of occurrence of the cold cloud shields in time-longitude space exhibited a westward propagating wave-like behavior with a 2-day frequency. This 2-day westward propagating variability was likely the result of equatorial inertiogravity wave propagation, possibly reinforced by diurnal variability of the boundary layer over the ocean [*Chen and Houze*, 1997]. The 2-day waves in the tropics [*Matsuno*, 1966; *Gill*, 1982; *Takayabu*, 1994] have a timescale much greater than that of an individual MCS.

[51] One might expect a synoptic or mesoscale wave in the environment to manifest itself as an envelope in which convective systems appear and disappear but move according to convective dynamics, independent of the parent wave's dynamics. Such envelope behavior manifests itself on larger scales of motion such as the Madden-Julian oscillation [*Nakazawa*, 1988]. However, in the 2-day frequency wave examples seen in Figure 29, several individual MCSs moved with the wave velocity, for example, the MCSs on 12 and 13 December. It thus appears that the MCS adopted the wave velocity. This behavior is consistent with phase-locked wave-MCS interaction, as in wave-CISK.

[52] On some occasions the MCSs in Figure 29 bifurcated, with one moving eastward while the other moved westward with the wave velocity (e.g., 14 December). Aircraft radar data obtained on 14 and 15 December at the times indicated in Figure 29 suggested that the eastward moving elements were moving in a manner consistent with cold pool dynamics. Thus it appears that MCS propagation was affected by both wave velocity and cold pool dynamics, with the wave velocity being the dominant effect during this particular regime. Some wave-CISK calculations have indicated that both wave and advective solutions exist [*Raymond*, 1983, 1984]. The bifurcation of the propagation into cold pool and wave components is reasonable in view of *Crook and Moncrieff*'s [1988] finding that large-scale convergence and lifting (as might be provided by the larger-scale wave) can promote formation of new convection with mesoscale organization independent of the cold pool forcing.

[53] Behavior analogous to that seen over the tropical ocean has been noted in a midlatitude continental setting. *Carbone et al.* [2002] plotted radar data over the United States east of the Rocky Mountains in time-longitude format and found that large echoes propagated eastward for long periods of time in a wave-like fashion (east of 100° longitude in Figure 30). They suggested that this attribute could make longer-range (2–3 days) MCS prediction more feasible in some cases. *Carbone et al.* [2002] did not determine what type of wave motion might have been affecting the echo movement on the 2- to 3-day timescale, but they included inertiogravity waves as one possibility, which would be similar to the

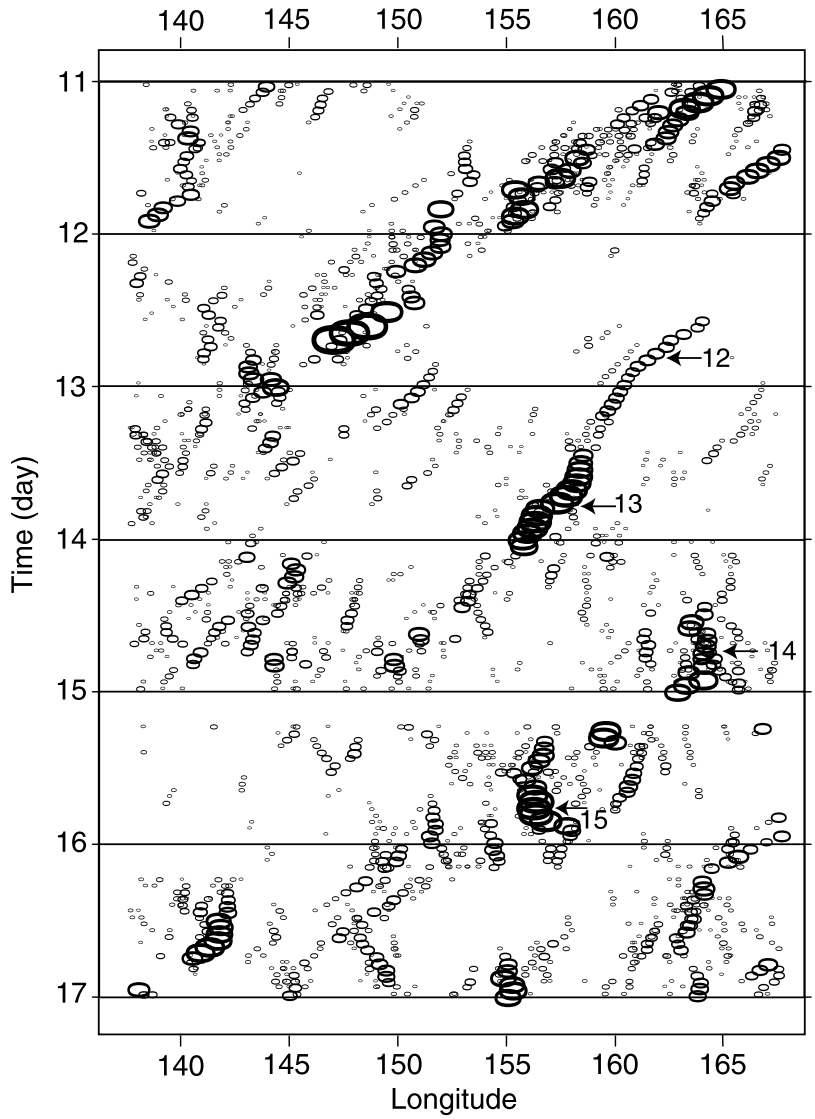

Figure 29. Mesoscale convective systems in TOGA COARE as tracked in satellite infrared data. Results are displayed in time-longitude space for 11–17 December 1992. Sizes of each oval are proportional to the sizes of the actual MCS image at a given instant. Arrows point out locations of research aircraft missions on 12–15 December. The date marker is at 0000 UTC (1100 local standard time at 156°E). From *Chen et al.* [1996].

behavior of the tropical MCSs over the west Pacific (Figure 29).

[54] *Mapes et al.* [2003] used satellite data and a numerical model to analyze MCSs moving from the Andes out over the tropical Pacific Ocean. They found that the diurnal heating cycle over the Andes triggered MCSs that moved out over the tropical Pacific Ocean. The diurnal propagation of the MCSs over the ocean was controlled by gravity waves driven by the diurnal heating of the elevated land surface of the Andes (Figure 31). The gravity wave response to the daytime heating was a compensating downward motion (or "warm phase") over the coastal plain and ocean in the evening (Figure 31a). After sundown, cooling over the elevated terrain led to a near-field gravity wave response of upward motion in the lower troposphere. This cool phase of the nighttime gravity wave response to diabatic cooling over the mountains favors convective development over the ocean at night. As the night goes on, the convection over the water develops into an MCS, which grows and moves seaward with gravity wave speed during the morning (Figure 31b).

[55] Another example of MCS velocity affected by thermally generated gravity wave dynamics occurs over the Bay of Bengal during the onset of the Asian monsoon. The bay has a highly concave coastline and generally is surrounded by rather high terrain (Figure 32). The Joint Air-Sea Monsoon Interaction Experiment (JASMINE) obtained data in this region in May 1999 [*Webster et al.*, 2002]. The period 20–27 May 1999 was convectively active over the bay; the winds were west southwesterly at low levels, turning to easterly aloft (Figure 33). As the high ground surrounding the bay heated up during the day, gravity waves

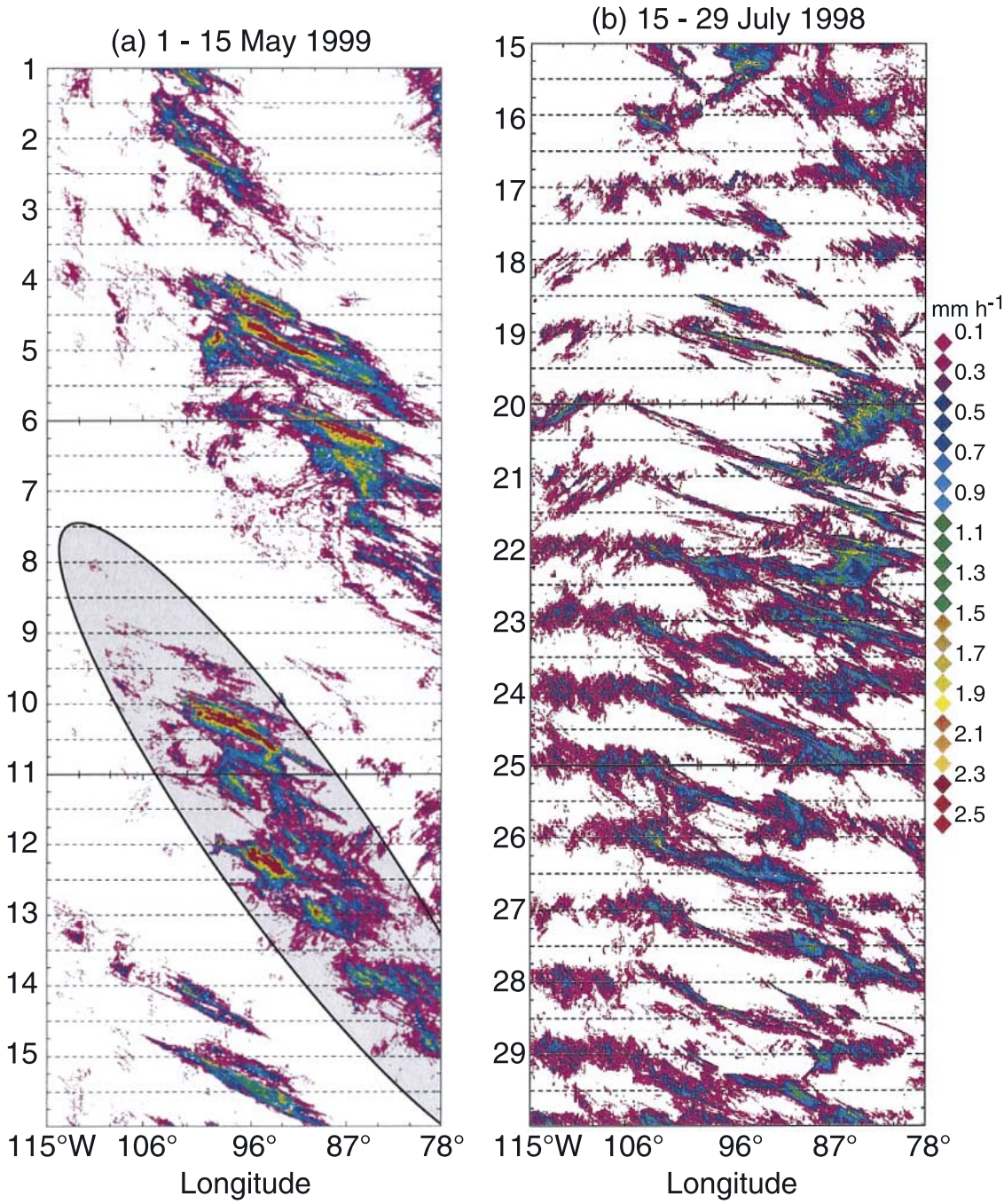

Figure 30. Time-longitude plot of radar-derived rain rate over the central United States for (a) 1–15 May 1999 and (b) 15–29 July 1998. Note the slow eastward propagation of precipitation envelopes in Figure 30a, within which there are faster propagating rain streaks. The shaded, elliptical area denotes one such envelope. In Figure 30b, there are mixed regimes including a nearly pure component of diurnal modulation in the western part of the domain. From *Carbone et al.* [2002].

excited by the heating presumably propagated out over the bay in the fashion described by *Mapes et al.* [2003]. Satellite infrared data plotted in time-latitude format (Figure 34) showed cold cloud tops propagating equatorward from the top of the bay out over the water (20–27 May). These large high-topped cloud systems were MCSs that reached maximum intensity over the central part of the bay.

[56] Details of the structure and propagation of several of the diurnally generated cloud systems seen in Figure 34 were documented in JASMINE by a C-band Doppler radar aboard the NOAA ship *Ronald H. Brown* stationed at 12°N. The radar shows that these cloud systems had the structure of leading-line/trailing-stratiform MCSs. Figure 35a shows a portion of one of these systems at three different times during its traverse of the area of radar coverage. It had a leading convective line on the southwest side of the system and a region of stratiform precipitation generally to the northeast of the line. Time-lapse sequences of the radar

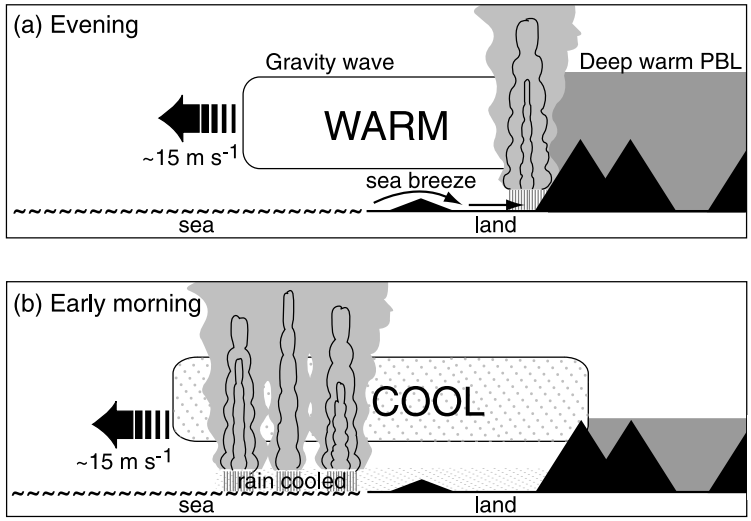

Figure 31. Schematic depiction of diurnal gravity waves emitted by the mixed layer over the mountainous terrain of western tropical South America and associated deep convection: (a) evening and (b) early morning. From *Mapes et al.* [2003].

images show that the progression of the leading line south was a combination of continuous (cold pool) and discrete propagation. At each of the times shown in Figure 35, patterns of convective cells were located ahead of the convective line. Such cells were always forming ahead of the approaching line and moving toward the MCS in a system-relative sense. Some of the cells ahead of the line were eventually incorporated into the line as part of a discrete propagation process evidently similar to that illustrated in Figure 27. At the time shown in Figure 35a, the leading convective line of the MCS had a break in it where a new segment of the line forming from cells ahead of the system was separated from the older line segment to the northwest.

[57] When the ship radar data are subjected to detailed three-dimensional spatial analysis and tracking in time, the echoes ahead of the MCS are seen to have been generally small and isolated rather than interconnected by contiguous echo. They were streaming east-northeastward, evidently advected by the lower tropospheric wind, and were typically of moderate depth. Being carried along by the wind would be expected in a simple convective environment. In contrast, the MCS leading-line and trailing-stratiform radar echo were deep and widespread, typical of an organized mesoscale system. The MCS moved toward the south or southeast, essentially across the predominately zonal environmental flow. The MCS moved in concert with the high cloud tops in the infrared time-latitude plots in Figure 34. Evidently, the gravity waves generated diurnally over the coastal high terrain phase locked with the convection offshore and gave the convection a deep organized interconnected aspect (i.e., formed an MCS) that propagated south or southeastward in a direction that could not be explained by simple advection. This example seems to be a clear case of the MCS propagation becoming one and the same with a wave generated by a process external to the MCS and behaving differently from the smaller nonwave-influenced convective cells streaming northeastward across the sea.

[58] Other types of waves (besides gravity and inertio-gravity waves) may affect MCS propagation velocities. In the east Pacific Intertropical Convergence Zone (ITCZ), easterly waves and Kelvin waves modulate convective activity. During the Tropical East Pacific Process Study (TEPPS) the NOAA ship *Ronald H. Brown* was located in the east Pacific ITCZ. *Serra and Houze* [2002] analyzed radar data collected on the *Ronald H. Brown* in TEPPS. When they plotted the radar data in time-longitude format, the radar echo pattern formed a generally streaky pattern showing that echoes were generally moving at a velocity of $\sim$8 m s^{-1},

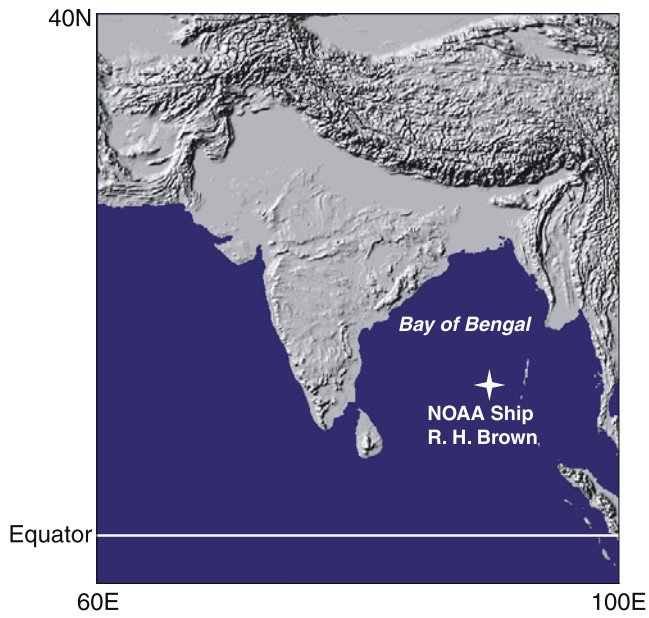

Figure 32. Map of the region where the field project Joint Air-Sea Monsoon Interaction Experiment (JASMINE) was held.

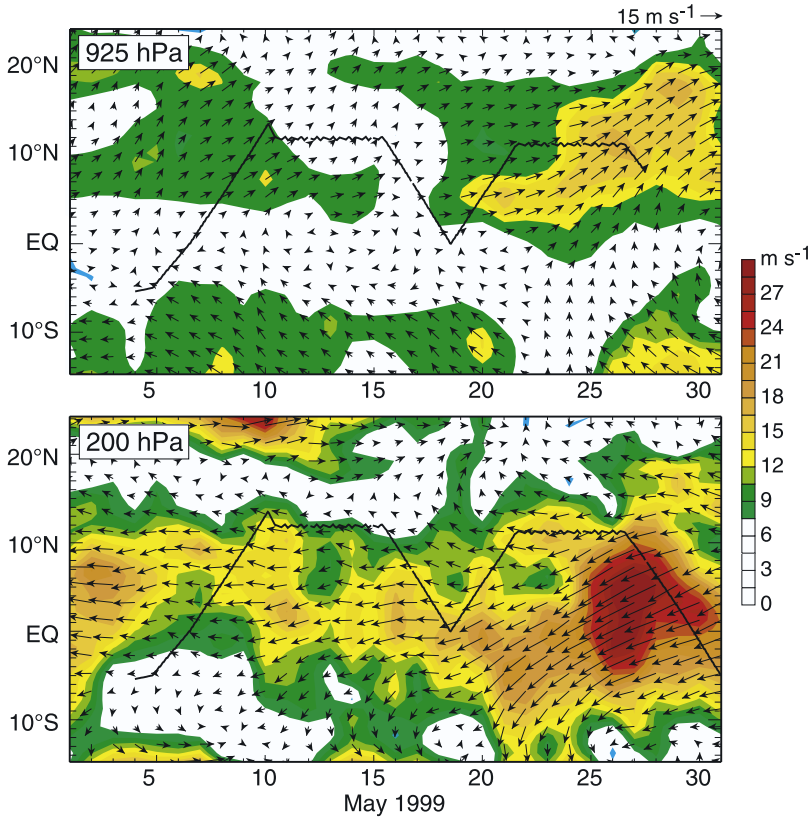

Figure 33. Daily averaged vector winds along 89°E for phase II of JASMINE. Color coding denotes wind speed according to the scale at right. The trace shows the ship track. From *Webster et al.* [2002].

which was equal to the zonal velocity of easterly waves evident in concurrent satellite data (Figure 36). On 19 August the westward streaks were superimposed on a broader eastward moving pattern, which was shown by *Straub and Kiladis* [2002] to be associated with a Kelvin wave.

7.6. MCV Effect on Propagation

[59] Another factor that sometimes affects MCS movement is the MCV that forms in the stratiform region (section 5). An MCS entering its dissipating phase sometimes degenerates to a remnant MCV [*Bartels and Maddox*, 1991], which may drift with the middle level flow, whose velocity may be different from either cold pool or discrete propagation of the active convection. The MCV can later generate a new cycle of convection [*Bosart and Sanders*, 1981; *Fritsch et al.*, 1994; *Fritsch and Forbes*, 2001], which again is dominated by cold pool–induced and/or discrete propagation. This pulsation between active convective phases and the MCV phase can lead to a zig-zag propagation velocity. Figure 37 shows the time-longitude track of an MCS dominated at first by cold pool propagation, then by slower MCV drift, and then again by cold pool propagation.

8. FACTORS LIMITING LIFETIME AND SIZE OF MCSs

[60] Mesoscale convective systems can be up to several hundred kilometers in dimension, depending on how their boundaries are defined. Some of the largest MCSs occur over the western tropical Pacific. Their large sizes in that region have led investigators to call them "superclusters," "superconvective systems," and similar names. *Chen et al.* [1996] used the 208 K infrared temperature contour to define the edge of convective cloud entities over the TOGA COARE region. Research flights in TOGA COARE indi-

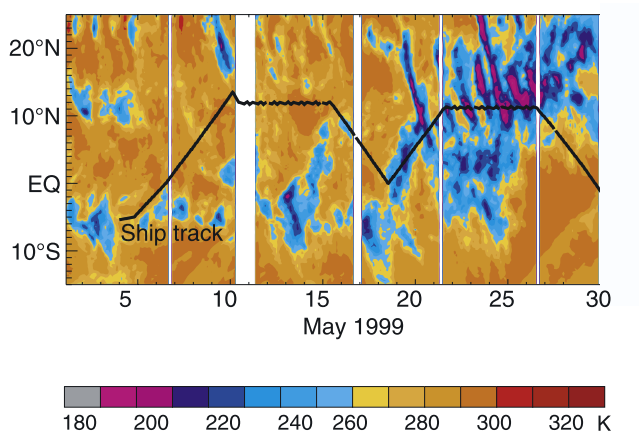

Figure 34. Time-latitude section of brightness temperature (see color-coded scale) from the European Space Agency METEOSAT-5 geostationary satellite. Data are averaged between 85° and 90°E. Cold temperatures are indicative of high cloud tops, while relatively clear periods appear as warm temperatures representing infrared radiation emitted at the surface or the moist boundary layer or from low tropospheric clouds. From *Webster et al.* [2002].

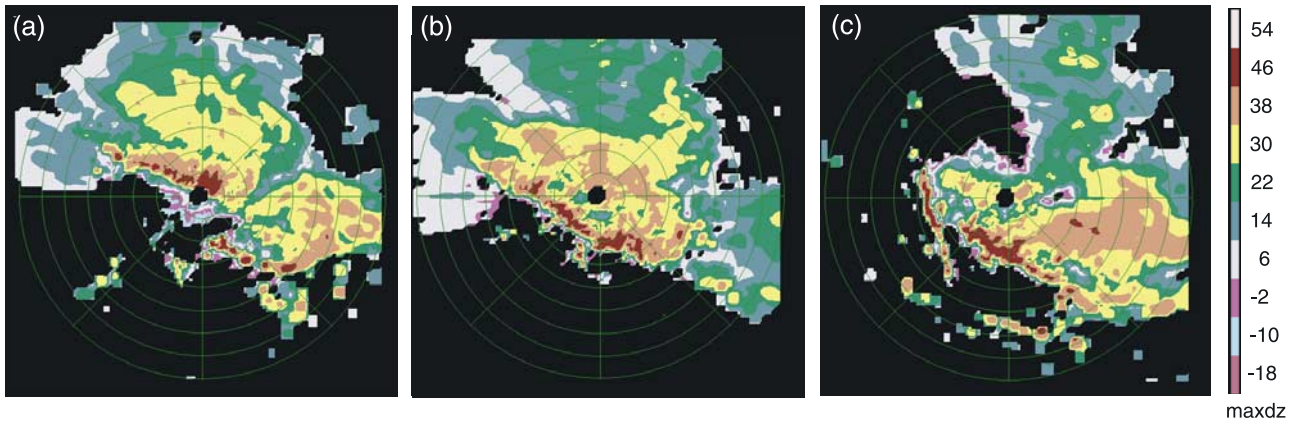

Figure 35. Radar echo patterns observed over the Bay of Bengal by the C-band radar on the NOAA ship *Ronald H. Brown* during JASMINE at (a) 1815 UTC 22 May 1999, (b) 2045 UTC 22 May 1999, and (c) 0045 UTC 23 May 1999. Colors indicate radar reflectivity at intervals of 8 dBZ, with the orange color centered at 46 dBZ. Range rings are at 30-km intervals.

cated that this cold contour roughly outlined the precipitating part of the cloud system. *Chen et al.* [1996] tracked the elements delineated by the 208 K contour by the overlap method of *Williams and Houze* [1987]. Figure 38 shows the population of tracked MCSs according to their lifetime and maximum dimension attained during that lifetime. Systems over 300 km in dimension were termed superconvective systems.

[61] How do MCSs get this large, and why do they not get any larger? Regarding the first question, *Yuter and Houze* [1998] examined TOGA COARE aircraft radar data obtained with the lower fuselage scanning C-band radar of the NOAA P3 aircraft at approximately the same time as infrared satellite images. They subdivided a 240 km $\times$ 240 km area centered on the aircraft into 24 km $\times$ 24 km grid elements, and they averaged the satellite-derived infrared temperature over each 24 km $\times$ 24 km element. The aircraft radar data had a recorded resolution of 2 km $\times$ 2 km and were subdivided into convective and stratiform components according to a standard algorithm (described in its various modifications by *Churchill and Houze* [1984], *Steiner et al.* [1995], *Yuter and Houze* [1997], and *Houze* [1997]). Figure 39 shows the statistics of the relationship of the 24-km average infrared temperature to the fractions of the 24 km $\times$ 24 km element covered by radar echo (precipitation), convective precipitation, and stratiform precipitation. The fraction of area covered by precipitation tends to increase as the mean infrared temperature decreases. The fraction of area covered by stratiform precipitation increases in a similar manner, while the fraction of area covered by convective cells is completely unrelated to the average infrared temperature of cloud top. Thus there is a limit of 20–30% of a 24 km $\times$ 24 km grid element that can be covered by convective precipitation at any given time regardless of cloud top height. When *Yuter and Houze* [1998] considered the entire 240 km $\times$ 240 km domain surrounding the aircraft, they found that the area covered by convective cells seldom exceeded 2000–3000 km^2, while the stratiform precipitation area could be as large as 40,000 km^2 (Figure 40). Thus, at both 24-km resolution and 240-km resolution, there is a limit to how much surface area can support active convection at any given time. The size of an MCS is thus effectively determined by the growth of the stratiform precipitation region.

[62] If the stratiform region consists of previously active convective elements, as suggested by *Houze* [1997], then the growth of the stratiform region is a manifestation of convective cells weakening and becoming stratiform while new cells form elsewhere in the immediate environment. The stratiform elements produced as a residual of the weakened cells accumulate to form the larger stratiform region of the MCS. If these stratiform residual elements of previously active convective cells have a dissipation time that is generally greater than the active cell lifetime, the stratiform elements accumulate in time, and the region grows in size overall. Over time, a balance could be reached between the formation rate of new convective precipitation and old stratiform precipitation dying off. The number of active convective cells possible at a given time limits this maximum size. MCSs would therefore reach maximum size only if the environment is able to sustain the maximum number of cells for a period. *Yuter and Houze* [1998] thus hypothesized that the MCS size in a given situation was set by the convective ''sustainability'' of the environment.

[63] If sustainability, defined as the ability of the environment to support the generation of new convective cells over time, determines the maximum size to which an MCS may build itself, the key question regarding the maximum spatial scale of an MCS becomes, What determines the sustainability? One factor is the thermodynamic structure of the boundary layer. *Kingsmill and Houze* [1999b] analyzed the low-altitude soundings taken by aircraft ascending and descending in the vicinity of radar-observed precipitation areas in TOGA COARE. They categorized the radar echoes as shallow, deep narrow, and deep broad. The latter would correspond to MCSs, which are both deep and have a larger horizontal dimension. The convective available potential energy (CAPE) in the vicinity of shallow and deep narrow

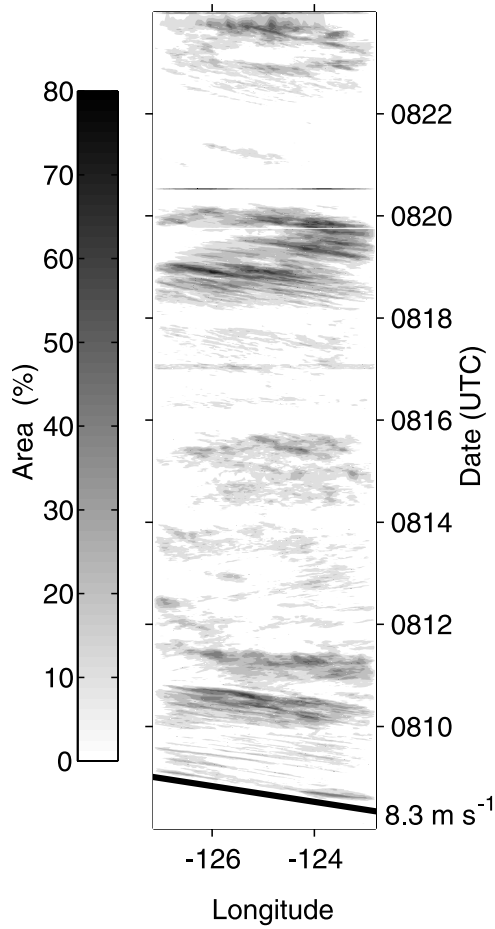

Figure 36. Time-longitude plot of ship radar data collected on 9–23 August 1997 at 7.8°N, 125°W in the middle of the east Pacific Intertropical Convergence Zone during the Tropical Eastern Pacific Process Study. Radar echo is represented as percent area covered by reflectivity >20 dBZ. The bold line indicates the easterly wave propagation speed of 8.3 m s^{-1} as determined from satellite data. The streaks in the radar data indicate that the echoes tended to move at a similar zonal velocity. On 19 August these streaks were superimposed on an eastward propagating pattern, evidently associated with a Kelvin wave. From *Serra and Houze* [2002].

convection was noticeably lower than that in the environment of deep broad echoes. In the vicinity of the deep broad MCSs the CAPE was generally high for parcels initiated from anywhere within the boundary layer (top of the boundary layer ~500 m). That is, in the vicinity of deep broad MCSs, there was a higher integrated CAPE (ICAPE, as defined by *Mapes* [1993] (Figure 41). This finding is consistent with the idea that a boundary layer that is warm and moist throughout its depth is necessary to sustain a broad convective system, i.e., an MCS.

[64] This result is consistent with the global pattern of stratiform rain fraction associated with tropical convection [*Schumacher and Houze*, 2003]. The highest stratiform rain fractions occur over the oceans, where a moist warm boundary layer exists over broad expanses (see section 10). Over tropical continents the stratiform rain fractions are less. This fact suggests that over land, MCS size is limited because the warm moist boundary layer becomes stable at night. The strong nocturnal cooling over land sharply limits the sustainability, whereas over the oceans the diurnal cycle is weak and the convection can continue overnight, allowing stratiform regions and MCS sizes to increase irrespective of the time of day. An exception over land would be when a low level jet replenishes the boundary layer through the night, as is the case along the Rocky Mountains and the Andes when large nocturnal "mesoscale convective complexes" form and reach maximum size overnight [*Laing and Fritsch*, 1997]. In this case the low level jet aids and abets the sustainability, which allows the MCS to develop a large stratiform area and a large size.

[65] Thus one factor determining how MCSs reach a certain maximum size appears to be the sustainability, which is a thermodynamic characteristic of the environment. Another factor that determines the limitation on the ultimate size of an MCS appears in some cases to be dynamic rather than thermodynamic. *Cotton et al.* [1989] and *Olsson and Cotton* [1997] find that many midlatitude MCSs exhibit balanced properties, for which the Rossby radius limits the system size and duration. The most prominent balanced circulation in an MCS is the MCV that develops in a long-lived MCC (section 5); the Rossby radius almost certainly sets the maximum size of these systems. In equatorial regions, where the Coriolis effect is small, the Rossby radius would not be expected to limit the size of the system, and strong MCVs are rare to nonexistent in MCSs in equatorial regions. Over the western tropical Pacific the very large superconvective systems often exceed the sizes of midlatitude MCCs (Figure 38). One can speculate that the systems over a tropical ocean (such as the west Pacific warm pool) can attain their greatest size because, first, they do not exhibit strong MCVs and are therefore not limited by a small Rossby radius [*Cotton et al.*, 1989]. Second, they exist in an environment with effectively infinite sustainability owing to the huge extent of the underlying warm ocean. New convection can keep on forming for an indefinite time period in and near an active MCS. A balance stage may then occur in which the MCS area covered by old stratiform precipitation is disappearing with age at the same rate that new convective area is being created. Thus the maximum size of superconvective systems over the western tropical Pacific is probably determined by the sustainability balance limit.

9. MOMENTUM REDISTRIBUTION BY MCSs

[66] Wherever a layer of buoyant air occurs, a hydrostatic low-pressure anomaly forms at the base of that layer in order to preserve mass continuity [see *Houze*, 1993, chapter 7]. Air accelerates laterally into this local minimum of pressure induced by the buoyant layer above. In an analysis of GATE aircraft data, *LeMone* [1983] found the small-scale hydrostatic low-pressure minimum located below the down shear tilted buoyant updraft of a line of convective cells of a mesoscale convective system. In addition to the pressure

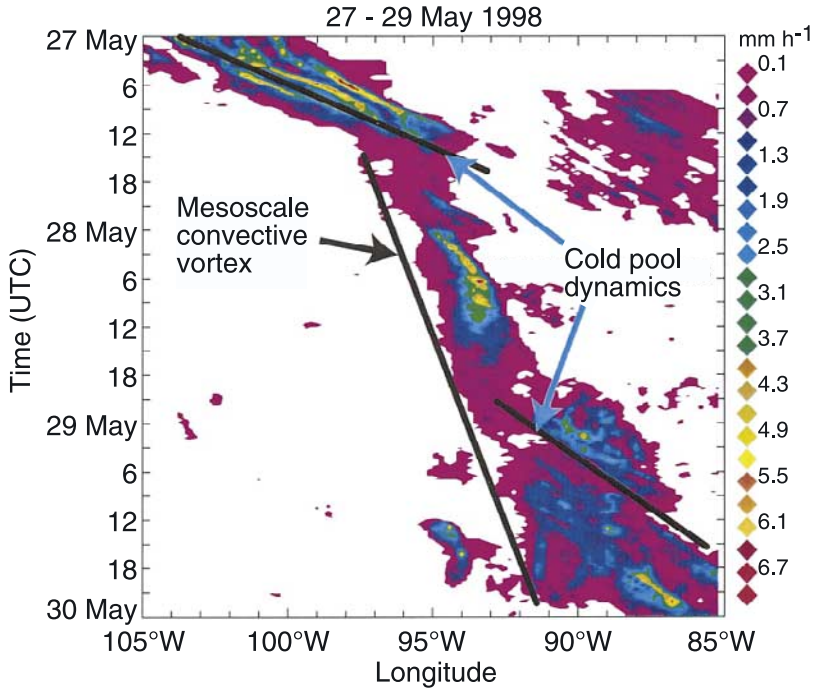

Figure 37. Time-longitude plot of radar-derived rain rate over the central United States for 27–29 May 1998. See text for discussion. From *Carbone et al.* [2002].

perturbation associated with an individual convective-scale updraft, as described by LeMone, we have seen that a larger (mesoscale) hydrostatic low develops at the base of the slightly buoyant stratiform cloud of a large MCS (section 5). Realistic simulations of leading-line/trailing-stratiform MCSs indicate that the mesolow below the stratiform cloud deck and the convective-scale low associated with the active convective cells tend to merge into a single mesolow with

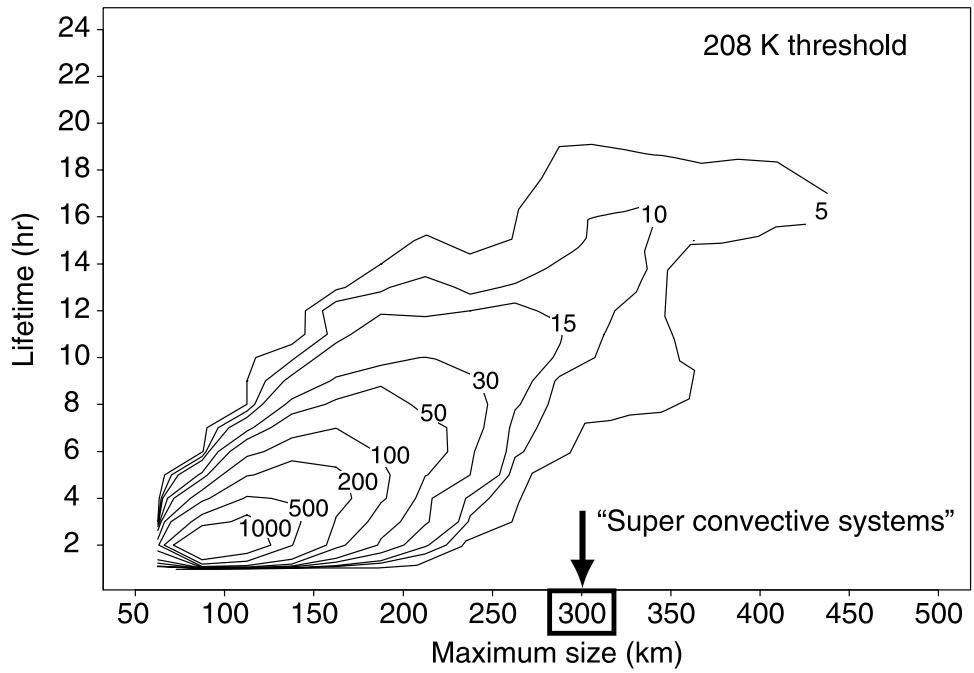

Figure 38. Timescales and space scales of MCSs in TOGA COARE. MCSs were defined by a cloud top temperature threshold of 208 K and by whether they exhibited continuity in both space and time. Frequency distribution shows occurrences of tracked MCSs (number per 25-km-size interval per hour) as a function of the maximum size (abscissa) reached by a convective system during its lifetime (from start to end of its life cycle). Adapted from *Chen et al.* [1996] and *Chen and Houze* [1997].

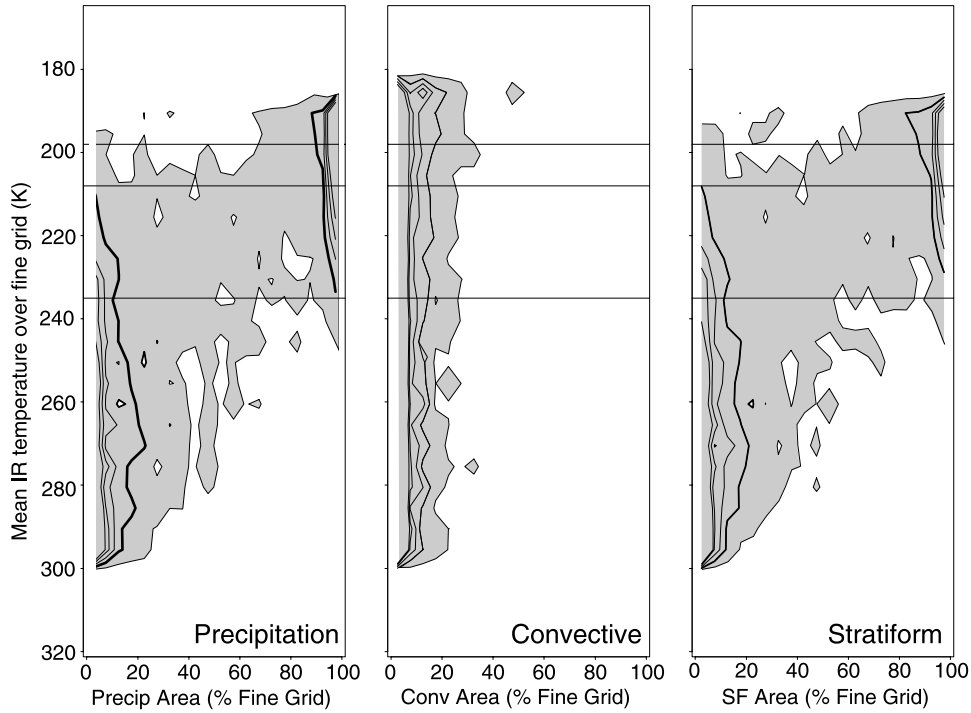

Figure 39. Comparison of TOGA COARE aircraft radar data with concurrent infrared satellite imagery. Figure 39 summarizes results from an analysis of the data at 24-km resolution. The mean infrared temperature is plotted against the percentage area covered by radar echo (as observed by the aircraft's lower fuselage C-band radar) in each 24 km × 24 km grid element. (left) Total precipitation echo coverage. Percentage area covered by the (middle) convective and (right) stratiform components of the radar echo in each grid element. The contours show the frequency occurrence of each combination of mean infrared temperature and percent area coverage. The histogram bin sizes are 28.8 km^2 (5% of grid area) and 5 K. Contour intervals are 0.2% of the data K^{-1} km^{-2}, starting at 0.1% K^{-1} km^{-2}. Horizontal lines indicate 200, 208, and 235 K, which are temperature thresholds commonly used in analysis of satellite data. Note that the stratiform area increases as the mean infrared temperature decreases. However, the convective coverage in a given 24 km × 24 km element is constant with respect to mean infrared temperature. From *Yuter and Houze* [1998].

the maximum perturbation of pressure at the back edge of the convective region, where it borders the stratiform region (e.g., Figure 42). The pressure anomaly field in the MCS also exhibits a mesohigh under the convective region at low levels and near the back edge of the stratiform region at high levels. These three pressure centers thus tilt backward through the system: high at low levels in the convective region, low in middle levels at the boundary of the convective and stratiform regions, and high at upper levels in the trailing-stratiform region. Figure 43 summarizes the pressure gradient forces (bold arrows in Figure 43a) resulting from the sloped positioning of the middle level low and upper and lower level highs. The middle level low leads to the acceleration of front-to-rear flow across the convective region. This acceleration aids the layer inflow into the convective uplift region (section 3). At the same time the mesolow also draws air rear to front across the stratiform region. This acceleration contributes to the formation of the middle level inflow into the stratiform region (section 4).

[67] In addition to pressure gradient accelerations induced by the MCS buoyancy field, the updrafts and downdrafts of the MCS redistribute momentum via vertical fluxes. *Moncrieff* [1978, 1981, 1992] has long advocated a method of computing the net effect on the large-scale momentum field of an idealized two-dimensional, steady state convective system. His formulation incorporates all the flux and pressure gradient acceleration effects into one net calculation. This approach is difficult, however, to apply to a system that is more complex in structure than the idealized two-dimensional, steady state system. As found in studies such as those of *McAnelly and Cotton* [1989], *Houze et al.* [1990], *Kingsmill and Houze* [1999a, 1999b], and *Parker and Johnson* [2000], MCSs exhibit a wide variety of complex structures other than the classical two-dimensional leading-line/trailing-stratiform structure. However, the various MCS structures are always divisible into convective and stratiform components. It is therefore helpful to break down the momentum processes in an MCS into fundamental convective and stratiform components. To obtain such a phenomenological breakdown of the momentum redistribution processes in an MCS, *Yang and Houze* [1996] have applied a traditional eddy flux formulation to a numerically

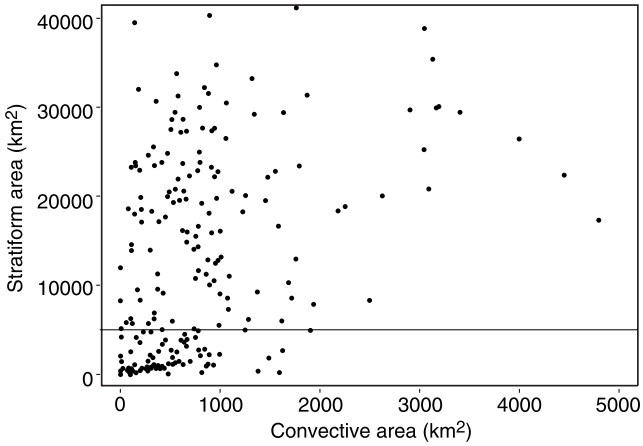

Figure 40. Analysis of TOGA COARE aircraft radar data. Figure 40 plots the area of convective precipitation versus the area of stratiform precipitation as observed within a 240 km × 240 km region surveyed by the lower fuselage C-band radar of the aircraft. The horizontal line at 5000 km^2 corresponds to the maximum convective precipitation area on the abscissa. Note that at any given time regardless of the size of stratiform area the convective area remains less than about 5000 km^2. Adapted from *Yuter and Houze* [1998].

simulated two-dimensional leading-line/trailing-stratiform MCS. In their calculations the overall effect of the model MCS on the large-scale momentum field (arrows in Figure 43b) is consistent with what would be predicted by the Moncrieff paradigm. The convergence of vertical fluxes by mean and eddy motions (see arrows in Figure 43a) produce the strongest effects in the convective region, where they increase the forward momentum at low levels and increase rearward momentum in middle levels. The convective updrafts carry lower level, rearward momentum upward. The convective downdrafts carry rear-to-front momentum downward. The momentum carried downward by the convective downdrafts is in part created by the pressure gradient force (PGF) across the stratiform region at middle levels when the convective downdrafts are initiated in middle levels with negatively buoyant air entrained from the neighboring stratiform region.

[68] The net momentum tendency over the large-scale region containing the system in this illustration is forward at low and high levels and rearward at middle levels (Figure 43b). At low levels the momentum transported downward in the convective downdrafts outweighs the rearward PGF in the convective region. In middle levels the rearward PGF in the mesolow in the convective region is offset by the forward PGF in the stratiform region. The upward transport of rearward momentum by the convective updrafts combines with the PGFs to produce the net rearward acceleration over the large-scale region. At upper levels the only significant acceleration is the forward PGF associated with the location of the upper level mesohigh near the rear of the stratiform region.

[69] The phenomenological breakdown of the net momentum feedback into several basic components helps to elucidate how momentum feedbacks might vary from one MCS to another. The example in Figure 43 is for an idealized MCS of the leading-line/trailing-stratiform type. The same basic features would be present in other types of MCSs but might manifest themselves with different intensity and in a variety of spatial configurations. A system with a stronger or bigger stratiform region might be expected to produce a different momentum feedback to the environment than a system with a smaller stratiform region. A system in which the convective cells are not linearly arranged might produce a different location of the middle level mesolow center (or perhaps no well-defined center at all, e.g., multiple small-scale low-pressure centers). The accelerations shown in Figure 43 might therefore be weaker, stronger, or directed wholly or partially orthogonal to those shown in this example, depending on the characteristics of the particular MCS.

[70] One variation on the momentum redistribution theme of the idealized example in Figure 43 occurs when the stratiform region subsidence becomes particularly strong and widespread. The stratiform region can then manifest a strong eddy flux of momentum, as the subsiding middle level inflow transports middle level momentum downward. Such an eddy flux was not present in the lower levels of the simulated MCS shown in Figure 43. However, some of the very large MCSs that occurred over the western Pacific in TOGA COARE had downward transports of momentum in their large stratiform regions. These downward transports were substantial because the stratiform regions cover such large areas. Figure 44 shows ship radar radial velocity data in a horizontal area approximately 100 km in dimension within the stratiform region of a large MCS in TOGA COARE. The colors show velocity toward (blue) and away from (yellow) the ship. During the 5-hour period shown, the MCS was moving slowly toward the south. The horizontal maps show that over this period the radial velocity in the sector west of the ship changed alternately from westerly to

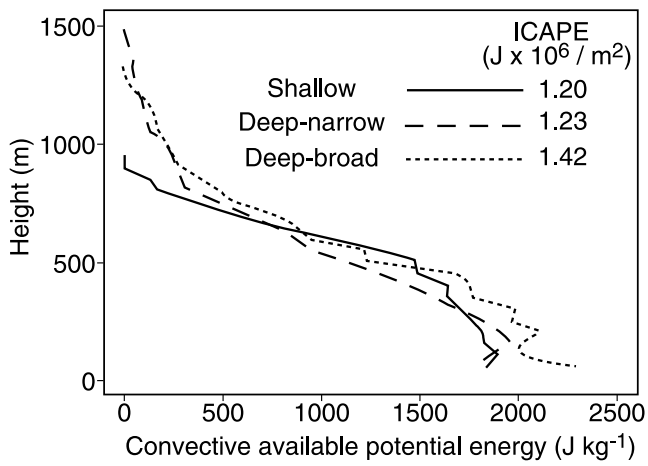

Figure 41. Convective available potential energy (CAPE) and integrated CAPE (ICAPE) computed from thermodynamic data obtained by aircraft during ascents and descents in the vicinities of MCSs sampled in TOGA COARE. From *Kingsmill and Houze* [1999b].

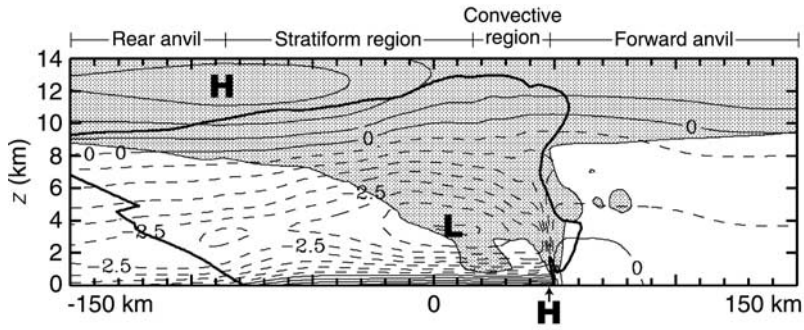

Figure 42. Perturbation pressure field in the mature stage of a squall line MCS simulated with a two-dimensional high-resolution model. Contours are in hPa. Negative perturbation isobars are dashed. Region of time-averaged nonprecipitating hydrometeor (cloud water and cloud ice) mixing ratio greater than 0.1 g kg^{-1} is shaded. From *Yang and Houze* [1996].

easterly. The accompanying vertical sections (along the red lines in the horizontal maps) show that the middle level inflow (indicated by the arrows) from the east occasionally subsided to low levels, completely reversing the prevailing low level flow direction over a large region. Since the stratiform region spans such a large area, the momentum redistribution can significantly affect the large-scale average momentum profile for the region affected by the MCS. D. B. Mechem, S. S. Chen, and R. A. Houze Jr. (Momentum transport processes of organized mesoscale convection over the western Pacific warm pool, submitted to *Quarterly Journal of the Royal Meteorological Society*, 2004) have demonstrated this effect in a cloud-resolving model. This effect was also inferred from GCM calculations by *Moncrieff and Klinker* [1997].

[71] The example in Figure 44 illustrates the potential impact of the momentum redistribution by the stratiform region, when the stratiform circulation becomes stronger than that often produced in cloud models. The momentum flux in the stratiform region is not only hard to simulate but also difficult to observe because the vertical air motions are too small to measure easily by available methods. Thus both modeling and observations can lead to underestimates of the effect of the stratiform region on the large-scale momentum field.

10. EFFECTS OF MCS HEATING ON THE LARGE-SCALE ENVIRONMENT

[72] A mesoscale convective system constitutes a disturbance of the mass field of the atmosphere. The buoyant updrafts displace mass, and the environment responds via gravity wave action, like a pond rippling in response to an object falling into the water (section 7.4). Since the vertical motion in the convective clouds is closely linked to latent heat release, the heating profile associated with a convective

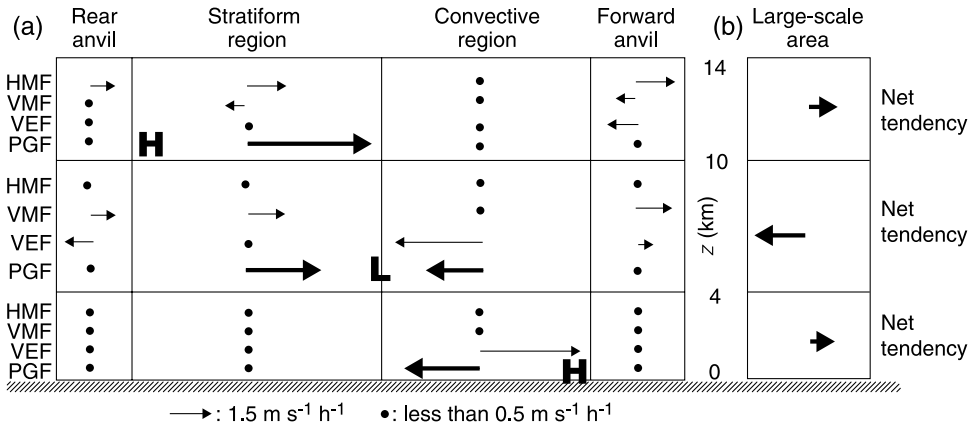

Figure 43. (a) A block diagram showing the balance of area-weighted momentum budget terms over four subregions of a squall line MCS. Rightward (leftward) arrows are for rear-to-front (front-to-rear) momentum tendency for individual terms in the cross-line momentum budget equation (HMF, horizontal mean flux, VMF, vertical mean flux, VEF, vertical eddy flux, and PGF, pressure gradient force). The length of the arrow is proportional to the layer-averaged tendency produced by each budget term. A dot is for the tendency <0.5 m s^{-1} h^{-1}. H and L indicate approximate locations of centers of mesoscale high- and low-pressure perturbations, respectively. (b) Same as in Figure 43a except for net momentum tendency. Adapted from *Yang and Houze* [1996].

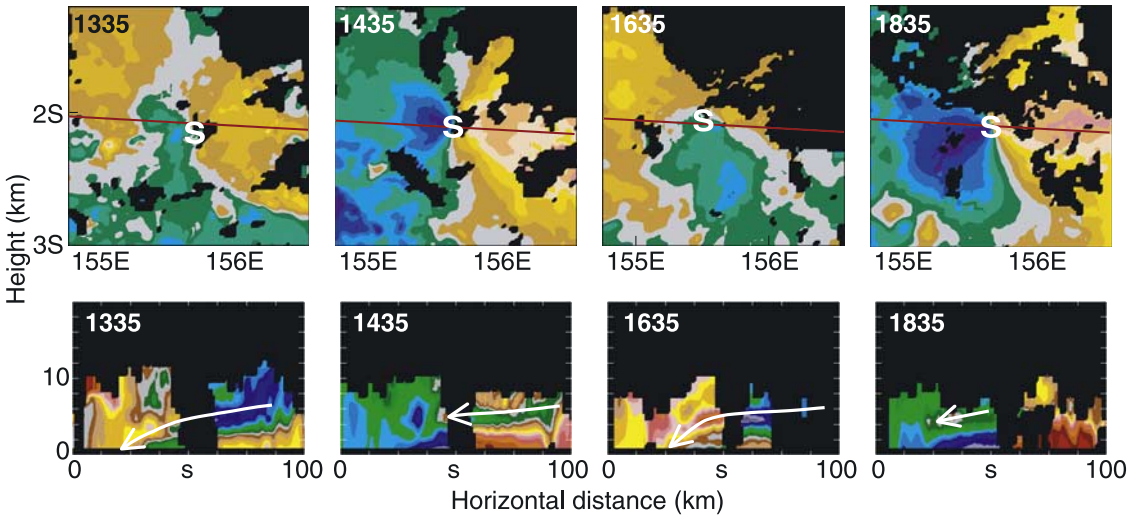

Figure 44. (top) Doppler radar radial velocity at the 0.5-km level obtained in a TOGA COARE MCS on 15 December 1992 with the radar on the ship *Xiangyanghong #5* (located at S). (bottom) Radial velocity in cross sections taken along the lines shown in the top plots. Colors indicate the radial velocity (in increments of 2 m s^{-1} in the top plots and 1 m s^{-1} in the bottom plots). Gray is centered on zero radial velocity. Cold colors indicate radial velocity toward the ship radar. Warm colors indicate radial velocity away from the radar. The color patterns in the top plots indicate a generally westerly wind across the ship at all times. The streamlines shown in the bottom plots indicate the middle level inflow subsiding and transporting momentum downward in the stratiform region of the MCS. Adapted from *Houze et al.* [2000].

cloud system indicates how the large-scale atmosphere must respond to the convection. As summarized in Figure 4, the heating profile of an MCS is composed of two modes, and the larger the contribution of the stratiform mode, the more the heating maximum intensifies and shifts to upper levels. *Nicholls et al.* [1991] and *Mapes* [1993] showed how these two modes of heating provoke distinctly different responses in the large-scale environment: The convective mode is deep (vertical wavelength twice the depth of the troposphere) and propagates rapidly, at a gravity wave speed proportional to the vertical wavelength, away from the MCS, while the stratiform mode (vertical wavelength of the depth of the troposphere) propagates away from the MCS at about half the speed of the convective mode.

[73] The distinct dichotomy of heating modes in Figure 4 has sometimes been questioned, because it is frequently difficult to identify distinctly the convective and stratiform precipitation areas in radar data. Probably this perception arises because of the wide variety of patterns of convective and stratiform precipitation that occur in MCSs [*McAnelly and Cotton*, 1989; *Houze et al.*, 1990]. It has been suggested that the convective/stratiform dichotomy might be a simplification of a more continuous spectrum of precipitation type. Observations, however, lead one to strongly reject this continuum hypothesis when considering how MCSs release heat to the atmosphere. *Mapes and Houze* [1995] performed an analysis completely independent of the reflectivity-based discrimination between convective and stratiform precipitation. They used only wind divergence profiles obtained within or in the vicinity of MCSs in TOGA COARE. These divergence profiles indicated the level-by-level mass (i.e., heating) disturbance imposed upon the large-scale environment. Mapes and Houze input the profiles into a linear spectral model, which simplified and decomposed the primitive equations into vertical wavelength components. Results of calculations with this model showed that the response of the large-scale atmosphere was dominated by two distinct modes. The faster propagating mode (52 m s^{-1}) corresponded to the convective-type

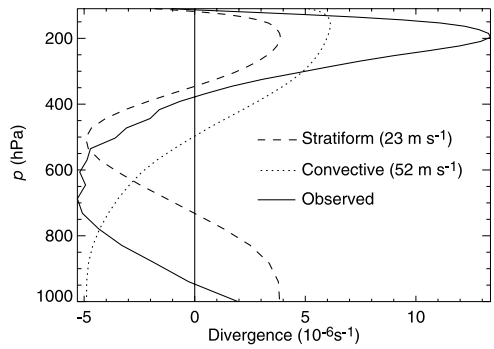

Figure 45. Divergence measured by rawinsondes when extensive, deep convection-generated cloud systems affected the intensive flux array (centered near 2°S, 156°E) over the western tropical Pacific during TOGA COARE. Sixteen cases were used to compute the net divergence (solid curve). The components of the net divergence constituted by the 52 and 23 m s^{-1} gravity wave responses to the mass disturbance are shown by the dotted and dashed curves, respectively. From *Houze* [1997], derived from calculations of *Mapes and Houze* [1995] and provided by B. Mapes, University of Colorado, Boulder.

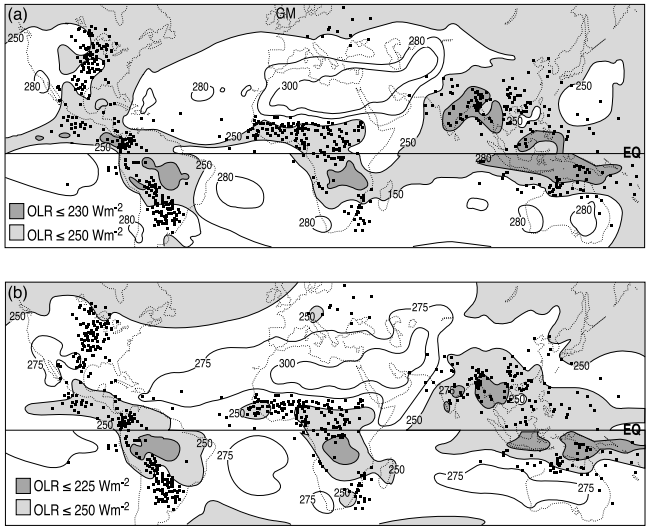

Figure 46. Global distribution of mesoscale convective complexes (dots) and regions of widespread frequent deep convection as inferred by outgoing long-wave radiation (OLR) minima (shading). From *Laing and Fritsch* [1997].

heating profile, characterized by convergence in the lower half of the troposphere and divergence in the upper half of the troposphere. The slower mode (23 m s^{-1}) corresponded to the stratiform-type heating profile, consisting of convergence in middle levels sandwiched between divergence at lower and upper levels. These two modes accounted for nearly all the net divergence (Figure 45). Since this calculation made no use whatsoever of radar reflectivity patterns or any other measurements of precipitation, it constituted a confirmation that the convective/stratiform separation of the radar echoes is the physically significant separation of modes as far as the large-scale atmospheric response to the MCS is concerned. If further subcategories of radar echo exist, the large-scale flow does not appear to care.

[74] *McAnelly et al.* [1997] found that before the rapidly moving (convective) mode propagated away, downward motion occurred in the environment and suppressed convection in the immediate environment of the MCS. However, when the slower moving (stratiform) mode dominated the environment, with upward motion in the lower troposphere, new convection was encouraged in the immediate environment, which is the effect that *Mapes* [1993] characterized as "gregarious convection."

[75] As the stratiform component of the heating becomes increasingly dominant, the more the net heating by an MCS intensifies and shifts to upper levels (Figure 4b) and the more the large-scale environment is affected by the stratiform mode of vertical velocity response. The upward shift of heating occurs in the middle stages of MCSs, as the stratiform region becomes more pronounced, and in MCCs it may last well into the later stages of the cloud system [*Cotton et al.*, 1989]. The intensification and upward shift of heating implies an increased vertical gradient of net heating by the MCS in the upper troposphere. This vertical gradient is a source of potential vorticity (PV). We have seen in section 5 that the MCV tends to form in the stratiform regions of MCSs and thus affect the lifetime and future structure and intensity of the mesoscale system. *Fritsch and Maddox* [1981a, 1981b] and *Fritsch and Brown* [1982] described the corresponding upper level anticyclonic response to the MCS. *Fritsch and Forbes* [2001] described how the PV generation by an MCS can affect the wind field in a region surrounding an individual MCS. *Nicholls et al.* [1991], *Mapes* [1993], *Mapes and Houze* [1995], and *Mapes* [1998] showed that the adjustment of the large-scale environment to the MCS heating is rapid, as the gravity wave bores move away from the system at speeds of ~50 m s^{-1} in response to the convective region heating profile and of ~20 m s^{-1} in response to the stratiform region heating profile (Figure 45). The final adjusted large-scale flow field will reflect the mean vertical gradient of heating within MCSs over a given region and time period. The greater the stratiform component of this heating, the greater is the upper level response of the large-scale circulation to the ensemble of MCSs. The response of the large-scale flow to populations of MCSs over large regions and long time periods will be discussed in section 11.

11. GLOBAL DISTRIBUTION AND IMPACTS OF MCSs

[76] Using satellite imagery, *Laing and Fritsch* [1997] have synthesized the global distribution of MCCs (Figure 46). MCCs are MCSs satisfying the definition of *Maddox* [1980]. These especially intense systems occur

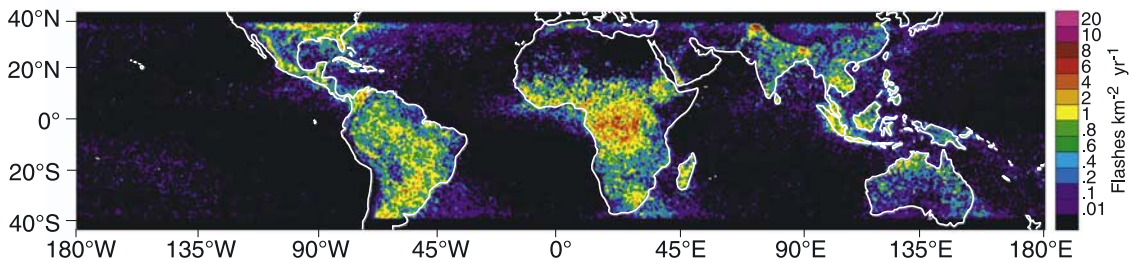

Figure 47. Annual average lightning flash density (flashes per month) for June, July, and August derived from the TRMM Lightning Image Sensor. Courtesy of S. Nesbitt, Colorado State University, Fort Collins.

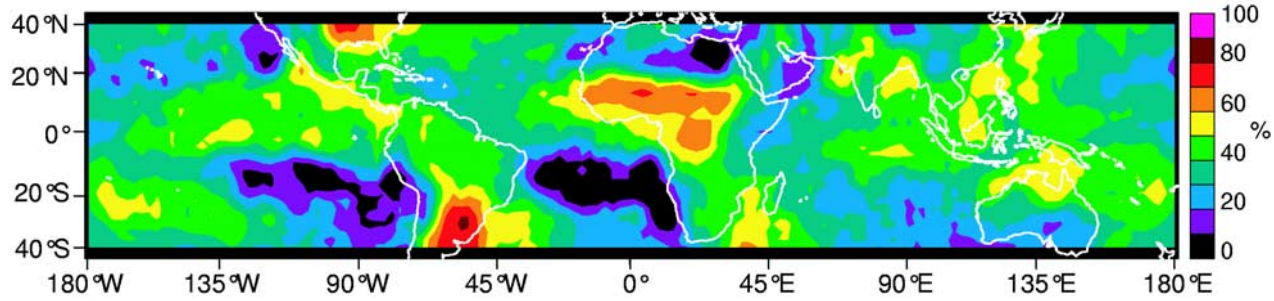

Figure 48. Percentage of MCSs detected by the TRMM Precipitation Radar (PR) that had extensive ice scattering in the 85-GHz channel of the TRMM Microwave Sensor. Derived by methods described by *Nesbitt et al.* [2000] and provided by S. Nesbitt, Colorado State University, Fort Collins.

primarily over land, where they probably benefit from the greater peak low level buoyancy generated by daytime heating. Once established, they appear to be maintained against nocturnal stabilization by a low level jet (e.g., east of the Rockies and Andes, as discussed in section 6) and/or the development of an MCV in the stratiform region of the system (section 5). Conditions over land often favor rapidly moving squall line MCSs, especially in zones of strong shear (e.g., over sub-Saharan Africa under the influence of the African easterly jet, as described by *Hamilton and Archbold* [1945], *Aspliden et al.* [1976], *Fortune* [1980], and *Hodges and Thorncroft* [1997]).

[77] The global pattern of MCSs shows other differences between land and ocean. Figure 47 shows the strong preference for lightning to occur over land. The most frequent occurrence of lightning over land is in the tropical and subtropical latitudes, with tropical Africa showing the most frequent lightning on Earth. We may safely assume that the largest proportion of lightning strikes occur in MCSs. Thus, again, we infer a dramatic difference between continental and oceanic MCSs. *Nesbitt et al.* [2000], using data from the Tropical Rainfall Measuring Mission (TRMM) satellite, obtained a similar and consistent result. They examined passive microwave radiance in the 85-GHz channel of the TRMM Microwave Imager (TMI) in combination with data from the TRMM Precipitation Radar (PR) (Figure 48). The tropical continental MCSs identified in this analysis exhibited strong scattering of the 85-GHz signal in the locations of most frequent lightning (see Figure 47). An extremely strong contrast in the ice-scattering characteristics of convection over land and ocean is evident between the sub-Saharan African continent and the adjacent tropical Atlantic Ocean (Figure 48).

[78] Differences between land and ocean convection are further evident in TRMM PR data. Figure 49a shows the TRMM PR annual mean rainfall, while Figure 49b shows the fraction of that rainfall categorized as stratiform. The largest stratiform fractions occur over the oceanic ITCZs of the Pacific and Atlantic.

[79] The Atlantic ITCZ stratiform rain fraction of over 40% contrasts with 20–30% stratiform over the adjacent African continent. The stratiform rain in these regions falls almost exclusively from the stratiform regions of MCSs. The stratiform regions of MCSs consist of deep ice clouds, extending in altitude from ~5 km to the tropopause. The TRMM data in Figure 49b therefore

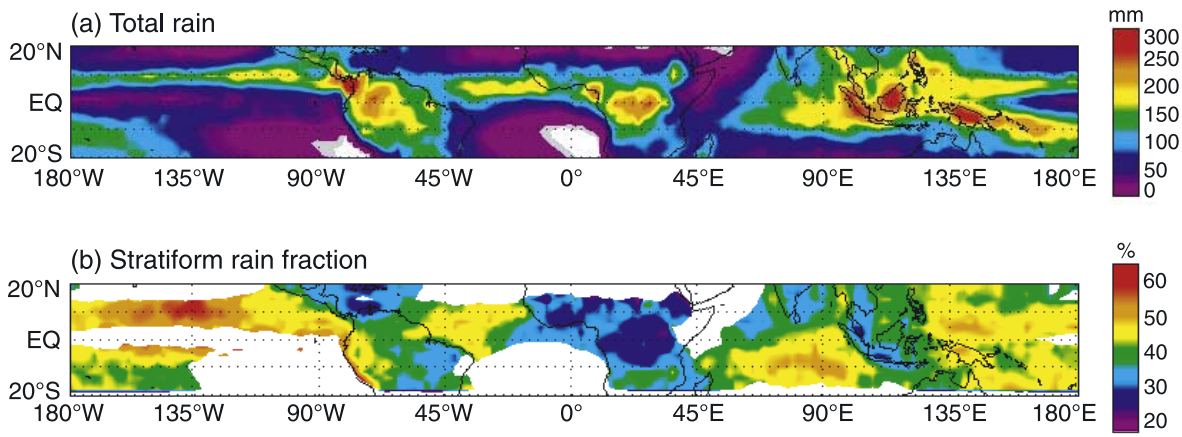

Figure 49. (a) Annual rainfall and (b) fraction of the annual rainfall that is stratiform, as determined from the TRMM PR by methods described by *Schumacher and Houze* [2003]. Courtesy of C. Schumacher.

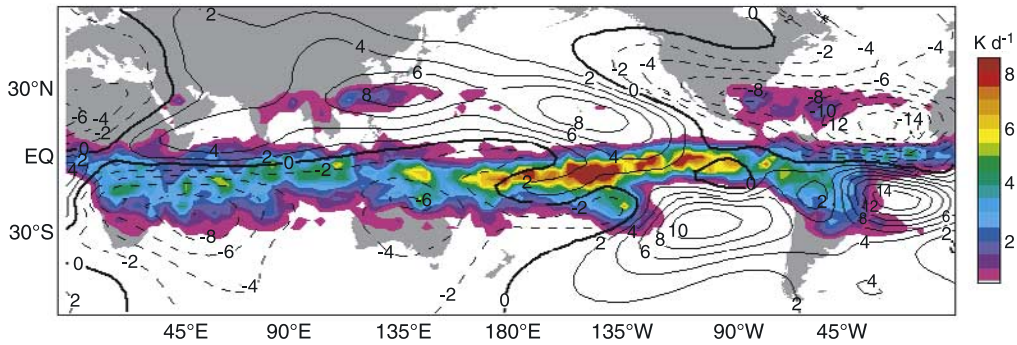

Figure 50. Contours of the 250-hPa stream function anomaly pattern computed from the TRMM precipitation-based heating for the 4-month El Niño season of 1998. The heating was based on the convective and stratiform components of the precipitation observed by the TRMM PR. Colored shading shows the heating at 400 hPa. The basic state wind field was determined from National Centers for Environmental Prediction (NCEP) reanalysis fields for the same time period as the precipitation. The stream function contour interval is 10^6 m^2 s^{-1}; negative contours are dashed. From *Schumacher et al.* [2004].

suggest more ice cloud over the ocean than over land. However, Figure 48 indicates greater microwave scattering by ice particles over the African continent than over the tropical Atlantic. From these two data sets it may be hypothesized that while deep stratiform ice clouds are more prevalent and produce more rain over the ocean than over land, the ice particles in the oceanic precipitating clouds are of a different nature than those in continental MCSs. Probably, the continental convection has higher buoyancy at low levels, stronger updrafts, more growth of ice particles by riming in convective cells, and more transport of large ice particles to upper levels by the convective updrafts. Since the lapse rates over the ocean tend to be closer to moist adiabatic, the buoyancy at low levels is less, and the updrafts are less likely to produce as much growth by riming and correspondingly less likely to produce large graupel particles and carry them to upper levels. Hence it is not surprising that the oceanic MCSs produce less ice scattering and less lightning. These differences between ice particles in continental and oceanic MCSs need to be verified by independent observations.

[80] The TRMM data in Figures 48 and 49b also provide an interesting comparison between the continents of Africa and South America. The MCSs over South America have higher stratiform rain fractions and lower ice scattering than do the MCSs over Africa. The South American MCSs have been investigated with polarimetric radar in recent field studies [e.g., *Cifelli et al.*, 2002]. Comparable polarimetric radar data sets need to be obtained over equatorial Africa before the differences between the two regions can be understood. Such measurements have been proposed as part of the African Monsoon Multidisciplinary Analysis Project (see the AMMA science plan at www.joss.ucar.edu/amma/).

[81] The Pacific ITCZ exhibits the highest stratiform rain fractions found anywhere in the tropics (over 60% in the annual mean pattern, see Figure 49b). As discussed in section 9, the larger the stratiform component of heating, the more the maximum of the net heating shifts to upper levels (Figure 4). *Schumacher et al.* [2004] estimated the global pattern of heating associated with tropical precipitation, as measured by the TRMM PR, by assigning heating profiles like those in Figure 4 to the TRMM PR rain field according to the amount of total rain that was stratiform at that location. Figure 50 shows an example of the heating field estimated in this way for an El Niño period, January–April 1998. The heating pattern at 400 hPa exhibits a maximum in the central tropical Pacific. This maximum at upper levels is accentuated by the fact that the stratiform rain fraction tends to be maximum in this region. The stratiform rain fraction maximum seen in this region annually (Figure 49b) is even more pronounced in the El Niño time period, when it reaches nearly 70%. The large magnitude of the stratiform rain fraction in this region means that the magnitude and altitude of the maximum heating is highest in this region at this time (as shown in Figure 4b). *Schumacher et al.* [2004] used this heating field as input to a simplified climate model and estimated the steady state response to the heating. As expected from theoretical calculations [*Gill*, 1980], counterrotating anticyclonic gyres characteristic of the Kelvin-Rossby wave response to the heating occur and extend into the subtropical latitudes. In a non-El Niño year (not shown) these gyres are weaker and located west of their location in Figure 50.

[82] The horizontal variability of the stratiform rain amount (obtained by multiplying the stratiform rain fraction in Figure 49b with the TRMM PR rain field in Figure 49a) leads to horizontal variation of the vertical profile of heating (Figure 4). Figure 51a shows a vertical cross section of the climate model–derived large-scale vertical motion (ω) and zonal wind along the equatorial belt outlined in Figure 50. The vertical motion is approximately proportional to the heating, while the zonal wind indicates the large-scale response to the heating. In the region of maximum stratiform rain fraction in the central Pacific ($\sim$150°W) the heating is concentrated at upper levels, as required by the nearly 70% stratiform rain fraction in that region, and the corresponding

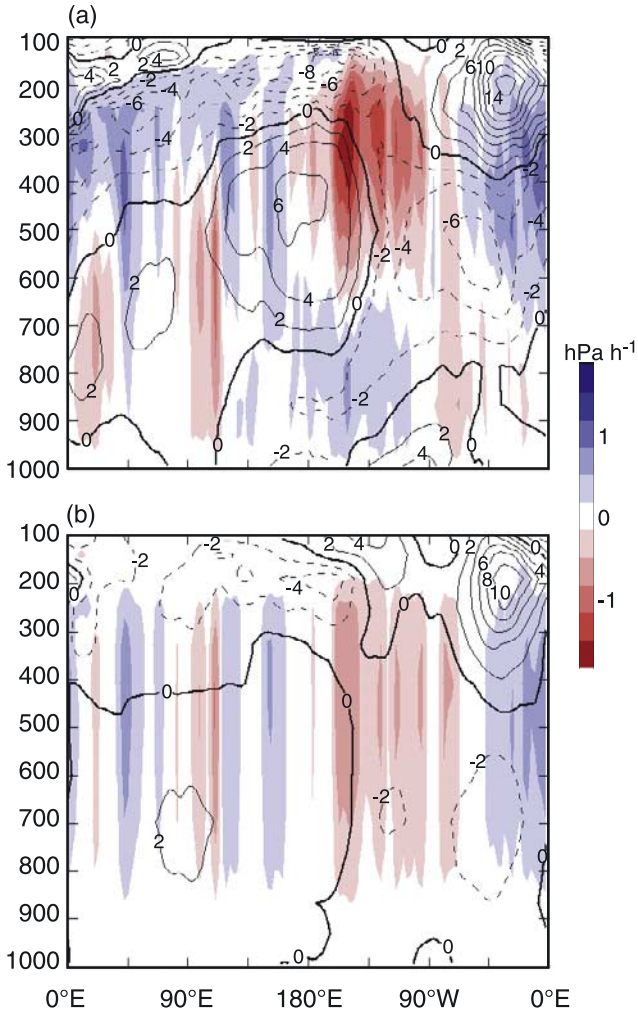

Figure 51. Vertical cross sections of anomaly fields of vertical motion (shaded) and zonal wind (contours in m s^{-1}, easterlies dashed) averaged along the equator from 8.5°N to 8.5°S for the NCEP reanalysis basic state for El Niño (January, February, March, and April 1998) and latent heating derived from the TRMM PR-observed precipitation. (a) Observed, spatially variable stratiform rain fraction shown by the TRMM PR. (b) A stratiform rain fraction assumed to be a uniform 40% (the tropics-wide average). In this case the circulation is weak and without structure. The structure seen in the observed case (Figure 51a) derives from the spatial variability of the stratiform rain fraction. From *Schumacher et al.* [2004].

zonal wind response is strongly divergent and highly concentrated at upper levels. In contrast, over the Indonesian region (~100°–120°E), where the stratiform rain fraction is <30%, the heating maximum is much lower and the upper level zonal wind response is weaker and spread over a deeper layer. This rich structure and intensity of the response of the large-scale circulation to the heating is lost if the stratiform rain fraction is not allowed to vary spatially but rather is assumed to be a constant 40% (the tropics-wide average) over the whole tropics (Figure 51b). Since the stratiform rain fraction is determined by the MCS population, it is clear that the variability of the MCS population over Earth is a vital element in the nature of the global circulation.

12. CONCLUSIONS

[83] Studies of MCSs over the past 10–15 years have led to new views of the structure, dynamics, and large-scale impacts of these important cloud systems. This review has highlighted the following new insights.

[84] The defining process of a convective cloud system is the nature of its vertical air motions, which arise from the buoyancy provided by the ambient thermodynamic stratification. Convective clouds have long been viewed as forming from buoyant bubbles or "parcels" of air emanating from the planetary boundary layer. While this view certainly describes nearly all smaller convective clouds, the organized vertical circulation in a large, mature MCS takes on a different type of organization, which is better described by layer lifting than parcel concepts. The upward air motion in an MCS may begin in the form of buoyant convective-scale parcels rooted in the boundary layer and rising high into the upper troposphere; however, after the MCS matures, a layer of air much deeper than the boundary layer enters and rises on a slantwise path through the system. This layer is often potentially unstable and overturns but, nonetheless, remains a coherent unit as it rises through the system. The overturning within the layer allows the highest-θ_e air to ascend to the top of the system. The nature of the overturning within the layer remains a topic of research; however, evidence from modeling suggests that buoyant elements triggered at the nose of the cold pool of an MCS develop characteristics of trapped gravity waves as they propagate rearward into the stratiform region. They also may develop a lateral component of overturning in the form of longitudinal rolls.

[85] The slantwise layer ascent appears to be part of a gravity wave response to the mean latent heat release in the convective region of an MCS. The layer lifting promotes the formation of the broad saturated upper stratiform cloud region of the MCS. Middle level inflow entering the stratiform region of an MCS and passing under the stratiform cloud deck is also a part of the gravity wave response to the heating in the convective region of the MCS. The middle level inflow initially enters the stratiform region from a direction controlled by the large-scale wind in the environment of the MCS. This middle level inflow is accelerated inward by pressure gradient forces within the MCS and effectively feeds the mesoscale downdraft. The subsidence results from cooling by sublimation of snow below the anvil on the outer perimeter of the system and by melting and evaporation of precipitation particles in the interior of the stratiform region of the MCS. An MCS does not always take the form of a crisply defined leading convective line with a trailing-stratiform region; however, it tends always to have a stratiform region with a middle level inflow guided into the system by the environmental relative wind. The "rear inflow" behind squall lines appears to be a particularly clear example of the more general phenomenon of middle level inflow into and mesoscale

descent within the lower reaches of a stratiform region of an MCS.

[86] A mesoscale vortex (MCV) tends to form in middle levels at the base of the stratiform cloud deck of the MCS. This vortex initiates in some cases as a "bookend," forming at the end of a convective line. In midlatitudes the Coriolis force enhances the cyclonic bookend vortex. The Coriolis-enhanced MCV accounts for the asymmetric squall line structure that often occurs in midlatitudes but seldom if ever in the tropics. The MCV, which is most prominent in longer-lived MCCs, tends to become inertially stable because the saturated conditions in the stratiform upper level cloud deck reduce the value of the static stability and hence decrease the Rossby radius of deformation. The inertial stability of the vortex suggests that it becomes a quasi-balanced flow maintained by a secondary vertical circulation, which, in turn, prolongs the life of the MCS by triggering new convection on the edges of the system. The MCV, or a weaker form of it, also occurs in MCSs in the tropics, where the Coriolis effect is weaker. The tropical MCVs may be a key factor in the development of an MCS into a tropical cyclone. Tropical cyclones tend to spin up as the MCVs of two or more MCSs rotate around a common centroid, which develops into the center of the cyclone. The mechanism by which the middle level cyclone congeals and builds downward toward the ocean surface is not clear.

[87] Several factors contribute to MCS propagation. In addition to the direct lifting of unstable air by an advancing cold pool, wave dynamics may affect the system propagation. The mass divergence produced by the heating profile of an MCS generates bores moving at gravity wave speed. The slower, shorter-wavelength bores may give the MCS an aspect of discrete propagation as the bores trigger new convective cells at a distance from the cold pool. These new cells may be incorporated by the convective region or form an entirely new convective region while an older convective region weakens and becomes stratiform.

[88] Waves generated external to the MCS may phase lock with the MCS as they continue to propagate. The pattern of movement of some larger MCSs suggests cooperation between the wave and an MCS in a manner seemingly consistent with wave-CISK concepts. In this case the velocity of movement of the MCS becomes one and the same with that of the wave. This velocity may be in a different direction than the preferred direction of cold pool propagation. Some MCSs bifurcate, with one portion directed by wave propagation and the other directed by cold pool propagation.

[89] The development and continual regeneration of the stratiform region determines the spatial size attained by an MCS. The stratiform region consists of material from previously active convective cells. This material is left behind as cells weaken or the tops of active cells are sheared off. The ultimate size of the stratiform region is therefore determined by the ability of the MCS to regenerate new convection. The amount of active convective activity supported at a given time in a given region is limited. If the stratiform elements have a dissipation time that is greater than the active cell lifetime, the stratiform region grows in size. Over time a balance can be reached between the formation rate of new convective precipitation and old stratiform precipitation. However, the number of convective cells possible at a given time limits this maximum size. MCSs reach this maximum size only if the environment is able to sustain the maximum number of cells over a long time period. Such an environment is said to possess "sustainability." One factor enhancing sustainability is a boundary layer that has a favorable thermodynamic structure that remains in place over a long period of time in the vicinity of the MCS. The highest stratiform rain fractions occur over the oceans, where a moist warm boundary layer exists over broad expanses, while over land, stratiform region development is limited, evidently because the warm moist boundary layer usually becomes stable at night. An exception occurs over land when a low level jet replenishes the boundary layer through the night, thus creating a continually replenished boundary layer capable of sustaining an MCS for a long period of time.

[90] For midlatitude MCCs, especially those that develop a strong MCV, the Rossby radius probably sets the maximum size of the system. In near-equatorial regions, where the Coriolis effect is small, a strong MCV is not favored. Apparently, this consideration indicates why MCSs tend to reach their maximum observed sizes over the west Pacific Ocean warm pool, where the broad expanse of high sea surface temperature gives the environment an essentially infinite sustainability. New convection can continue to form for an indefinite time period in and near an active MCS. The ultimate MCS size is therefore determined by a balance stage in which the MCS area covered by old stratiform components is disappearing with age at the same rate that a new convective area is being created by continuous or discrete propagation and that old convection is converting to stratiform cloud and precipitation.

[91] MCSs vertically redistribute momentum by two processes: horizontal acceleration by pressure gradient forces that develop within the system and vertical eddy fluxes associated with their internal circulations. Two-dimensional, steady state idealizations describe well the momentum redistribution by squall line MCSs but have difficulty describing the momentum redistribution in all the diverse MCS structures that occur. Dividing the systems into convective and stratiform components separates the momentum redistribution into fundamental components that vary from one MCS to the next. The net change in the environmental momentum profile can be strongly affected by the stratiform component, and the final vertical profile of momentum in the environment is a function of the size of the stratiform region relative to the convective region.

[92] The vertical profile of heating also varies systematically between the convective and stratiform regions of MCSs, without regard to whether the internal arrangement of the convective and stratiform components has a leading-line/trailing-stratiform structure or not. The distinctly characteristic heating profiles of the convective and stratiform regions constitute two distinct wavelengths of forcing; the convective heating wavelength is $2H$, while the stratiform wavelength is H, where H represents the depth of the

troposphere. These two wavelengths of forcing produce distinct effects on the large-scale environment of the MCS; as the stratiform component of the heating becomes greater, the more the net heating by an MCS intensifies and shifts to upper levels. Analyses of wind data within and surrounding MCSs show that these two modes dominate the divergent response of the environment to the MCS. Since only the convective and stratiform modes are significant to the large-scale response to the MCS, additional categories of radar echo structure, though perhaps helpful in other pursuits, are not necessary to understand the heating impact of MCSs on the large-scale wind field.

[93] MCS structures exhibit subtle but important variations from one geographical/climatic regime to another. In the tropics, deep stratiform ice clouds are more prevalent and produce more rain over the ocean than over the land. Passive microwave radiances at 85 GHz suggest that the ice particles in the oceanic precipitating clouds are systematically smaller than over the land. The convective cells within the MCSs over continents likely have higher buoyancy at low levels and therefore stronger updrafts, more growth of ice particles by riming in convective cells, and more transport of large ice particles to upper levels.

[94] Global horizontal variability of the stratiform rain amount from MCSs leads to horizontal variation of the vertical profile of heating. This variation is especially evident across the tropics. The central Pacific ITCZ exhibits the highest stratiform rain fractions in the tropics (over 60% in the annual mean pattern and over 70% during El Niño–Southern Oscillation periods). This variability in MCS structure leads to variation of the upper level response to MCSs. The upper level flow response to the MCSs is strongest and most elevated in altitude in connection with the central Pacific ITCZ. Accounting for the spatial variability of the stratiform rain fraction is thus essential to capturing accurately the large-scale atmospheric response to MCSs.

[95] **ACKNOWLEDGMENTS.** The author appreciates the invitation extended by Brian Colle and James Doyle to present an overview of mesoscale convective systems at the American Meteorological Society's *10th Conference on Mesoscale Processes*, Portland, Oregon, in June 2003. That invitation and presentation was the stimulus for this review article. The author is grateful for helpful comments on the manuscript from W. R. Cotton, Dale Durran, Robert Fovell, Mitchell Moncrieff, Joanne Simpson, Bradley Smull, and Sandra Yuter. Candace Gudmundson edited the manuscript, and Kay Dewar and Beth Tully refined the figures. The author's work on this paper was supported by NASA grants NAG5-9668, NAG5-13654, NAG5-11685, and NSF ATM-9900710 and by the Joint Institute for the Study of the Atmosphere and Ocean under NOAA Cooperative Agreements NA17RJ1232 and NA67R50155, contribution number 1047.

[96] The Editor responsible for this paper was Kendal McGuffie. He thanks two anonymous reviewers and one cross-disciplinary reviewer.

REFERENCES

Abdullah, A. J. (1949), Cyclogenesis by a purely mechanical process, *J. Meteorol.*, *6*, 86–97.

Arakawa, A., and W. Schubert (1974), Interaction of a cumulus cloud ensemble with the large-scale environment, *J. Atmos. Sci.*, *35*, 674–701.

Aspliden, C. L., Y. Tourre, and J. B. Sabine (1976), Some climatological aspects of West African disturbance lines during GATE, *Mon. Weather Rev.*, *104*, 1029–1035.

Bartels, D. L., and R. A. Maddox (1991), Midlevel cyclonic vortices generated by mesoscale convective systems, *Mon. Weather Rev.*, *119*, 104–118.

Bister, M., and K. A. Emanuel (1997), The genesis of Hurricane Guillermo: TEXMEX analyses and a modeling study, *Mon. Weather Rev.*, *125*, 2662–2682.

Bosart, L. F., and F. Sanders (1981), The Johnstown flood of July 1977: A long-lived convective system, *J. Atmos. Sci.*, *38*, 1616–1642.

Braun, S. A., and R. A. Houze Jr. (1997), The evolution of the 10–11 June 1985 PRE-STORM squall line: Initiation, development of rear inflow, and dissipation, *Mon. Weather Rev.*, *125*, 478–504.

Bretherton, C. S., and P. K. Smolarkiewicz (1989), Gravity waves, compensating subsidence, and detrainment around cumulus clouds, *J. Atmos. Sci.*, *46*, 740–759.

Browning, K. A., J. C. Fankhauser, J.-P. Chalon, P. J. Eccles, R. C. Strauch, F. H. Merrem, D. J. Musil, E. L. May, and W. R. Sand (1976), Structure of an evolving hailstorm. Part V: Synthesis and implications for hail growth and hail suppression, *Mon. Weather Rev.*, *104*, 603–610.

Bryan, G. H., and J. M. Fritsch (2000), Moist absolute instability: The sixth static stability state, *Bull. Am. Meteorol. Soc.*, *81*, 1207–1230.

Bryan, G. H., and J. M. Fritsch (2003), On the existence of convective rolls in the convective region of squall lines, paper presented at 10th Conference on Mesoscale Processes, Am. Meteorol. Soc., Portland, Oreg., 23–27 June.

Carbone, R. E., J. D. Tuttle, D. A. Ahijevych, and S. B. Trier (2002), Inferences of predictability associated with warm season precipitation episodes, *J. Atmos. Sci.*, *59*, 2033–2056.

Charney, J. G., and A. Eliassen (1964), On the growth of the hurricane depression, *J. Atmos. Sci.*, *21*, 68–75.

Chen, S. S., and W. M. Frank (1993), A numerical study of the genesis of extratropical convective mesovortices. Part I: Evolution and dynamics, *J. Atmos. Sci.*, *50*, 2401–2426.

Chen, S. S., and R. A. Houze Jr. (1997), Diurnal variation and life-cycle of deep convective systems over the tropical Pacific warm pool, *Q. J. R. Meteorol. Soc.*, *123*, 357–388.

Chen, S. S., R. A. Houze Jr., and B. E. Mapes (1996), Multiscale variability of deep convection in relation to large-scale circulation in TOGA COARE, *J. Atmos. Sci.*, *53*, 1380–1409.

Chong, M., P. Amayenc, G. Scialom, and J. Testud (1987), A tropical squall line observed during the COPT 81 experiment in West Africa. Part I: Kinematic structure inferred from dual-Doppler radar data, *Mon. Weather Rev.*, *115*, 670–694.

Churchill, D. D., and R. A. Houze Jr. (1984), Development and structure of winter monsoon cloud clusters on 10 December 1978, *J. Atmos. Sci.*, *41*, 933–960.

Cifelli, R., W. A. Petersen, L. D. Carey, S. A. Rutledge, and M. A. F. Silva Dias (2002), Radar observations of the kinematic, microphysical, and precipitation characteristics of two MCSs in TRMM LBA, *J. Geophys. Res.*, *107*(D20), 8077, doi:10.1029/2000JD000264.

Corfidi, S. F., J. H. Merritt, and J. M. Fritsch (1996), Predicting the movement of mesoscale convective complexes, *Weather Forecasting*, *11*, 41–46.

Cotton, W. R., and R. A. Anthes (1989), *Storm and Cloud Dynamics*, 881 pp., Academic, San Diego, Calif.

Cotton, W. R., M.-S. Lin, R. L. McAnelly, and C. J. Tremback (1989), A composite model of mesoscale convective complexes, *Mon. Weather Rev.*, *117*, 765–783.

Cram, J. M., R. A. Pielke, and W. R. Cotton (1992), Numerical simulation and analysis of a prefrontal squall line. Part

II: Propagation of the squall line as an internal gravity wave, *J. Atmos. Sci.*, *49*, 209–225.

Crook, N. A., and M. W. Moncrieff (1988), The effect of large-scale convergence on the generation and maintenance of deep moist convection, *J. Atmos. Sci.*, *45*, 3606–3624.

Davies, H. C. (1979), Phase-lagged wave-CISK, *Q. J. R. Meteorol. Soc.*, *105*, 325–353.

Davis, C. A., and M. L. Weisman (1994), Balanced dynamics of mesoscale vortices produced in simulated convective systems, *J. Atmos. Sci.*, *51*, 2005–2030.

Emanuel, K. A. (1982), Inertial instability and mesoscale convective systems. Part II: Symmetric CISK in a baroclinic flow, *J. Atmos. Sci.*, *39*, 1080–1097.

Fortune, M. (1980), Properties of African squall lines inferred from time-lapse satellite imagery, *Mon. Weather Rev.*, *108*, 153–168.

Fortune, M. A., W. R. Cotton, and R. L. McAnelly (1992), Frontal-wave-like evolution in some mesoscale convective complexes, *Mon. Weather Rev.*, *120*, 1279–1300.

Fovell, R. G. (2002), Upstream influence of numerically simulated squall line storms, *Q. J. R. Meteorol. Soc.*, *128*, 893–912.

Fovell, R. G., and P.-H. Tan (1998), The temporal behavior of numerically simulated multicell-type storms. Part II: The convective cell life cycle and cell regeneration, *Mon. Weather Rev.*, *126*, 551–577.

Fritsch, J. M., and J. M. Brown (1982), On the generation of convectively driven mesohighs aloft, *Mon. Weather Rev.*, *110*, 1554–1563.

Fritsch, J. M., and G. S. Forbes (2001), Mesoscale convective systems, *Meteorol. Monogr.*, *28*, 323–357.

Fritsch, J. M., and R. A. Maddox (1981a), Convectively driven mesoscale weather systems aloft. Part I. Observations, *J. Appl. Meteorol.*, *20*, 9–19.

Fritsch, J. M., and R. A. Maddox (1981b), Convectively driven mesoscale weather systems aloft. Part II. Numerical simulations, *J. Appl. Meteorol.*, *20*, 20–26.

Fritsch, J. M., J. D. Murphy, and J. S. Kain (1994), Warm core vortex amplification over land, *J. Atmos. Sci.*, *51*, 1781–1806.

Gamache, J. F., and R. A. Houze Jr. (1982), Mesoscale air motions associated with a tropical squall line, *Mon. Weather Rev.*, *110*, 118–135.

Gill, A. (1980), Some simple solutions for heat-induced tropical circulation, *Q. J. R. Meteorol. Soc.*, *106*, 447–462.

Gill, A. E. (1982), Studies of moisture effects in simple atmospheric models: The stable case, *Geophys. Astrophys. Fluid Dyn.*, *19*, 119–152.

Hamilton, R. A., and J. W. Archbold (1945), Meteorology of Nigeria and adjacent territory, *Q. J. R. Meteorol. Soc.*, *71*, 231–262.

Hayashi, Y. (1970), A theory of large-scale equatorial waves generated by condensation heat and accelerating the zonal wind, *J. Meteorol. Soc. Jpn.*, *48*, 140–160.

Hodges, K. I., and C. D. Thorncroft (1997), Distribution and statistics of African mesoscale convective weather systems based on the ISCCP Meteosat imagery, *Mon. Weather Rev.*, *125*, 2821–2837.

Houze, R. A., Jr. (1977), Structure and dynamics of a tropical squall-line system, *Mon. Weather Rev.*, *105*, 1540–1567.

Houze, R. A., Jr. (1982), Cloud clusters and large-scale vertical motions in the tropics, *J. Meteorol. Soc. Jpn.*, *60*, 396–410.

Houze, R. A., Jr. (1993), *Cloud Dynamics*, 573 pp., Academic, San Diego, Calif.

Houze, R. A., Jr. (1997), Stratiform precipitation in regions of convection: A meteorological paradox?, *Bull. Am. Meteorol. Soc.*, *78*, 2179–2196.

Houze, R. A., Jr., and A. K. Betts (1981), Convection in GATE, *Rev. Geophys.*, *19*, 541–576.

Houze, R. A., Jr., and E. N. Rappaport (1984), Air motions and precipitation structure of an early summer squall line over the eastern tropical Atlantic, *J. Atmos. Sci.*, *41*, 553–574.

Houze, R. A., Jr., S. A. Rutledge, M. I. Biggerstaff, and B. F. Smull (1989), Interpretation of Doppler weather-radar displays in mid-latitude mesoscale convective systems, *Bull. Am. Meteorol. Soc.*, *70*, 608–619.

Houze, R. A., Jr., B. F. Smull, and P. Dodge (1990), Mesoscale organization of springtime rainstorms in Oklahoma, *Mon. Weather Rev.*, *118*, 613–654.

Houze, R. A., Jr., S. S. Chen, D. E. Kingsmill, Y. Serra, and S. E. Yuter (2000), Convection over the Pacific warm pool in relation to the atmospheric Kelvin-Rossby wave, *J. Atmos. Sci.*, *57*, 3058–3089.

Jorgensen, D., and B. F. Smull (1993), Mesovortex circulations seen by airborne Doppler radar within a bow echo mesoscale convective system, *Bull. Am. Meteorol. Soc.*, *74*, 2146–2157.

Kingsmill, D. E., and R. A. Houze Jr. (1999a), Kinematic characteristics of air flowing into and out of precipitating convection over the west Pacific warm pool: An airborne Doppler radar survey, *Q. J. R. Meteorol. Soc.*, *125*, 1165–1207.

Kingsmill, D. E., and R. A. Houze Jr. (1999b), Thermodynamic characteristics of air flowing into and out of precipitating convection over the west Pacific warm pool, *Q. J. R. Meteorol. Soc.*, *125*, 1209–1229.

Klimowski, B. A. (1994), Initiation and development of rear inflow within the 28–29 June 1989 North Dakota mesoconvective system, *Mon. Weather Rev.*, *122*, 765–779.

Knievel, J. C., and R. H. Johnson (2002), The kinematics of a midlatitude, continental mesoscale convective system and its mesoscale vortex, *Mon. Weather Rev.*, *130*, 1749–1770.

Knievel, J. C., and R. H. Johnson (2003), A scale-discriminating vorticity budget for a mesoscale vortex in a midlatitude, continental mesoscale convective system, *J. Atmos. Sci.*, *60*, 781–794.

Lafore, J.-P., and M. W. Moncrieff (1989), A numerical investigation of the organization and interaction of the convective and stratiform regions of tropical squall lines, *J. Atmos. Sci.*, *46*, 521–544.

Laing, A. G., and J. M. Fritsch (1997), The global population of mesoscale convective complexes, *Q. J. R. Meteorol. Soc.*, *123*, 389–405.

Leary, C. A. (1980), Temperature and humidity profiles in mesoscale unsaturated downdrafts, *J. Atmos. Sci.*, *37*, 1005–1012.

Leary, C. A., and R. A. Houze Jr. (1979), Melting and evaporation of hydrometeors in precipitation from anvil clouds of deep tropical convection, *J. Atmos. Sci.*, *36*, 669–679.

LeMone, M. A. (1983), Momentum transport by a line of cumulonimbus, *J. Atmos. Sci.*, *40*, 1815–1834.

Ligda, M. G. H. (1956), The radar observations of mature prefrontal squall lines in the midwestern United States, in *Summary of the Lectures Held During the VI Congress of OSTIV in St-Yan, France, 6–14 July 1956 and Other Selected Technical and Meteorological Papers*, *Publ. IV*, 3 pp., Organ. Sci. et Tech. Int. du Vol a Voile, Bleiswijk, Netherlands.

Lindzen, R. S. (1974), Wave-CISK in the tropics, *J. Atmos. Sci.*, *31*, 156–179.

Loehrer, S. M., and R. H. Johnson (1995), Surface pressure and precipitation life cycle characteristics of PRE-STORM mesoscale convective systems, *Mon. Weather Rev.*, *123*, 600–621.

Ludlam, F. H. (1980), *Clouds and Storms: The Behavior and Effect of Water in the Atmosphere*, 405 pp., Pa. State Univ. Press, University Park, Pa.

Maddox, R. A. (1980), Mesoscale convective complexes, *Bull. Am. Meteorol. Soc.*, *61*, 1374–1387.

Mapes, B. E. (1993), Gregarious tropical convection, *J. Atmos. Sci.*, *50*, 2026–2037.

Mapes, B. E. (1998), The large-scale part of tropical mesoscale convective system circulations: A linear vertical spectral band model, *J. Meteorol. Soc. Jpn.*, *76*, 29–55.

Mapes, B. E., and R. A. Houze Jr. (1995), Diabatic divergence profiles in western Pacific mesoscale convective systems, *J. Atmos. Sci.*, *52*, 1807–1828.

Mapes, B. E., T. T. Warner, and M. Xu (2003), Diurnal patterns of rainfall in northwestern South America, Part III: Diurnal gravity waves and nocturnal convection offshore, *Mon. Weather Rev.*, *131*, 830–844.

Matsuno, T. (1966), Quasi-geostrophic motions in the equatorial area, *J. Meteorol. Soc. Jpn.*, *44*, 25–43.

McAnelly, R. L., and W. R. Cotton (1989), The precipitation life cycle of mesoscale convective complexes, *Mon. Weather Rev.*, *117*, 784–808.

McAnelly, R. L., J. E. Nachamkin, W. R. Cotton, and M. E. Nicholls (1997), Upscale evolution of MCSs; Doppler radar analysis and analytical investigation, *Mon. Weather Rev.*, *125*, 1083–1110.

Mechem, D. B., R. A. Houze Jr., and S. S. Chen (2002), Layer inflow into precipitating convection over the western tropical Pacific, *Q. J. R. Meteorol. Soc.*, *128*, 1997–2030.

Menard, R. D., and J. M. Fritsch (1989), A mesoscale convective complex-generated inertially stable warm core vortex, *Mon. Weather Rev.*, *117*, 1237–1261.

Miller, D., and J. M. Fritsch (1991), Mesoscale convective complexes in the western Pacific region, *Mon. Weather Rev.*, *119*, 2978–2992.

Moncrieff, M. W. (1978), The dynamical structure of two-dimensional steady convection in constant vertical shear, *Q. J. R. Meteorol. Soc.*, *104*, 543–568.

Moncrieff, M. W. (1981), A theory of organised steady convection and its transport properties, *Q. J. R. Meteorol. Soc.*, *107*, 29–50.

Moncrieff, M. W. (1992), Organized convective systems: Archetypal dynamical models, mass and momentum flux theory, and parameterization, *Q. J. R. Meteorol. Soc.*, *118*, 819–850.

Moncrieff, M. W., and E. Klinker (1997), Organized convective systems in the tropical western Pacific as a process in general circulation models: A TOGA COARE case-study, *Q. J. R. Meteorol. Soc.*, *123*, 805–827.

Moncrieff, M. W., and M. J. Miller (1976), The dynamics and simulation of tropical squall lines, *Q. J. R. Meteorol. Soc.*, *102*, 373–394.

Nakazawa, T. (1988), Tropical super clusters within intraseasonal variations over the western Pacific, *J. Meteorol. Soc. Jpn.*, *66*, 823–839.

Nehrkorn, T. (1986), Wave-CISK in a baroclinic base state, *J. Atmos. Sci.*, *43*, 2773–2791.

Nesbitt, S. W., E. J. Zipser, and D. J. Cecil (2000), A census of precipitation features in the tropics using TRMM: Radar, ice scattering, and ice observations, *J. Clim.*, *13*, 4087–4106.

Nicholls, M. E., R. A. Pielke, and W. R. Cotton (1991), Thermally forced gravity waves in an atmosphere at rest, *J. Atmos. Sci.*, *48*, 1869–1884.

Olsson, P. Q., and W. R. Cotton (1997), Balanced and unbalanced circulations in a primitive equation simulation of a midlatitude MCC. Part II: Analysis of balance, *J. Atmos. Sci.*, *54*, 479–497.

Ooyama, K. V. (1971), A theory on parameterization of cumulus convection, *J. Meteorol. Soc. Jpn.*, *49*, 744–756.

Pandya, R., and D. Durran (1996), The influence of convectively generated thermal forcing on the mesoscale circulation around squall lines, *J. Atmos. Sci.*, *53*, 2924–2951.

Parker, M. D., and R. H. Johnson (2000), Organizational modes of midlatitude mesoscale convective systems, *Mon. Weather Rev.*, *128*, 3413–3436.

Payne, S. W., and M. M. McGarry (1977), The relationship of satellite inferred convective activity to easterly waves over West Africa and the adjacent ocean during phase III of GATE, *Mon. Weather Rev.*, *105*, 413–420.

Raymond, D. J. (1976), Wave-CISK and convective mesosystems, *J. Atmos. Sci.*, *33*, 2392–2398.

Raymond, D. J. (1983), Wave-CISK in mass flux form, *J. Atmos. Sci.*, *40*, 2561–2572.

Raymond, D. J. (1984), A wave-CISK model of squall lines, *J. Atmos. Sci.*, *41*, 1946–1958.

Raymond, D. J., and A. M. Blyth (1986), A stochastic mixing model for nonprecipitating cumulus clouds, *J. Atmos. Sci.*, *43*, 2708–2718.

Raymond, D. J., and H. Jiang (1990), A theory for long-lived convective systems, *J. Atmos. Sci.*, *47*, 3067–3077.

Rickenbach, T. M., and S. A. Rutledge (1998), Convection in TOGA COARE: Horizontal scale, morphology, and rainfall production, *J. Atmos. Sci.*, *55*, 2715–2729.

Riehl, H., and J. S. Malkus (1958), On the heat balance in the equatorial trough zone, *Geophysica*, *6*, 503–538.

Ritchie, E. A., and G. J. Holland (1997), Scale interactions during the formation of Typhoon Irving, *Mon. Weather Rev.*, *125*, 1377–1396.

Ritchie, E. A., J. Simpson, W. T. Liu, J. Halverson, C. Velden, K. F. Brueske, and H. Pierce (2003), Present day satellite technology for hurricane research: A closer look at formation and intensification, in *Hurricane! Coping With Disaster*, edited by R. Simpson, chap. 12, pp. 249–289, AGU, Washington, D. C.

Rotunno, R., J. B. Klemp, and M. L. Weisman (1988), A theory for strong, long-lived squall lines, *J. Atmos. Sci.*, *45*, 463–485.

Schmidt, J. M., and W. R. Cotton (1990), Interactions between upper and lower tropospheric gravity waves on squall line structure and maintenance, *J. Atmos. Sci.*, *47*, 1205–1222.

Schumacher, C., and R. A. Houze Jr. (2003), Stratiform rain in the tropics as seen by the TRMM Precipitation Radar, *J. Clim.*, *16*, 1739–1756.

Schumacher, C., R. A. Houze Jr., and I. Kraucunas (2004), The tropical dynamical response to latent heating estimates derived from the TRMM Precipitation Radar, *J. Atmos. Sci.*, *61*, 1341–1358.

Serra, Y., and R. A. Houze Jr. (2002), Observations of variability on synoptic timescales in the east Pacific ITCZ, *J. Atmos. Sci.*, *59*, 1723–1743.

Silva Dias, M. F., A. K. Betts, and D. E. Stevens (1984), A linear spectral model of tropical mesoscale systems: Sensitivity studies, *J. Atmos. Sci.*, *41*, 1704–1716.

Simpson, J., E. Ritchie, G. J. Holland, J. Halverson, and S. Stewart (1997), Mesoscale interactions in tropical cyclone genesis, *Mon. Weather Rev.*, *125*, 2643–2661.

Skamarock, W. C., M. L. Weisman, and J. B. Klemp (1994), Three-dimensional evolution of simulated long-lived squall lines, *J. Atmos. Sci.*, *51*, 2563–2584.

Smull, B. F., and R. A. Houze Jr. (1987), Rear inflow in squall lines with trailing-stratiform precipitation, *Mon. Weather Rev.*, *115*, 2869–2889.

Steiner, M., R. A. Houze Jr., and S. E. Yuter (1995), Climatological characterization of three-dimensional storm structure from operational radar and rain gauge data, *J. Appl. Meteorol.*, *34*, 1978–2007.

Straub, K. H., and G. N. Kiladis (2002), Observations of a convectively coupled Kelvin wave in the eastern Pacific ITCZ, *J. Atmos. Sci.*, *59*, 30–53.

Takayabu, Y. N. (1994), Large-scale cloud disturbances associated with equatorial waves. Part II: Westward-propagating inertio-gravity waves, *J. Meteorol. Soc. Jpn.*, *72*, 451–465.

Tepper, M. (1950), A proposed mechanism of squall lines: The pressure jump line, *J. Meteorol.*, *7*, 21–29.

Thorpe, A. J., M. J. Miller, and M. W. Moncrieff (1982), Two-dimensional convection in non-constant shear: A model of mid-latitude squall lines, *Q. J. R. Meteorol. Soc.*, *108*, 739–762.

Velasco, I., and J. M. Fritsch (1987), Mesoscale convective complexes in the Americas, *J. Geophys. Res.*, *92*, 9591–9613.

Webster, P. J., et al. (2002), The JASMINE pilot study, *Bull. Am. Meteorol. Soc.*, *83*, 1603–1630.

Williams, M., and R. A. Houze Jr. (1987), Satellite-observed characteristics of winter monsoon cloud clusters, *Mon. Weather Rev.*, *115*, 505–519.

Xu, Q., and J. H. E. Clark (1984), Wave-CISK and mesoscale convective systems, *J. Atmos. Sci.*, *41*, 2089–2107.

Yanai, M., S. Esbensen, and J. H. Chu (1973), Determination of bulk properties of tropical cloud clusters from large-scale heat and moisture budgets, *J. Atmos. Sci.*, *30*, 611–627.

Yang, M.-J., and R. A. Houze Jr. (1995a), Multicell squall-line structure as a manifestation of vertically trapped gravity waves, *Mon. Weather Rev.*, *123*, 641–661.

Yang, M.-J., and R. A. Houze Jr. (1995b), Sensitivity of squall-line rear inflow to ice microphysics and environmental humidity, *Mon. Weather Rev.*, *123*, 3175–3193.

Yang, M.-J., and R. A. Houze Jr. (1996), Momentum budget of a squall line with trailing-stratiform precipitation: Calculations from a high-resolution numerical model, *J. Atmos. Sci.*, *53*, 3629–3652.

Yuter, S. E., and R. A. Houze Jr. (1995a), Three-dimensional kinematic and microphysical evolution of Florida cumulonimbus. Part II: Frequency distribution of vertical velocity, reflectivity, and differential reflectivity, *Mon. Weather Rev.*, *123*, 1941–1963.

Yuter, S. E., and R. A. Houze Jr. (1995b), Three-dimensional kinematic and microphysical evolution of Florida cumulonimbus. Part III: Vertical mass transport, mass divergence, and synthesis, *Mon. Weather Rev.*, *123*, 1964–1983.

Yuter, S. E., and R. A. Houze Jr. (1997), Measurements of raindrop size distributions over the Pacific warm pool and implications for Z-R relations, *J. Appl. Meteorol.*, *36*, 847–867.

Yuter, S. E., and R. A. Houze Jr. (1998), The natural variability of precipitating clouds over the western Pacific warm pool, *Q. J. R. Meteorol. Soc.*, *124*, 53–99.

Zhang, D.-L. (1992), The formation of a cooling-induced mesovortex in the trailing-stratiform region of a midlatitude squall line, *Mon. Weather Rev.*, *120*, 2763–2785.

Zhang, D.-L., and J. M. Fritsch (1988), A numerical investigation of a convectively generated, inertially stable, extratropical warm-core mesovortex over land. Part I: Structure and evolution, *Mon. Weather Rev.*, *116*, 2660–2687.

Zhang, D.-L., and K. Gao (1989), Numerical simulation of an intense squall line during 10–11 June 1985 PRE-STORM. Part II: Rear inflow, surface pressure perturbations, and stratiform precipitation, *Mon. Weather Rev.*, *117*, 2067–2094.

Zipser, E. J. (1969), The role of organized unsaturated convective downdrafts in the structure and rapid decay of an equatorial disturbance, *J. Appl. Meteorol.*, *8*, 799–814.

Zipser, E. J. (1977), Mesoscale and convective-scale downdraughts as distinct components of squall-line circulation, *Mon. Weather Rev.*, *105*, 1568–1589.

R. A. Houze Jr., Department of Atmospheric Sciences, University of Washington, Seattle, WA 98195, USA. (houze@atmos.washington.edu)